

63-3-2

402 333

402333

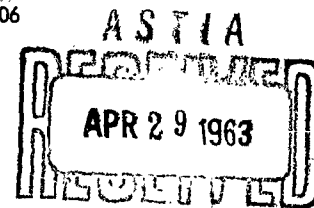
ASD-TDR-62-1004

FURTHER INVESTIGATION OF NOTCH SENSITIVITY
OF REFRACTORY METALS

TECHNICAL DOCUMENTARY REPORT NO. ASD-TDR-62-1004
December 1962

Directorate of Materials and Processes
Aeronautical Systems Division
Air Force Systems Command
Wright-Patterson Air Force Base, Ohio

Project No. 7351, Task 735106



TISIA

A

(Prepared under Contract No. AF 33(616)-7604
by Battelle Memorial Institute, Columbus, Ohio)

CATALOGED BY ASTIA
AD NO. _____

NOTICES

When Government drawings, specifications, or other data are used for any purpose other than in connection with a definitely related Government procurement operation, the United States Government thereby incurs no responsibility nor any obligation whatsoever, and the fact that the Government may have formulated, furnished, or in any way supplied the said drawings, specifications, or other data, is not to be regarded by implication or otherwise as in any manner licensing the holder or any other person or corporation, or conveying any rights or permission to manufacture, use, or sell any patented invention that may in any way be related thereto.

Qualified requesters may obtain copies of this report from the Armed Services Technical Information Agency, (ASTIA), Arlington Hall Station, Arlington 12, Virginia.

This report has been released to the Office of Technical Services, U. S. Department of Commerce, Washington 25, D. C., for sale to the general public.

Copies of this report should not be returned to the Aeronautical Systems Division unless return is required by security considerations, contractual obligations, or notice on a specific document.

FOREWORD

This report was prepared by Battelle Memorial Institute under United States Air Force Contract No. AF 33(616)-7604. This contract was initiated under Project No. 7351, "Metallic Materials", Task No. 735106, "Behavior of Metals". The project was administered under the direction of the Directorate of Materials and Processes, Deputy for Technology, Aeronautical Systems Division, with Lt. Robert T. Ault acting as project engineer.

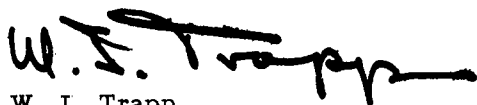
This report covers the period from October 1, 1961, through August 31, 1962.

ABSTRACT

Molybdenum and Mo-0.5Ti alloy with various degrees of cold work and different recrystallized grain sizes were tested to determine their low-temperature properties. Sufficient cold work (>25 per cent; about 68 per cent is sufficient) markedly reduced the ductile-to-brittle transition temperature of both materials, whereas increasing the recrystallized grain size increased this parameter. Mechanical notches resulted in pronounced degradation of properties in fibered structures, but were much less detrimental to recrystallized structure. This behavior was attributed to the controlling (detrimental) effect of grain boundaries in the fracture of recrystallized molybdenum or Mo-0.5Ti, regardless of material geometry.

The fracture toughness of unalloyed molybdenum, tungsten, tantalum, and columbium was studied over a range of temperatures chosen to include the ductile-brittle transition. Sheet specimens, 2 x 8 x 0.050 inch, containing sharp central notches were employed. Both wrought and recrystallized conditions were examined for each material. The effect of specimen orientation relative to the rolling direction was studied for molybdenum. Where possible, results were reported in terms of the fracture toughness parameters K_{IC} and K_{IC} . In an effort to provide some basic rationale for the behavior of a brittle material in the presence of notches, a model of an idealized partially relaxed crack was adopted. Using theoretical values of the stress at the tip of such a crack, the resultant macroscopic strain was calculated by means of parameters relating to dislocation density and velocity. This approach leads to an understanding of the parameters determining the response of a given metal to a running crack. The values of these parameters for molybdenum are experimentally determined.

This technical documentary report has been reviewed and is approved.



W. J. Trapp
Chief, Strength and Dynamics Branch
Directorate of Materials and Processes

TABLE OF CONTENTS

	<u>Page</u>
INTRODUCTION	1
SUMMARY	1
Metallurgical Variables	1
Fracture Toughness	2
Mechanisms	2
MATERIALS AND HEAT TREATMENTS	2
METALLURGICAL-VARIABLES STUDY	4
Experimental Procedures	4
Preparation of Specimens	4
Mechanical Testing	7
Experimental Results	7
Effects of Structure on Stress-Strain Curves	7
Effects of Structure on Low-Temperature Tensile Properties	7
Effect of Notch Acuity	34
Conclusions	34
FRACTURE-TOUGHNESS STUDIES	34
Experimental Procedures	38
Specimen Preparation	38
Mechanical Testing	40
Experimental Results	42
Molybdenum	42
Stress Relieved	47
Recrystallized	47
Tungsten	48
Stress Relieved	48
Recrystallized	48
Tantalum and Columbium	48
Practical Implications of Fracture-Toughness Results	52
Conclusions	52
MECHANISM OF NOTCH EMBRITTLEMENT	54
Development and Application of Model Relating to	
Crack Propagation in Refractory Metals	54
Model of a Partially Relieved Crack	55
Rate of Plastic Relaxation	57
Crack-Propagation Model	63
Results and Discussion	65
Determination of Dislocation Parameters for Molybdenum	
Relevant to the Crack-Propagation Model	76
Dislocation-Density Measurements	77
Measurements of Stress Dependence of Velocity	80

TABLE OF CONTENTS (Continued)

	<u>Page</u>
The Strain-Rate Dependence of the Lower Yield Stress	80
Measurement of Lüders' Band-Front Velocity	90
Stress Dependence of Delay Time	91
Stress-Relaxation Method	95
Discussion	96
GENERAL DISCUSSION	99
Theoretical Aspects	100
Metallurgical Aspects	101
Effects of Composition	102
Effects of Mechanical Variables	103
Fracture Toughness Aspects	103
Conclusions	103
REFERENCES	105
APPENDIX I	107
APPENDIX II	121

LIST OF TABLES

<u>Table</u>	
1.	Material Specifications 3
2.	Heat-Treatment Schedule 5
3.	Effect of Heat Treatment on Transition Temperature and Notch Sensitivity 31
4.	Calculated Values of the Stress-Concentration Factor α as a Function of Distance x and Hole Geometry a/r 59
5.	Values of the Dislocation Multiplication Parameters, C and β , for the Refractory Metals 59
6.	Values of the Dislocation-Velocity Parameter, n , for the Refractory Metals 61
7.	Estimates of the Dislocation Parameters ρ_0 , C , and n Appropriate for the Refractory Metals 62
8.	Value of the Integral I as a Function of a Crack Geometry a/r and Strain-Rate-Sensitivity Exponent n 65

LIST OF TABLES
(Continued)

<u>Table</u>	<u>Page</u>
9. Brittle-Crack-Penetration Transition Temperatures Predicted for Slow and Fast-Moving Cracks and Measured for Precracked Tensile Specimens	76
10. Values of n Obtained From the Literature for Fine- and Coarse-Grained Molybdenum	95
11. Tensile and Notch Tensile Properties of As-Wrought Molybdenum With 25 Per Cent Work.	107
12. Tensile and Notch Tensile Properties of As-Wrought Molybdenum With 68 Per Cent Work.	108
13. Tensile and Notch Tensile Properties of Stress-Relieved Molybdenum With 68 Per Cent Work (1/2 Hr at 538 C).	109
14. Tensile and Notch Tensile Properties of Stress-Relieved Molybdenum With 68 Per Cent Work (1/2 Hr at 871 C).	110
15. Tensile and Notch Tensile Properties of Recrystallized Molybdenum With 68 Per Cent Work (1/2 Hr at 1316 C)	111
16. Tensile and Notch Tensile Properties of Recrystallized Molybdenum With 68 Per Cent Work (1/2 Hr at 1928 C)	112
17. Tensile and Notch Tensile Properties of Recrystallized Molybdenum With 68 Per Cent Work (1/2 Hr at 2096 C)	113
18. Tensile and Notch Tensile Properties of As-Wrought Molybdenum-0.5 Per Cent Titanium With 25 Per Cent Work	114
19. Tensile and Notch Tensile Properties of As-Wrought Molybdenum-0.5 Per Cent Titanium With 68 Per Cent Work	115
20. Tensile and Notch Tensile Properties of Stress-Relieved Molybdenum-0.5 Per Cent Titanium With 68 Per Cent Work (1/2 Hr at 538 C).	116
21. Tensile and Notch Tensile Properties of Stress-Relieved Molybdenum-0.5 Per Cent Titanium With 68 Per Cent Work (1/2 Hr at 1093 C)	117
22. Tensile and Notch Tensile Properties of Recrystallized Molybdenum-0.5 Per Cent Titanium With 68 Per Cent Work (1/2 Hr at 1593 C)	118
23. Tensile and Notch Tensile Properties of Recrystallized Molybdenum-0.5 Per Cent Titanium With 68 Per Cent Work (1/2 Hr at 1928 C)	119
24. Tensile and Notch Tensile Properties of Recrystallized Molybdenum-0.5 Per Cent Titanium With 68 Per Cent Work (1/2 Hr at 2096 C)	120

LIST OF TABLES (Continued)

<u>Table</u>		<u>Page</u>
25.	Tensile Strength and Fracture-Toughness Properties of Wrought, Stress-Relieved Molybdenum Sheet (Longitudinal)	121
26.	Tensile Strength and Fracture-Toughness Properties of Wrought, Stress-Relieved Molybdenum Sheet (Transverse)	122
27.	Tensile Strength and Fracture-Toughness Properties of Recrystallized Molybdenum Sheet (Longitudinal)	123
28.	Tensile Strength and Fracture-Toughness Properties of Recrystallized Molybdenum Sheet (Transverse).	124
29.	Tensile Strength and Fracture-Toughness Properties of Wrought, Stress-Relieved Tungsten Sheet	125
30.	Tensile Strength and Fracture-Toughness Properties of Recrystallized Tungsten Sheet	126
31.	Tensile Strength and Fracture-Toughness Properties of Wrought, Stress-Relieved Tantalum Sheet	127
32.	Tensile Strength and Fracture-Toughness Properties of Recrystallized Tantalum Sheet	127
33.	Tensile Strength and Fracture-Toughness Properties of Wrought, Stress-Relieved Columbium Sheet	128
34.	Tensile Strength and Fracture-Toughness Properties of Recrystallized Columbium Sheet	128

LIST OF FIGURES

<u>Figure</u>		
1.	Notched- and Unnotched-Tensile-Specimen Specifications	6
2.	Effect of Working Reduction on the Engineering Stress-Strain Curve of Molybdenum at 150 C	8
3.	Stress-Strain Curves for Recrystallized Molybdenum at 150 C	8
4.	Tensile and Notch Tensile Properties of Wrought (25 Per Cent) Molybdenum	10
5.	Tensile and Notch Tensile Properties of Wrought (68 Per Cent) Molybdenum	11

LIST OF FIGURES
(Continued)

<u>Figure</u>		<u>Page</u>
6.	Tensile Properties and Notch Tensile Properties of Wrought (68 Per Cent) Stress-Relieved (1/2 Hr at 540 C) Molybdenum	12
7.	Tensile and Notch Tensile Properties of Wrought (68 Per Cent) Stress-Relieved (1/2 Hr at 870 C) Molybdenum.	13
8.	Tensile and Notch Tensile Properties of Small-Grained Recrystallized (1/2 Hr at 1320 C) Molybdenum).	14
9.	Tensile and Notch Tensile Properties of Medium-Grained Recrystallized (1/2 Hr at 1930 C) Molybdenum	15
10.	Tensile and Notch Tensile Properties of Large-Grained Recrystallized (1/2 Hr at 2090 C) Molybdenum	16
11.	Tensile and Notch Tensile Properties of Wrought (25 Per Cent) Mo-0.5Ti	17
12.	Tensile and Notch Tensile Properties of Wrought (68 Per Cent) Mo-0.5Ti	18
13.	Tensile and Notch Tensile Properties of Wrought (68 Per Cent) Stress- Relieved (1/2 Hr at 540 C) Mo-0.5Ti	19
14.	Tensile and Notch Tensile Properties of Wrought (68 Per Cent) Stress- Relieved (1/2 Hr at 1000 C) Mo-0.5Ti	20
15.	Tensile and Notch Tensile Properties of Small-Grained Recrystallized (1/2 Hr at 1590 C) Mo-0.5Ti	21
16.	Tensile and Notch Tensile Properties of Medium-Grained Recrystallized (1/2 Hr at 1930 C) Mo-0.5Ti.	22
17.	Tensile and Notch Tensile Properties of Large-Grained Recrystallized (1/2 Hr at 2090 C) Mo-0.5Ti	23
18.	Effects of Structure on Unnotch Tensile Strength	24
19.	Effect of Structure on Notch Tensile Strength	25
20.	Effect of Structure on Notch-Unnotch Strength Ratio of Mo-0.5Ti Alloy.	27
21.	Effect of Structure on the Transition Characteristics of Molybdenum and Mo-0.5Ti	28
22.	Effect of Structure on Notch Ductility	29
23.	Brittle Fracture Surface of Molybdenum Specimens	33

LIST OF FIGURES
(Continued)

<u>Figure</u>		<u>Page</u>
24.	Design of Smooth and Notched Tensile Specimens	39
25.	Configuration of Central Notch for Evaluation of Fracture Toughness for Tantalum and Columbium, Molybdenum, and Tungsten	41
26.	Tensile Strength and Fracture Toughness of Wrought, Stress-Relieved Molybdenum (Longitudinal) as a Function of Test Temperature	43
27.	Tensile Strength and Fracture Toughness of Wrought, Stress-Relieved Molybdenum (Transverse) as a Function of Test Temperature	44
28.	Tensile Strength and Fracture Toughness of Recrystallized Molybdenum (Longitudinal) as a Function of Test Temperature . . .	45
29.	Tensile Strength and Fracture Toughness of Recrystallized Molybdenum (Transverse) as a Function of Test Temperature . . .	46
30.	Tensile Strength and Fracture Toughness of Wrought, Stress-Relieved Tungsten as a Function of Test Temperature . . .	49
31.	Tensile Strength and Fracture Toughness of Recrystallized Tungsten as a Function of Test Temperature	50
32.	Effect of Test Temperature on Strength of Smooth and Center-Cracked Sheet Specimens of Tantalum and Columbium . . .	51
33.	Dependence of Fracture Stress on Fracture Toughness for Various Crack Lengths ($2a \ll W$), as Predicted by Fracture- Mechanics Theory (Assuming no Slow-Crack Extension)	53
34.	The Model of a Partially Relaxed Crack	56
35.	Calculated Stress Concentration α for an Elliptical Crack, Length $2a$ and Root Radius r , as a Function of Distance	58
36.	Schematic Presentation of Stress and Strain Ahead of a Moving Crack	64
37.	The Value of the Integral I as a Function of the Dislocation- Velocity Parameter n for Different Values of a/r , the Crack-Plastic Zone Geometry	66
38.	The Value of the Integral I as a Function of a/r , the Crack-Plastic Zone Geometry, for Different Values of the Dislocation Velocity Parameter n	67

LIST OF FIGURES
(Continued)

<u>Figure</u>		<u>Page</u>
39.	The Relation Between α^* , the Maximum Stress Concentration at the Elastic Plastic Boundary and a/r , the Crack-Plastic Zone	68
40.	The Influence of the Dislocation Parameter n on the Relative Plastic Zone Size a/r , the Maximum Stress-Concentration Factor α^* , and the Maximum Stress σ^* in Advance of a Moving Crack According to Equation (26) ($\sigma_y/\sigma_{nom} = 2$, $\rho_0 = 10^3$, $C = 10^9$, $f = 0.1$, $\epsilon_y = 10^{-3}$, $\epsilon_p^* = 10^{-3}$, $\dot{\epsilon}_p = 10^{-3}/\text{sec}$).	69
41.	Influence of the Multiplication Rate C and Initial Mobile Dislocation Density ρ_0 on the Relative Plastic-Zone Size a/r , the Maximum Stress-Concentration Factor α^* , and the Maximum Stress σ^* in Advance of a Moving Crack According to Equation (26) ($\sigma_y/\sigma_{nom} = 2$, $n = 5$, $f = 0.1$, $\epsilon_y = 10^{-3}$, $\epsilon_p^* = 10^{-3}$, $\dot{\epsilon}_p = 10^{-3}/\text{sec}$)	70
42.	Influence of the Multiplication Rate C and the Initial Mobile Dislocation Density ρ_0 on the Relative Plastic-Zone Size a/r , the Maximum Stress-Concentration Factor α^* in Advance of a Moving Crack According to Equation (26) ($\sigma_y/\sigma_{nom} = 2$, $n = 10$, $f = 0.1$, $\epsilon_y = 10^{-3}$, $\epsilon_p^* = 10^{-3}$, $\dot{\epsilon}_p = 10^{-3}/\text{sec}$)	71
43.	Influence of the Multiplication Rate C and the Initial Mobile Dislocation Density ρ_0 on the Relative Plastic-Zone a/r on the Maximum Stress-Concentration Factor α^* , and the Maximum Stress σ^* in Advance of a Moving Crack According to Equation (26) ($\sigma_y/\sigma_{nom} = 2$, $n = 20$, $f = 0.1$, $\epsilon_y = 10^{-3}$, $\epsilon_p^* = 10^{-3}$, $\dot{\epsilon}_p = 10^{-3}/\text{sec}$)	72
44.	Maximum Stress Concentration Factor α^* and Maximum Stress in Advance of a Moving Crack Predicted by Equation (26) for Tungsten, Molybdenum, and Columbium for the Dislocation Parameters Given in Table 5 ($\sigma_y/\sigma_{nom} = 2$, $f = 0.1$, $\epsilon_y = 10^{-3}$, $\epsilon_p^* = 10^{-3}$, $\dot{\epsilon}_p = 10^{-3}/\text{sec}$)	75
45.	Typical Microstructures of the Coarse- and Fine-Grained Material	78
46.	Microstructures Showing the Difference in Precipitate Distribution in the Coarse- and Fine-Grained Molybdenum	79
47.	Typical Etch-Pitting Results	81
48.	Transmission Electron Micrographs of Fine-Grained Molybdenum in the Annealed Condition	82

LIST OF FIGURES
(Continued)

<u>Figure</u>		<u>Page</u>
49.	Transmission Electron Micrographs of Coarse-Grained Molybdenum in the Annealed Condition, Showing the Effect of Inclusions	83
50.	Typical Dislocation Densities in Coarse-Grained Molybdenum at Various Strains	84
51.	Variation of Dislocation Density With Strain in Coarse-Grained Molybdenum	85
52.	Design of Test Bar	87
53.	Variation of Upper Yield Stress With Strain Rate in Molybdenum	88
54.	Variation of Lower Yield Stress With Strain Rate in Fine-Grain Molybdenum	89
55.	Typical Stress-Strain Curve Showing a Strain Rate Change During Lüders' Propagation	92
56.	Lüders' Bands in Fine-Grained Molybdenum, Showing Contrast at the Band Front	93
57.	Stress Dependence of Lüders' Band-Front Velocity	94
58.	Relaxation Curves for Coarse-Grained Molybdenum	97
59.	Relaxation Curves for Fine-Grained Molybdenum	98

INTRODUCTION

In view of the tendency toward low-temperature brittleness exhibited by many refractory metals, their response to cracks, notches, or internal flaws is an important metallurgical consideration and design problem. The notch sensitivity of refractory metals has been the subject of past research at Battelle Memorial Institute(1,2)*. Earlier studies were directed toward characterizing the ductile-to-brittle transition behavior and notch sensitivity of several commercial-grade refractory metals (molybdenum, tungsten, columbium, and tantalum) and refractory metal alloys (Mo-0.5Ti, Ta-10W, and F-48). The effects of interstitial oxygen and hydrogen on the low-temperature behavior of tantalum and columbium were evaluated in subsequent studies.

To improve understanding of the low-temperature behavior of refractory metals, the current program was expanded to include:

- (1) Studies on the effects of metallurgical variables (working reduction, stress-relief temperature, and grain size) on the low-temperature mechanical behavior of molybdenum and Mo-0.5Ti.
- (2) Fracture-toughness determinations for molybdenum, tungsten, tantalum, and columbium over the temperature range for ductile-to-brittle transition.
- (3) Basic studies of material properties relating to notch embrittlement.

SUMMARY

Metallurgical Variables

The effects of working reduction and heat treatment on the ductile-to-brittle transition temperature and notch behavior of molybdenum and Mo-0.5Ti were evaluated.

Although light working reductions (25 per cent) had little effect on the transition temperature of recrystallized material, greater reductions (68 per cent) markedly lowered the transition temperature. The major effect of increased reduction was a narrowing of the transition range; the lower temperature of this range remained constant. Notch behavior was relatively unaffected by working reductions up to 68 per cent. Stress-relief annealing lowered the transition temperature and improved notch behavior of wrought structures somewhat. Varying the stress-relief temperature had little effect on properties.

Recrystallization increased the transition temperature markedly, the greatest increase being associated with the largest recrystallized grain size.

The effects of notches were more pronounced with wrought than with recrystallized structures. Fibered structures were markedly sensitive to notches at

*References are listed on page 102.

Manuscript released by authors October 25, 1962, for publication as ASD Technical Documentary Report.

temperatures below about 0 C, whereas recrystallized structures were not particularly notch sensitive at temperatures as low as -75 C. This was attributed to the controlling effect grain boundaries have on fracture initiation in both notched and unnotched specimens with recrystallized structures. Detailed consideration of strength characteristics of recrystallized structures impugns their reliability at temperatures lower than about 150 C.

Fracture Toughness

Results of fracture-toughness tests on unalloyed refractory metals indicate that tantalum and columbium can be expected to perform reliably at temperatures as low as -196 C, even in the presence of sharp cracks, whereas molybdenum and tungsten have very little fracture resistance at room temperature or below. Wrought molybdenum exhibited appreciable fracture toughness above about 90 C; the corresponding temperature for wrought tungsten was about 260 C. For molybdenum and tungsten, specimens with recrystallized structures exhibited (1) generally lower fracture-toughness values, (2) a more gradual ductile-brittle transition, and (3) a somewhat higher transition temperature than those with wrought structures. Specimen orientation relative to the rolling direction appeared to have little effect on fracture toughness in molybdenum.

Mechanisms

The consequences of a simple model of crack propagation have been examined. The factors which seem most important in deciding the response of a metal to a running crack are the intrinsic fracture strength and the parameters describing the stress dependence of dislocation velocity, the initial dislocation density, and the rate of dislocation multiplication.

According to the model, the tensile stress at the tip of a running crack in tungsten may sometimes exceed the theoretical strength of the matrix. In less brittle molybdenum, stresses of up to about 7 times the static yield are experienced which may be expected to exceed the macroscopic fracture strength. As opposed to this type of behavior, under the influence of the stresses at a crack tip, columbium is able to relax and so blunt the crack. In this case it appears to be difficult for a running crack to produce sufficiently high stresses as to be self-sustaining.

Various indirect experimental methods for determining the stress dependence of dislocation velocity have been investigated and evaluated. An ultimate assessment of their value awaits experimental verification by the direct method.

MATERIALS AND HEAT TREATMENTS

The materials used in this research program were purchased from commercial producers and are representative of those in current production. Fabrication histories and analyses are reported in Table 1.

TABLE 1. MATERIAL SPECIFICATIONS

Material	Vendor	Fabrication History	Analyses, ppm				
			C	N	O	H	Ti
Molybdenum rod (68% work)	Universal-Cyclops Steel Corporation	Material hot-cold worked from 0.450-in. -diam recrystallized bar to 0.255-in. diam below 870 C and ground to 0.250-in. diam; total work from final recrystallization was 68 per cent	330	<10	6	<1	--
Molybdenum rod (25% work)	Ditto	Material hot-cold worked from 0.294-in. -diam recrystallized bar to 0.255-in. diam below 870 C and ground to 0.250-in. diam; total work from final recrystallization was 25 per cent	240	<10	5	<1	--
Molybdenum sheet	"	Commercial, stress-relieved, 50-mil sheet	290	<10	4	<1	--
Mo-0.5Ti rod (68% work)	"	Material hot-cold worked from 0.450-in. -diam recrystallized bar to 0.255-in. diam. below 1093 C and ground to 0.250-in. diam; total work from final recrystallization was 68 per cent	290	<10	1	<1	0.49%
Mo-0.5Ti rod (25% work)	"	Material hot-cold worked from 0.294-in. -diam recrystallized bar to 0.255-in. diam below 1093 C and ground to 0.250-in. diam; total work from final recrystallization was 25 per cent	260	40	78	<1	
Tungsten sheet	General Electric Co.	Commercial, stress-relieved, 50-mil sheet	20	<10	28	<1	--
Tantalum sheet	Wah Chang Corp.	Ditto	50	20	44	<1	--
Columbium sheet	Ditto	"	40	110	228	<1	--

Heat treatments for the selected test conditions of each material are indicated in Table 2. All heat treatments were conducted in vacuum on high-purity argon.

No observable microstructural change accompanied the stress-relief treatments. The small-grained, recrystallized structures of molybdenum and Mo-0.5Ti were relatively "clean" and free of second-phase particles. However, numerous precipitate particles could be seen, both within the grains and in the grain boundaries, of the coarse-grained structures.

METALLURGICAL-VARIABLES STUDY*

Most refractory metals undergo a transition from ductile-to-brittle behavior at low temperature. This brittle behavior is the result of a loss of strength that occurs at temperatures where the critical stress for fracture is less than the stress required to promote macroscopic plastic flow. In the simple case for pure tensile stresses applied at a given rate, the limits for this behavior can be adequately established by defining the temperature at which the material becomes brittle. However, realistic designs are seldom so simple, and material deficiencies (cracks, inclusions, etc.) further complicate the problem.

A technique used in the past to assist in the definition of design criteria utilizes notched tensile specimens, which reduces the maximum shear stress in the test section, thereby inhibiting plastic flow. This results in strengthening attributable to the notch under conditions where the material is ductile. However, this should also increase the flow stress relative to the cleavage fracture stress, resulting in the brittle failure of notched specimens at higher temperatures than with unnotched specimens. Thus, at a given temperature where simple tensile properties would predict reliable behavior, the abnormally high value for the nominal stress required for slip in notched specimens may exceed that required for fracture, and catastrophic brittle failure would result.

Thus, empirical design information relating the effects of notches to behavior as reflected by strength and ductility observations may serve to define critical temperatures below which unreliable behavior can be expected. The first phase of this program was designed to investigate the low-temperature tensile and notch tensile behavior of molybdenum and the Mo-0.5Ti alloy in several fibered and recrystallized conditions to assist in developing design parameters for their use.

Experimental Procedures

Preparation of Specimens

All mechanical-test specimens were machined from previously heat-treated specimen blanks.

Notched and unnotched tensile specimens for the study of metallurgical variables were machined to the specifications described in Figure 1.

*Authored by E. S. Bartlett, A. G. Imgram, and H. R. Ogden.

TABLE 2. HEAT-TREATMENT SCHEDULE

Material	Condition	Heat Treatment	Hardness, VHN	Grain Size (Mean Linear Intercept), min	Specimen Use		
					Metallurgical Variables	Fracture Toughness	Mechanism of Notch Embrittlement
Molybdenum rod (68% work)	As wrought		247	--			
	Low temperature, stress relieved	1/2 hr at 540 C	230	--			
	High temperature, stress relieved	1/2 hr at 870 C	246	--			
	Recrystallized, small grain	1/2 hr at 1320 C	183	0.021			
	Recrystallized, medium grain	1/2 hr at 1930 C	177	0.163			
Molybdenum rod (25% work)	Recrystallized, large grain	1/2 hr at 2090 C	175	0.320			
	As wrought	--	221	--			
Mo-0.5Ti rod (68% work)	As wrought	--	264	--			
	Low temperature, stress relieved	1/2 hr at 540 C	262	--			
	High temperature, stress relieved	1/2 hr at 1000 C	261	--			
	Recrystallized, small grain	1/2 hr at 1590 C	203	0.028			
Mo-0.5Ti rod (25% work)	Recrystallized, medium grain	1/2 hr at 1930 C	199	0.194			
	Recrystallized, large grain	1/2 hr at 2090 C	199	0.285			
	As wrought	--	233	--			
Molybdenum sheet	High temperature, stress relieved	1 hr at 800 C	253	--			
	Recrystallized	1 hr at 1200 C	174	0.045			
	High temperature, stress relieved	1 hr at 1100 C	450	--			
Tungsten sheet	Recrystallized	1 hr at 1500 C	358	0.038			
Tantalum sheet	High temperature, stress relieved	1 hr at 800 C	140	--			
	Recrystallized	1 hr at 1200 C	98	0.040			
Columbium sheet	High temperature, stress relieved	1 hr at 800 C	165	--			
	Recrystallized	1 hr at 1300 C	98	0.025			

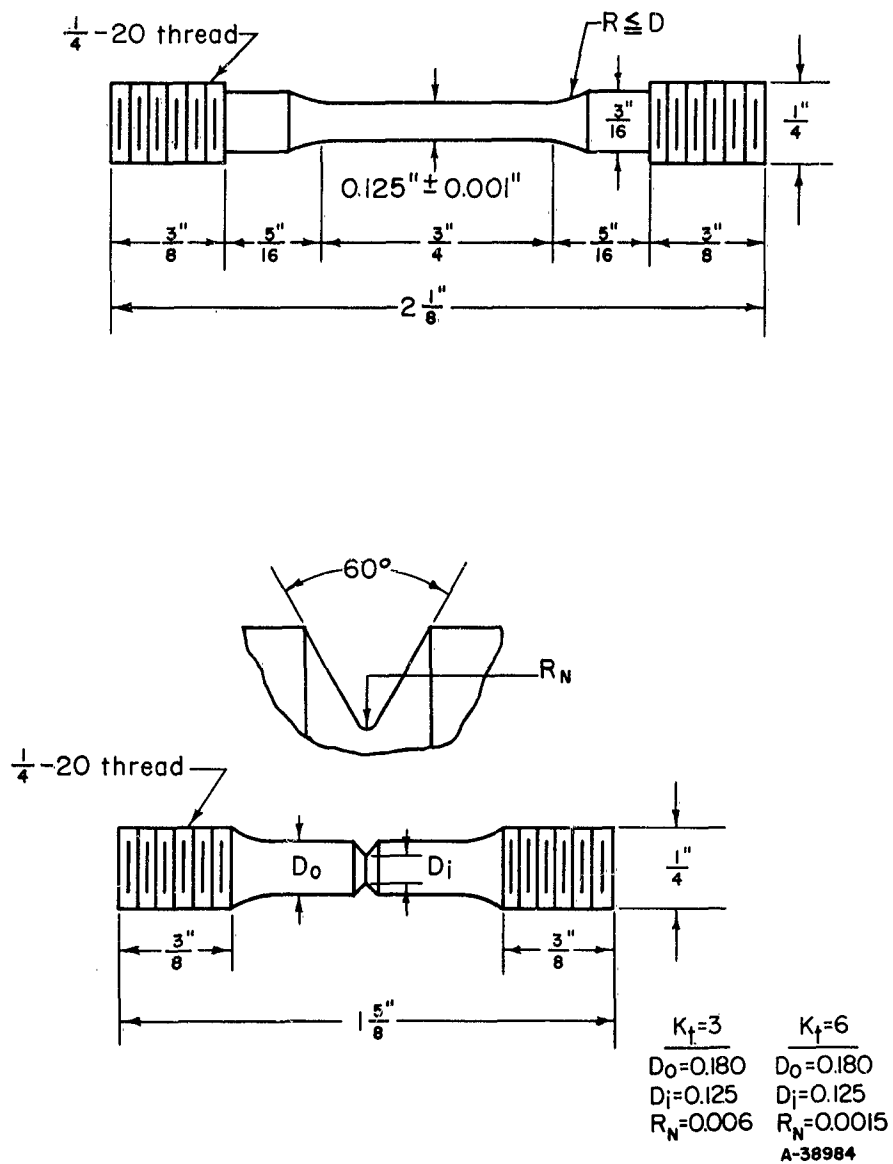


FIGURE 1. NOTCHED- AND UNNOTCHED-TENSILE-SPECIMEN SPECIFICATIONS

Mechanical Testing

Notched and unnotched specimens of each material and structural condition were tested at a series of temperatures selected to encompass the ductile-to-brittle transition.

Tests were conducted in a Baldwin-Southwark Universal Testing Machine. Unnotched specimens were tested at a constant crosshead speed of 0.02 inch per minute, whereas notched specimens were tested at a constant crosshead speed of 0.005 inch per minute. Load-extension curves to the breaking point were obtained for each specimen at all test temperatures.

Ultimate tensile strength, 0.2 per cent offset yield strength, reduction in area, and per cent elongation were recorded for each unnotched specimen. For notched specimens, ultimate tensile strength and reduction in area were determined. Point of failure (at or below maximum load) and mechanism of fracture (shear or cleavage) were noted for both notched and unnotched specimens.

Experimental Results

Effects of Structure on Stress-Strain Curves

Figure 2 illustrates the effect of working reduction on the engineering stress-strain curve of molybdenum at 150 C. Specimens with a recrystallized structure exhibited a sharp yield point. With light working reduction (25 per cent) no yield point could be detected, and the total elongation to fracture was decreased. Heavier working reductions (68 per cent) reintroduced a yield point (probably because of aging during fabrication), and further reduced elongation. The rate of work hardening also decreased with increasing amounts of prior cold work. Stress-relief annealing did not significantly alter the stress-strain curve of the heavily worked material. Effects similar to those shown in Figure 2 were observed for the Mo-0.5Ti alloy.

The effect of grain size on the stress-strain curves of recrystallized molybdenum at 150 C is illustrated in Figure 3. A pronounced yield point was observed with the small-grained structure, but was not detected for either of the coarse-grained structures. Work-hardening rates were higher with the coarse-grained structures. These effects are probably related to the presence of second-phase particles which may act as dislocation generating sources in the coarse-grained structures and/or the relatively high interstitial content which permits dislocation locking in the fine-grained structure. Increasing the grain size also markedly decreased the total elongation to fracture and the capacity for necking.

Stress-strain curves for Mo-0.5Ti followed the same general pattern shown in Figure 3.

Effects of Structure on Low-Temperature Tensile Properties

The tensile and notched tensile properties of molybdenum and Mo-0.5Ti are presented for the various structural conditions as follows:

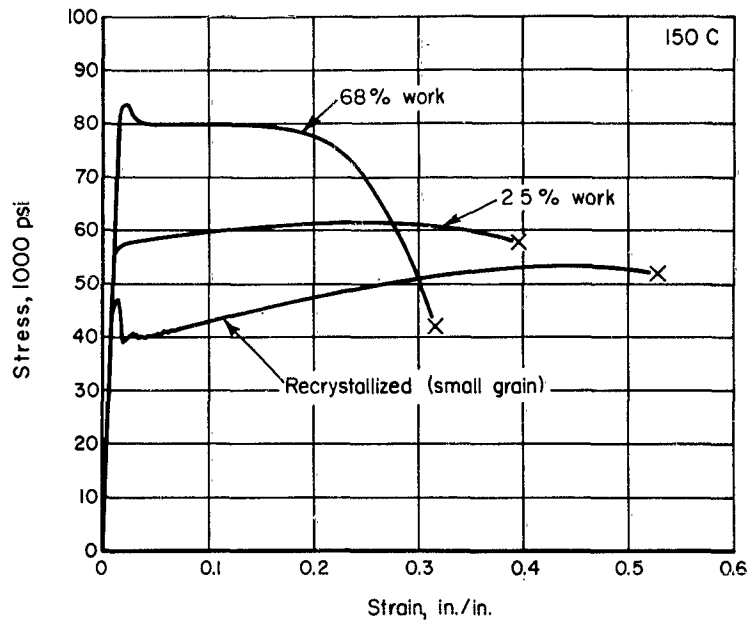


FIGURE 2. EFFECT OF WORKING REDUCTION ON THE ENGINEERING STRESS-STRAIN CURVE OF MOLYBDENUM AT 150 C

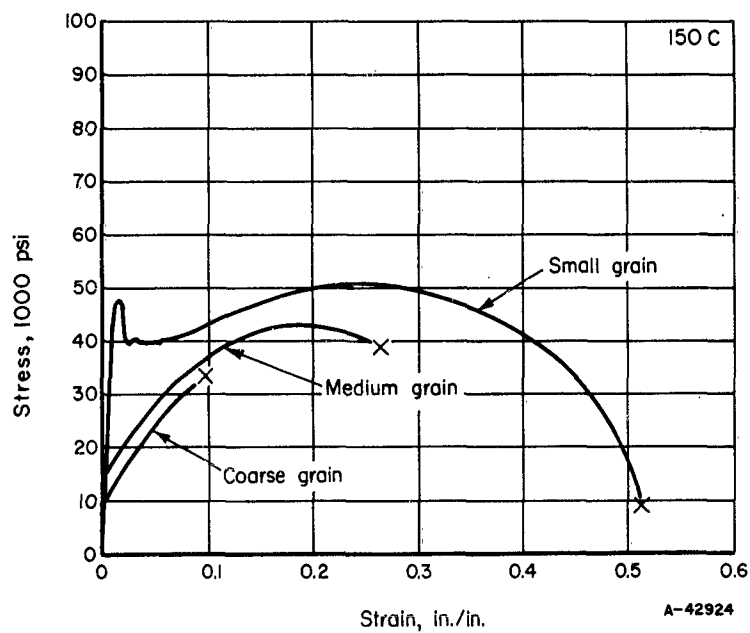


FIGURE 3. STRESS-STRAIN CURVES FOR RECRYSTALLIZED MOLYBDENUM AT 150 C

	<u>Mo</u>	<u>Mo-0.5Ti</u>
As Wrought		
25 Per Cent Work	Figure 4	Figure 11
68 Per Cent Work	Figure 5	Figure 12
Stress Relieved (68 Per Cent Work)		
Low Temperature	Figure 6	Figure 13
High Temperature	Figure 7	Figure 14
Recrystallized		
Small Grain ^(a)	Figure 8	Figure 15
Medium Grain	Figure 9	Figure 16
Large Grain	Figure 10	Figure 17

(a) Includes data for two notch acuities.

Tabulated data are presented in Appendix I.

The effects of metallurgical structure upon the tensile strength of molybdenum and Mo-0.5Ti are illustrated in Figure 18. Stress relief of the more severely worked material appeared to effect additional slight increases in strength at the lower temperatures. However, this can be more logically assumed to represent a decrease in the tendency toward fracture instability* of the wrought structure rather than an absolute increase in strength. Upon recrystallization, tensile strengths were markedly less for coarse-grained structures than for fine-grained structures. Furthermore, the rate of increase in tensile strength with decreasing temperature was appreciably less for the coarse-grained structures than for the fine-grained or fibered structures. In most cases where tests were conducted at temperatures of -196 C, tensile strengths were less than observed at -75 C, and in all cases investigated, the rate of change of strength with temperature was much lower at temperatures less than -75 than at temperatures greater than -75 C. This indicates that the threshold temperature for fracture instability in unnotched specimens lies between -196 and -75 C, probably closer to -75 C, regardless of metallurgical condition.

Figure 19 describes the effects of metallurgical structure on notch tensile strength of the two materials. These parameters indicate differences in behavior between unalloyed molybdenum and the Mo-0.5Ti alloy. Considering first the parameters for molybdenum, wrought structures exhibited notch strength properties that allowed the definition of sharp notch strength peaks at 25 C. Stress relief and recrystallization

*Fracture instability denotes the condition wherein fracture occurs at less than the expected level of stress, based upon extrapolation of data obtained at higher temperatures.

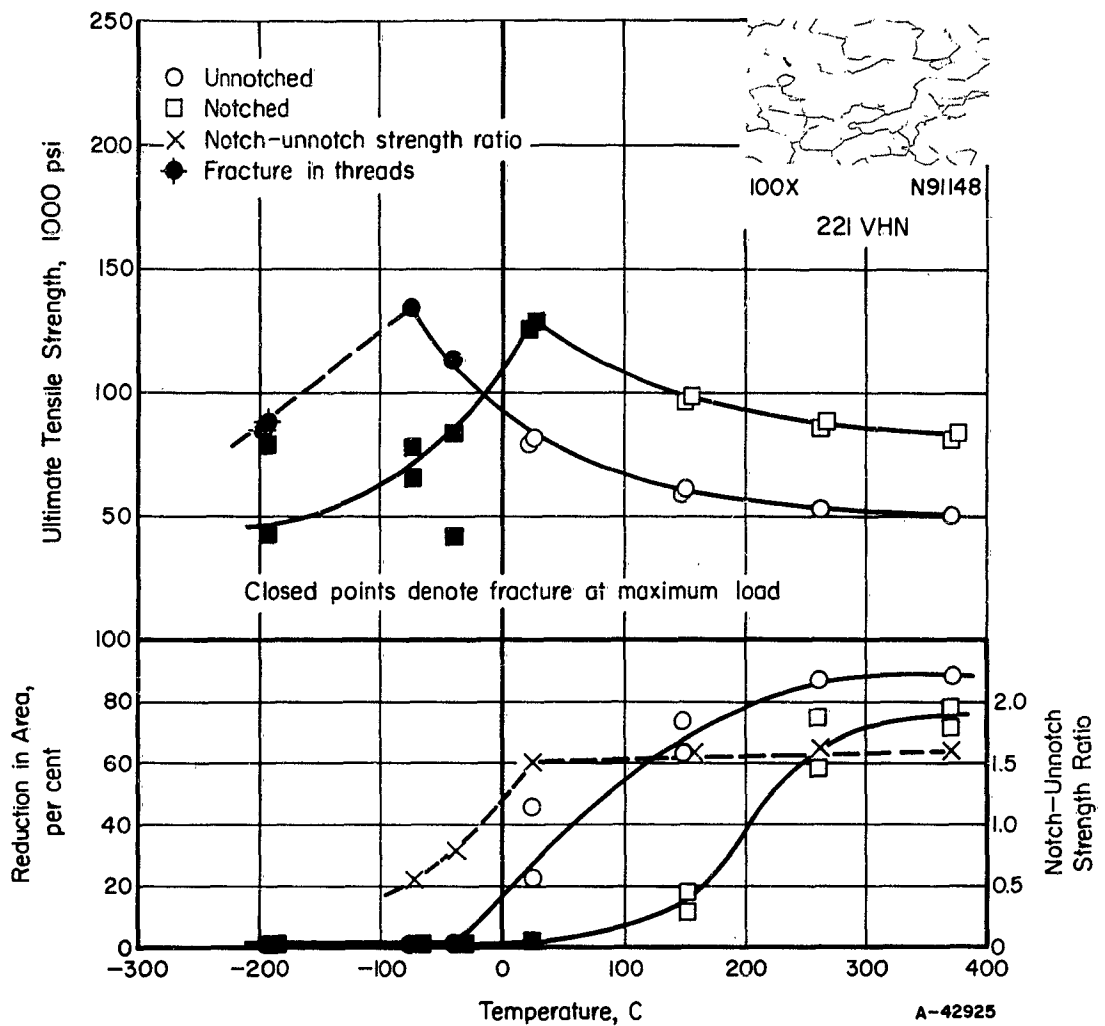


FIGURE 4. TENSILE AND NOTCH TENSILE PROPERTIES OF WROUGHT (25 PER CENT) MOLYBDENUM

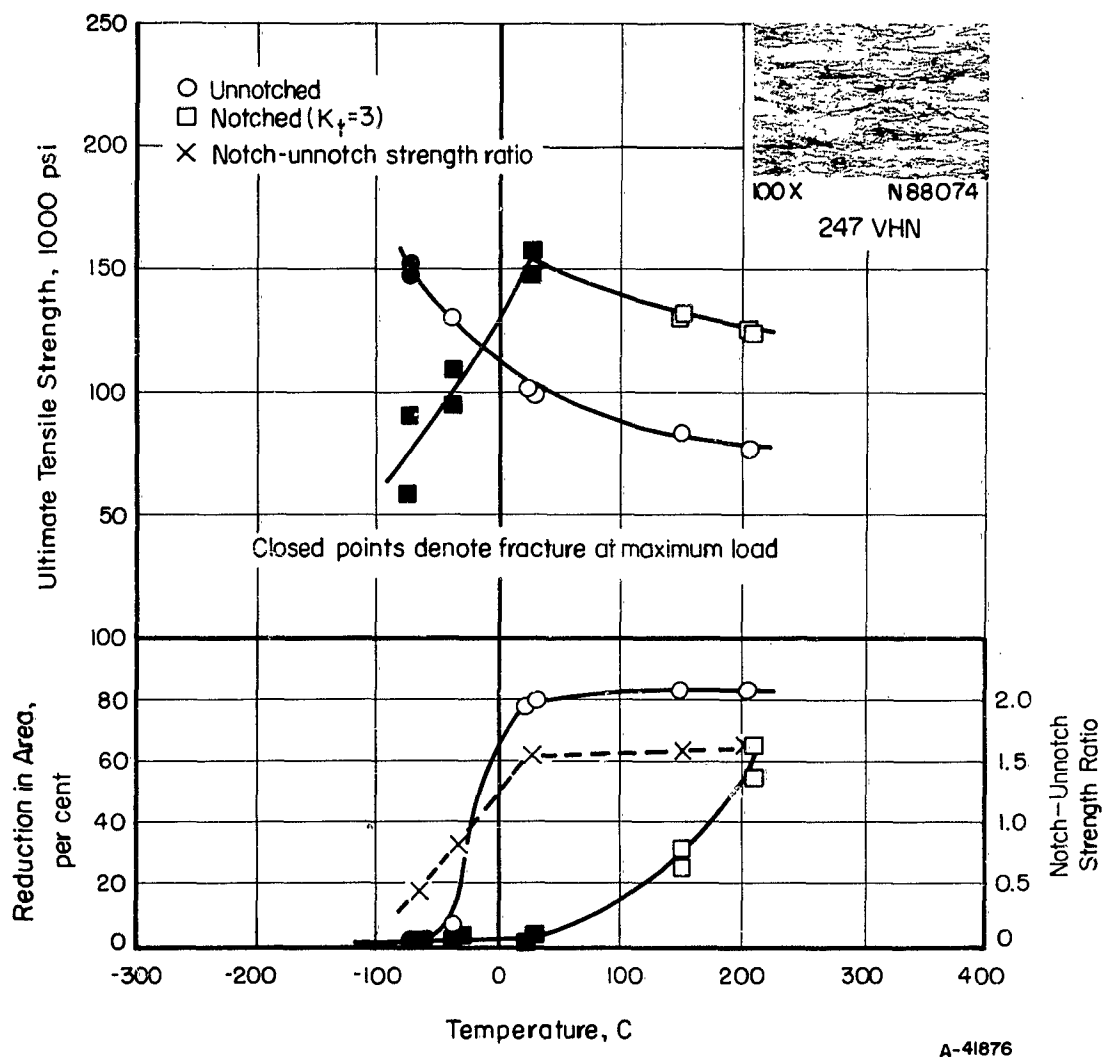


FIGURE 5. TENSILE AND NOTCH TENSILE PROPERTIES OF WROUGHT (68 PER CENT) MOLYBDENUM

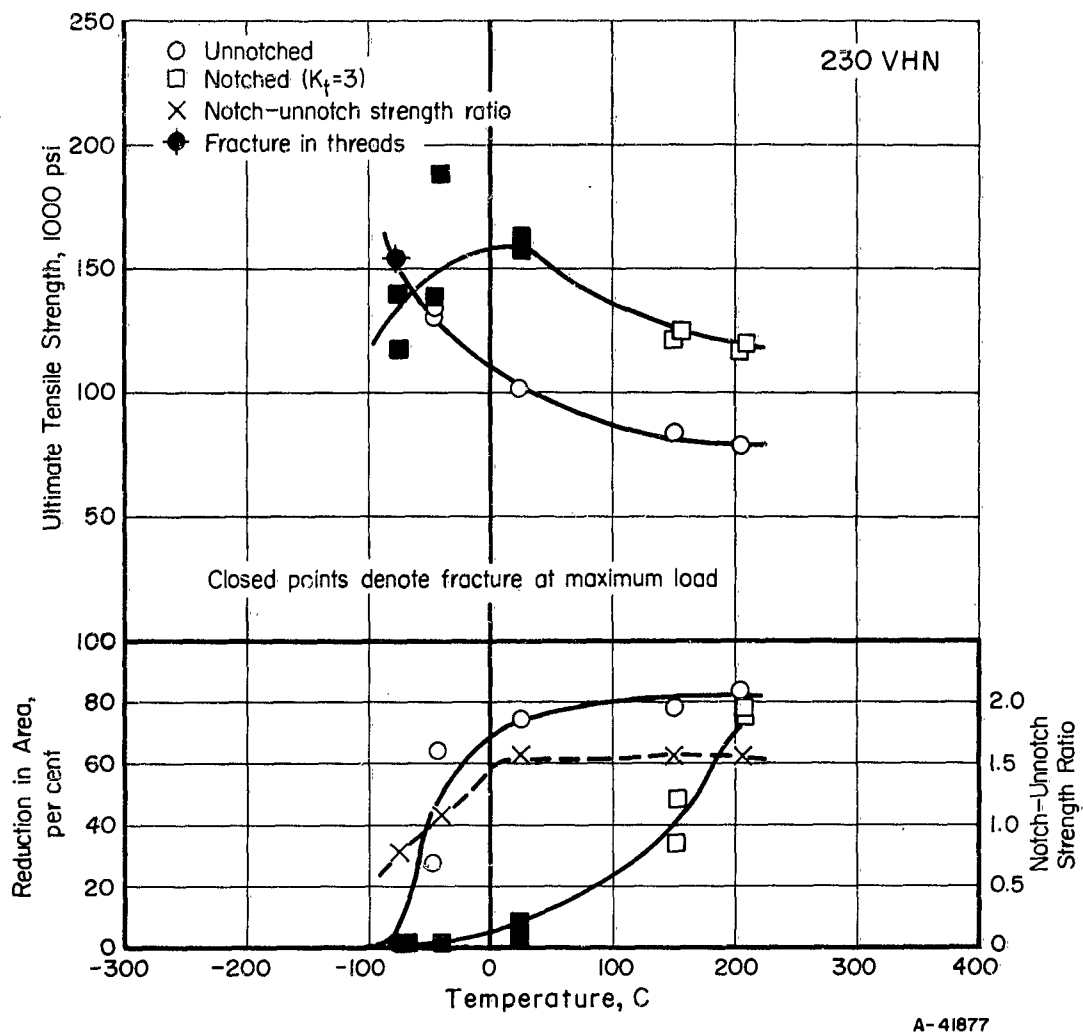


FIGURE 6. TENSILE PROPERTIES AND NOTCH TENSILE PROPERTIES OF WROUGHT (68 PER CENT) STRESS-RELIEVED (1/2 HR AT 540 C) MOLYBDENUM

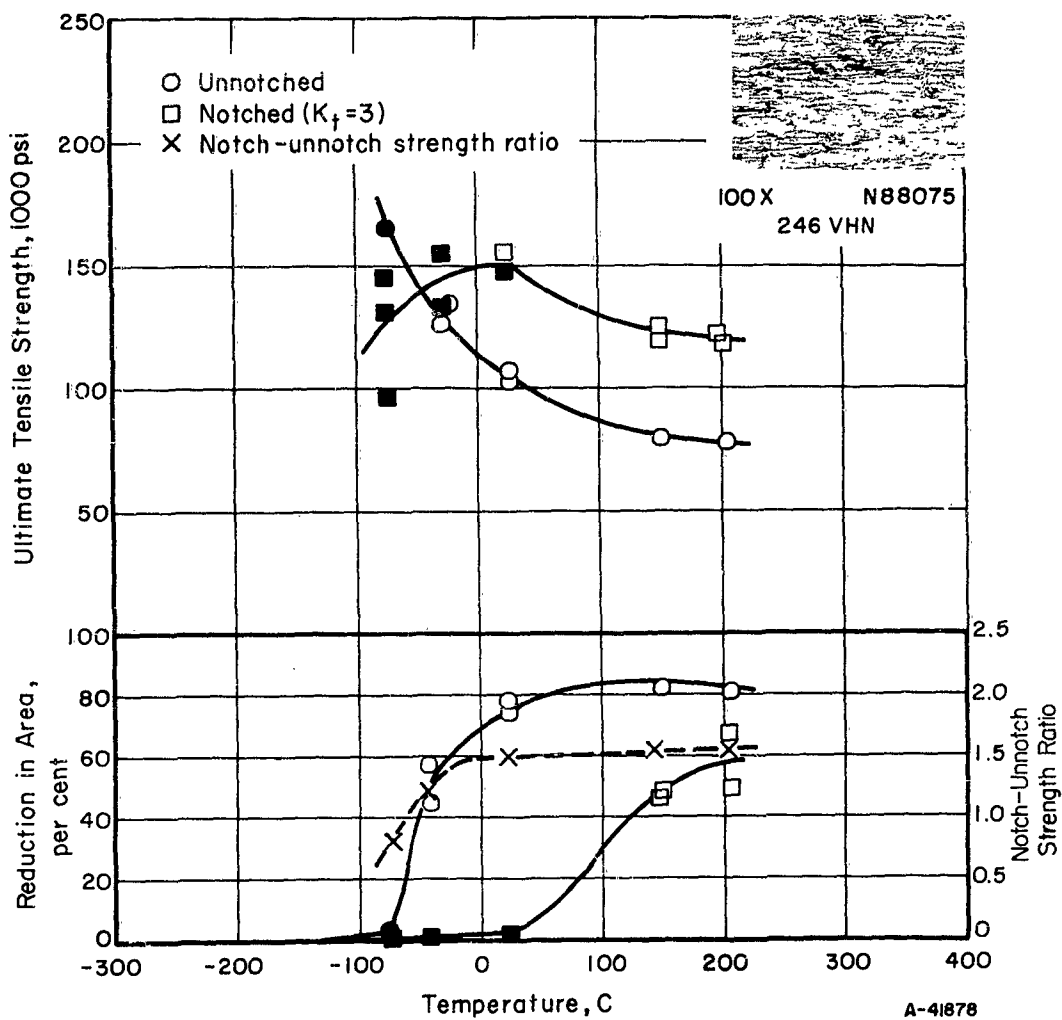


FIGURE 7. TENSILE AND NOTCH TENSILE PROPERTIES OF WROUGHT (68 PER CENT) STRESS-RELIEVED (1/2 HR AT 870 C) MOLYBDENUM

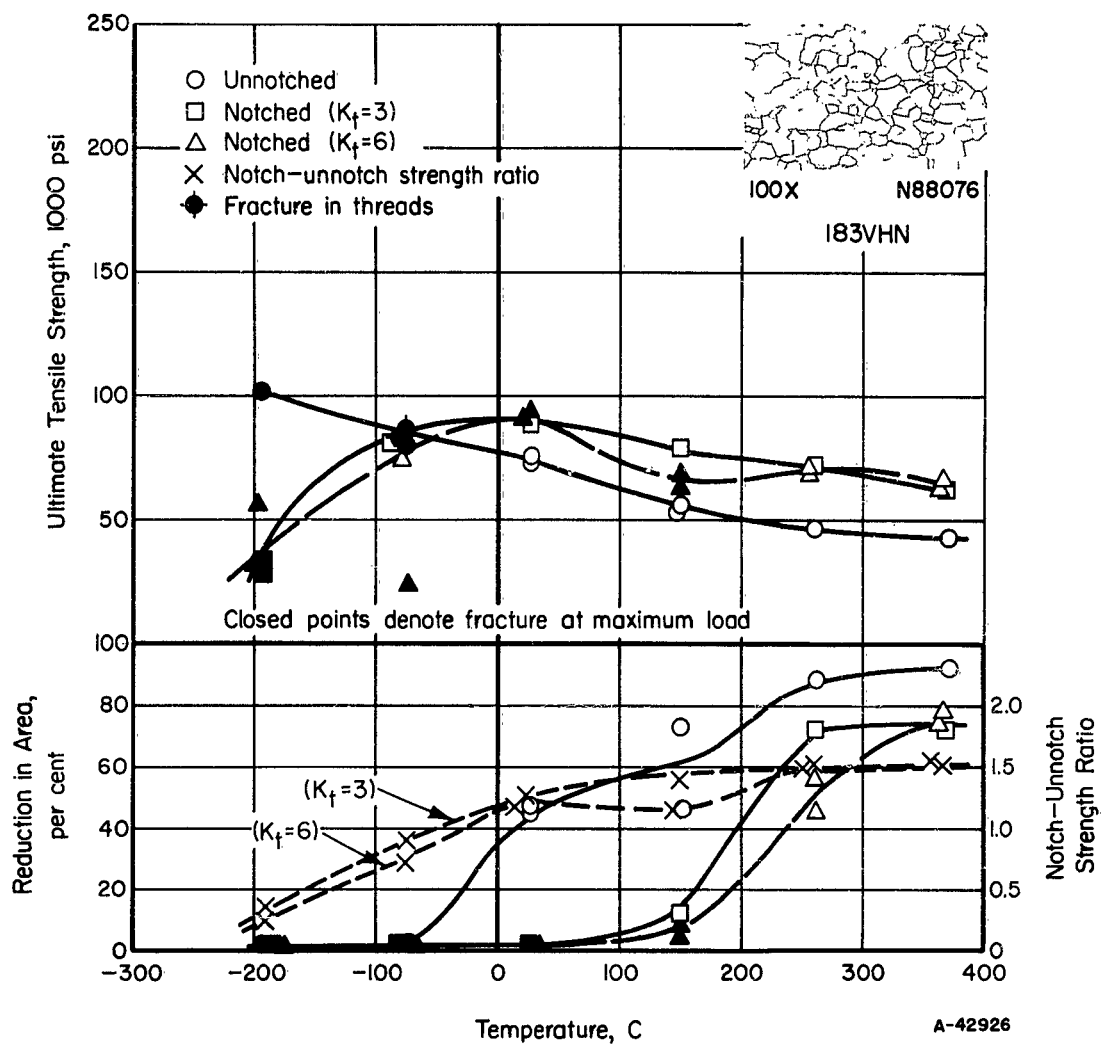


FIGURE 8. TENSILE AND NOTCH TENSILE PROPERTIES OF SMALL-GRAINED RECRYSTALLIZED (1/2 HR AT 1320 C) MOLYBDENUM

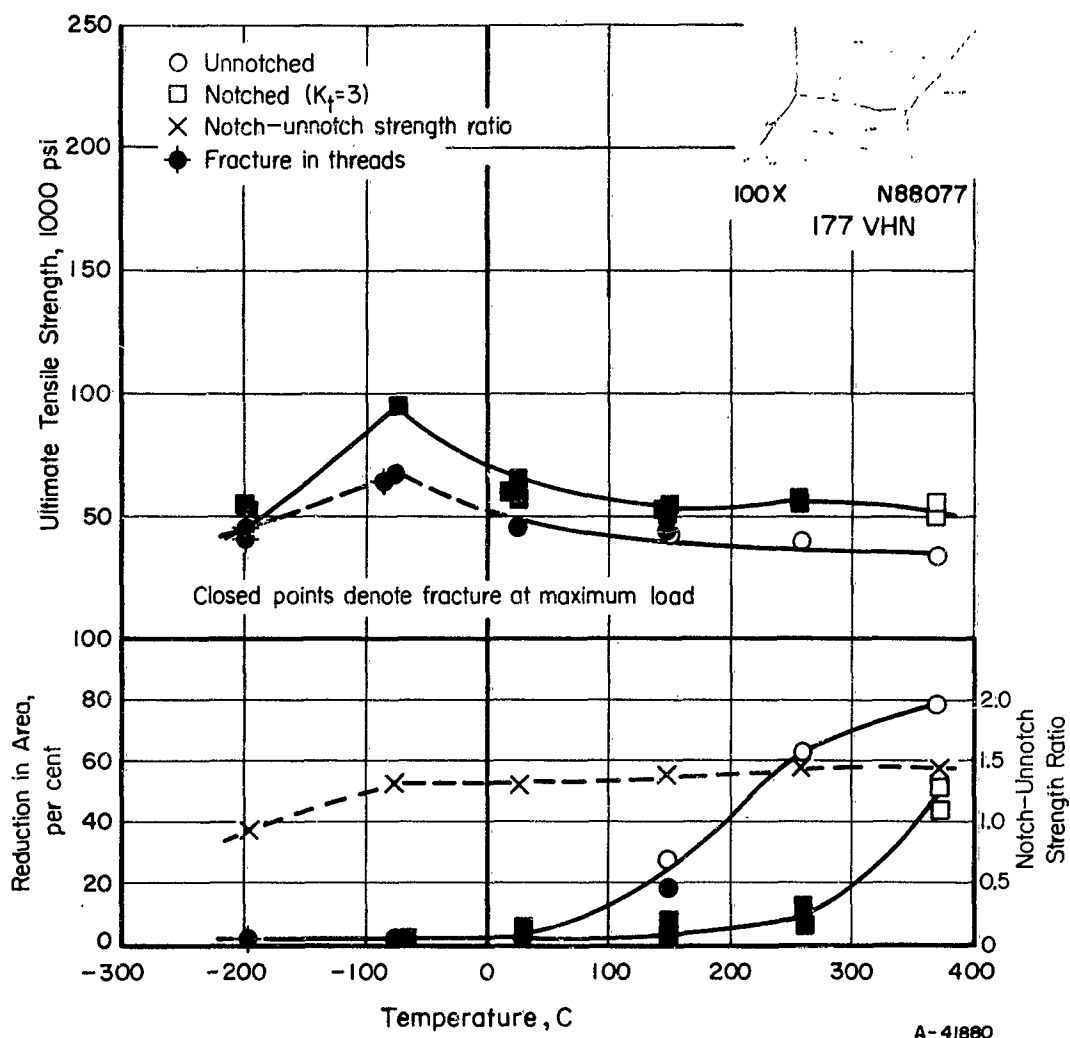


FIGURE 9. TENSILE AND NOTCH TENSILE PROPERTIES OF MEDIUM-GRAINED RECRYSTALLIZED (1/2 HR AT 1930 C) MOLYBDENUM

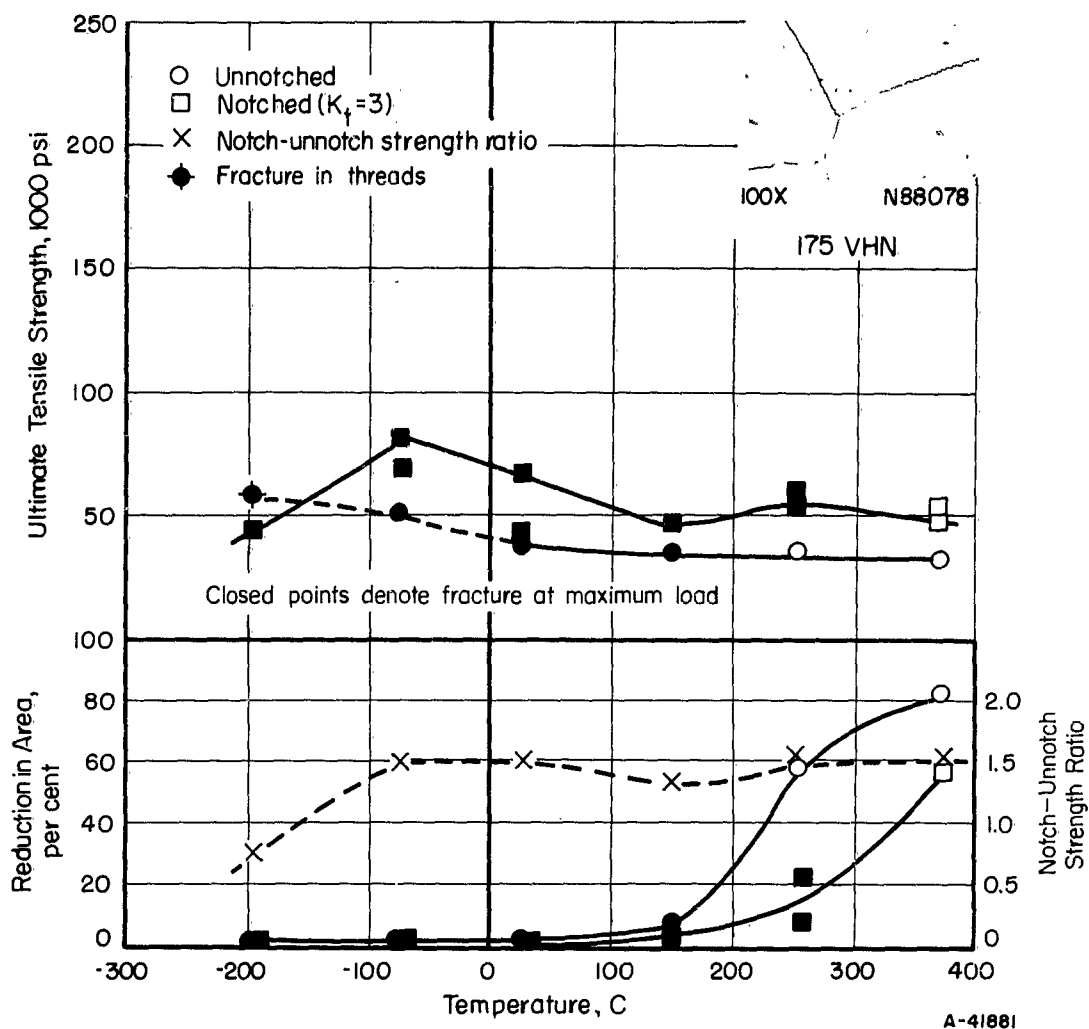


FIGURE 10. TENSILE AND NOTCH TENSILE PROPERTIES OF LARGE-GRAINED RECRYSTALLIZED (1/2 HR AT 2090 C) MOLYBDENUM

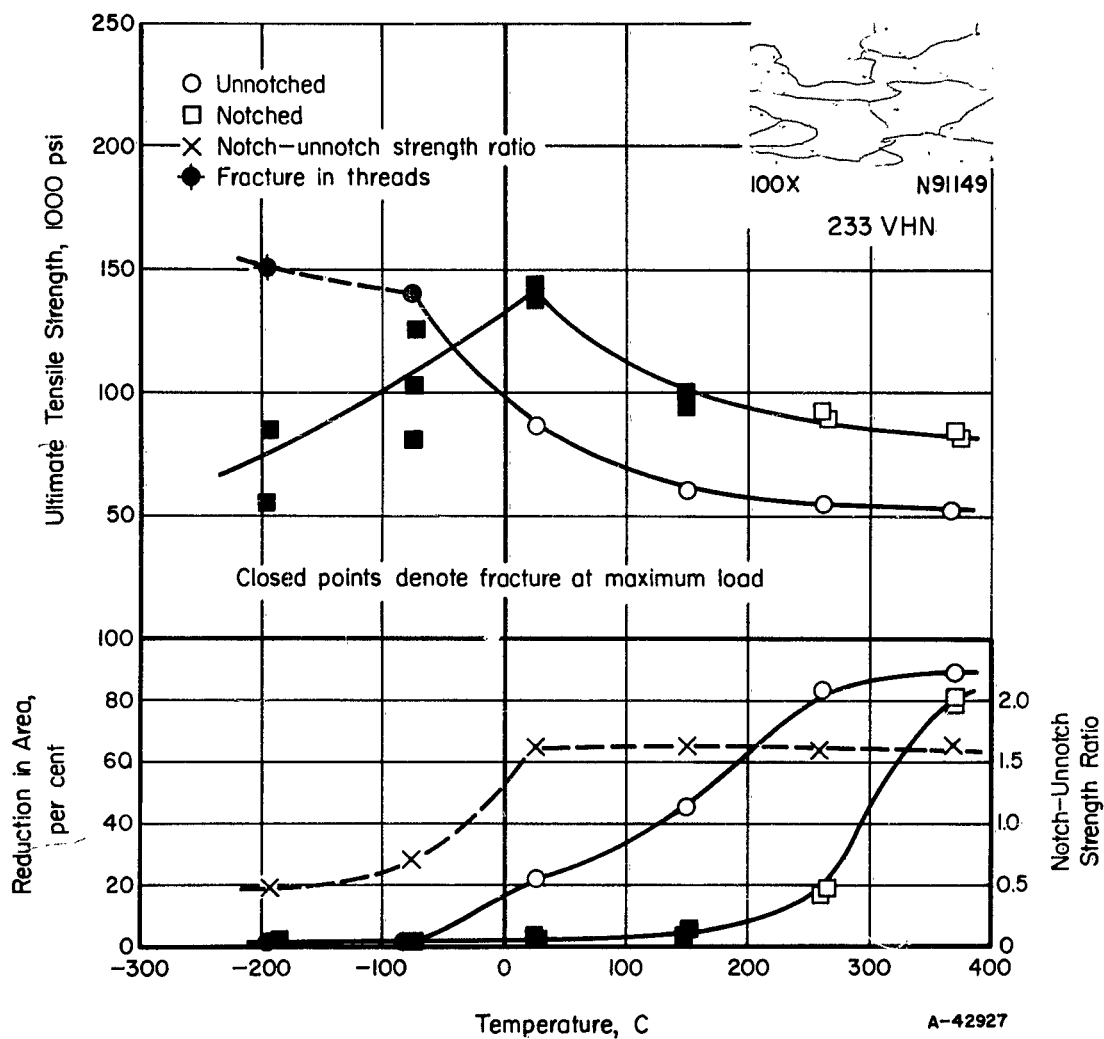


FIGURE 11. TENSILE AND NOTCH TENSILE PROPERTIES OF WROUGHT (25 PER CENT) Mo-0.5Ti

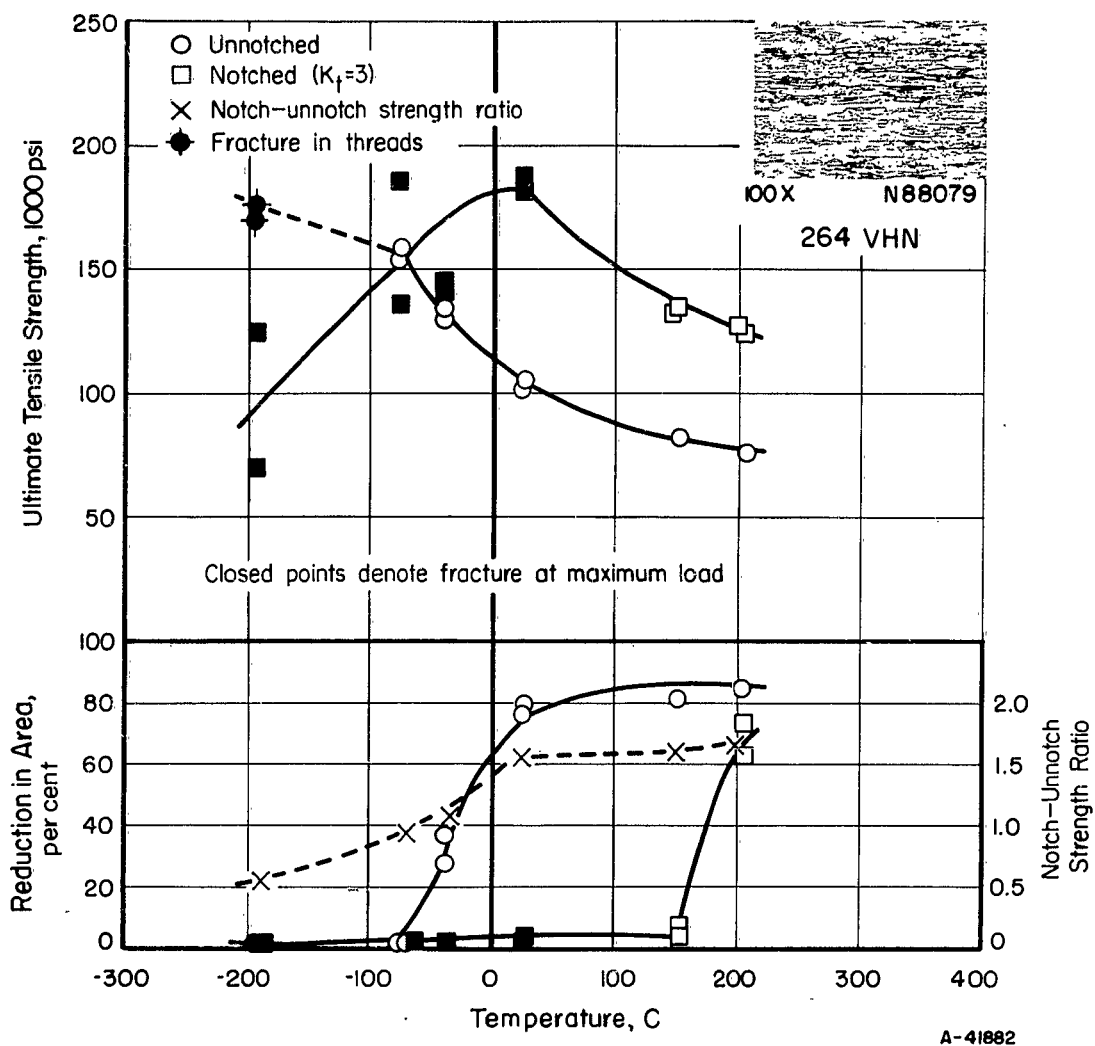


FIGURE 12. TENSILE AND NOTCH TENSILE PROPERTIES OF WROUGHT (68 PER CENT) Mo-0.5Ti

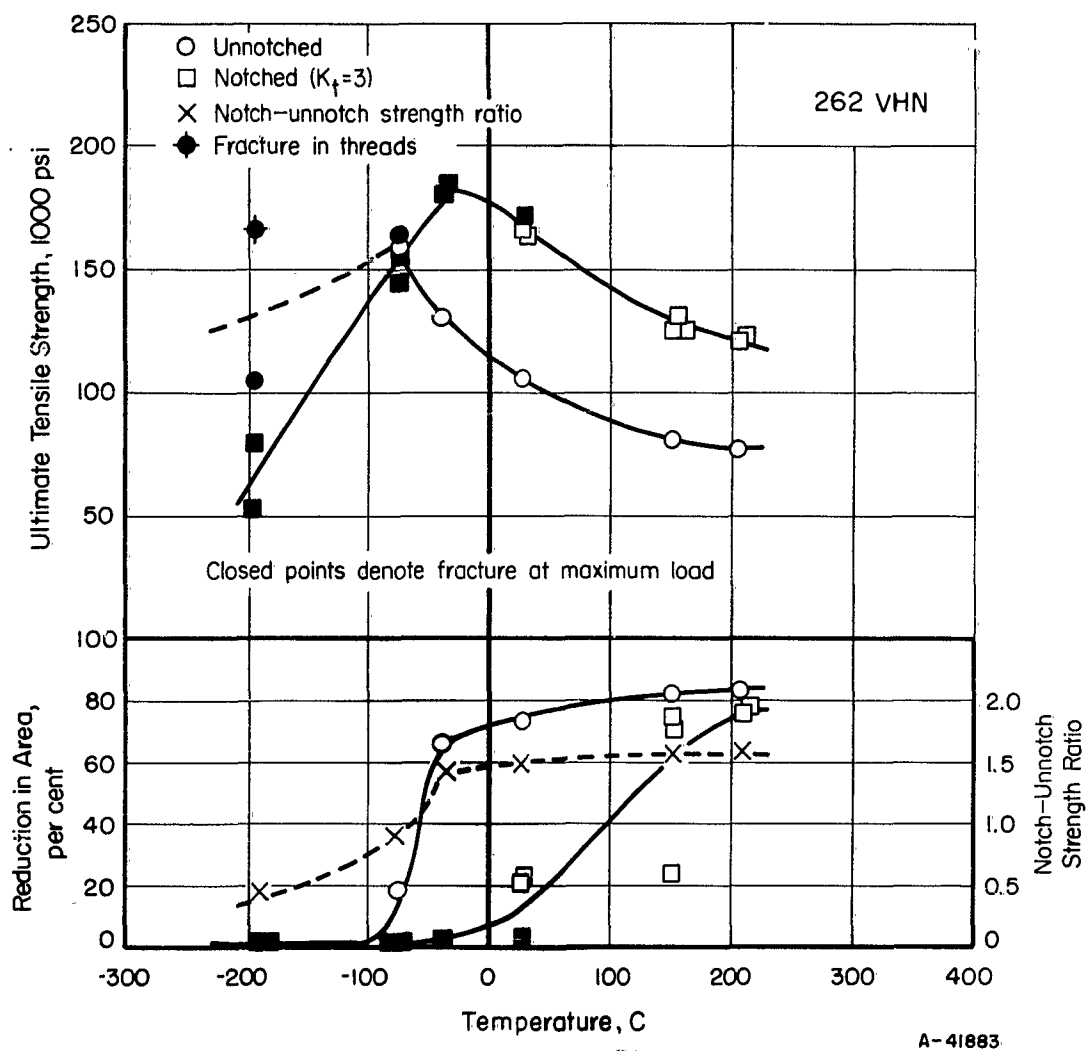


FIGURE 13. TENSILE AND NOTCH TENSILE PROPERTIES OF WROUGHT (68 PER CENT) STRESS-RELIEVED (1/2 HR AT 540 C) Mo-0.5Ti

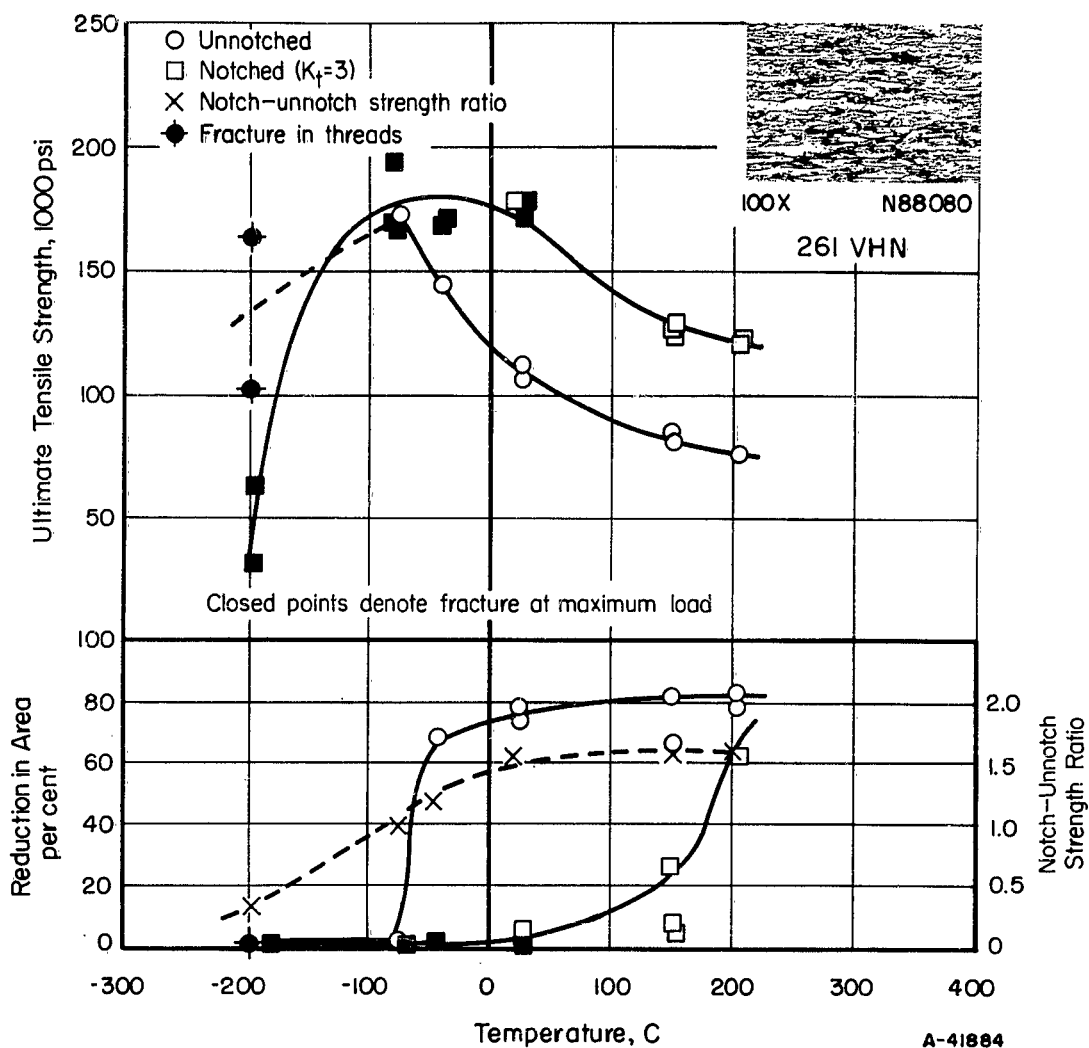


FIGURE 14. TENSILE AND NOTCH TENSILE PROPERTIES OF WROUGHT (68 PER CENT) STRESS-RELIEVED (1/2 HR AT 1000 C) Mo-0.5Ti

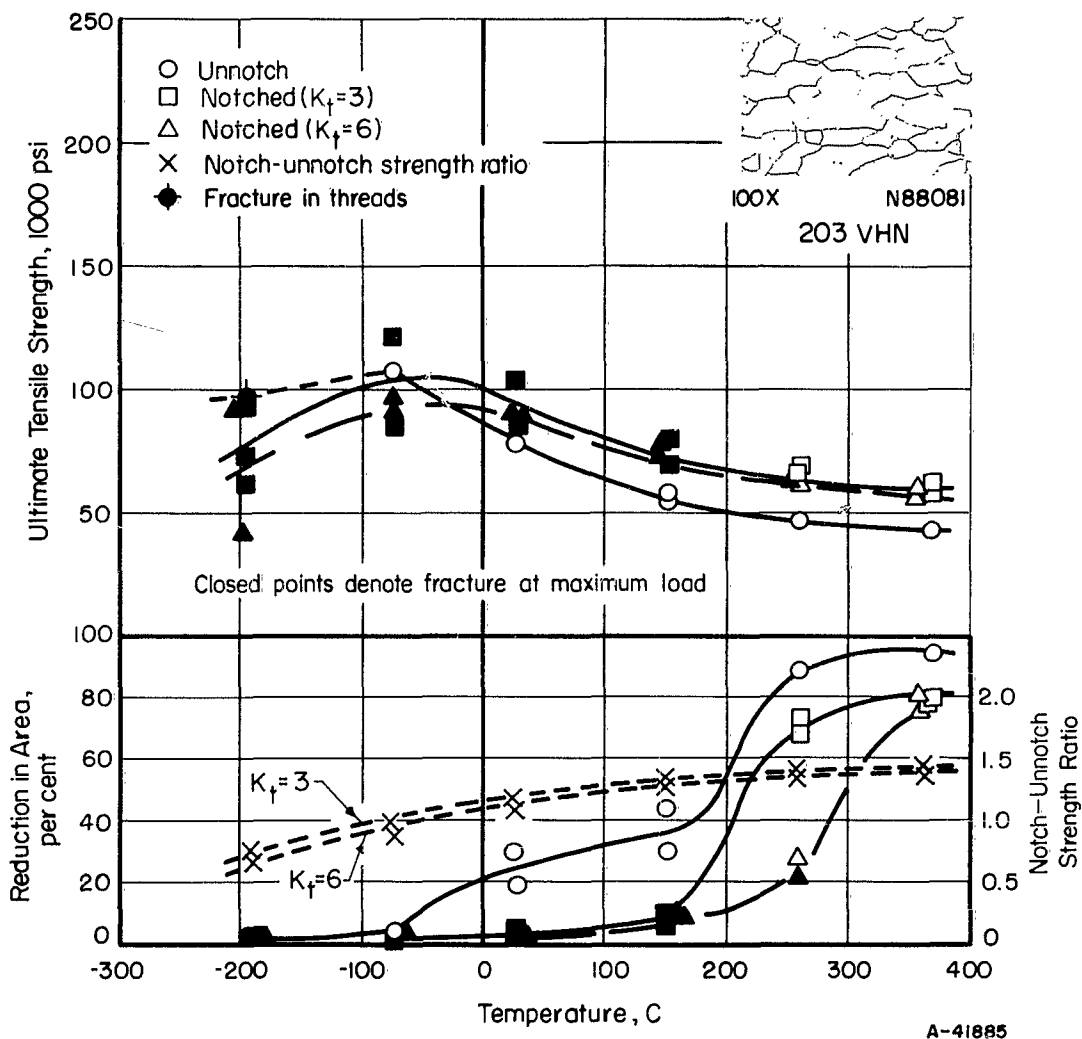


FIGURE 15. TENSILE AND NOTCH TENSILE PROPERTIES OF SMALL-GRAINED RECRYSTALLIZED (1/2 HR AT 1590 C) Mo-0.5Ti

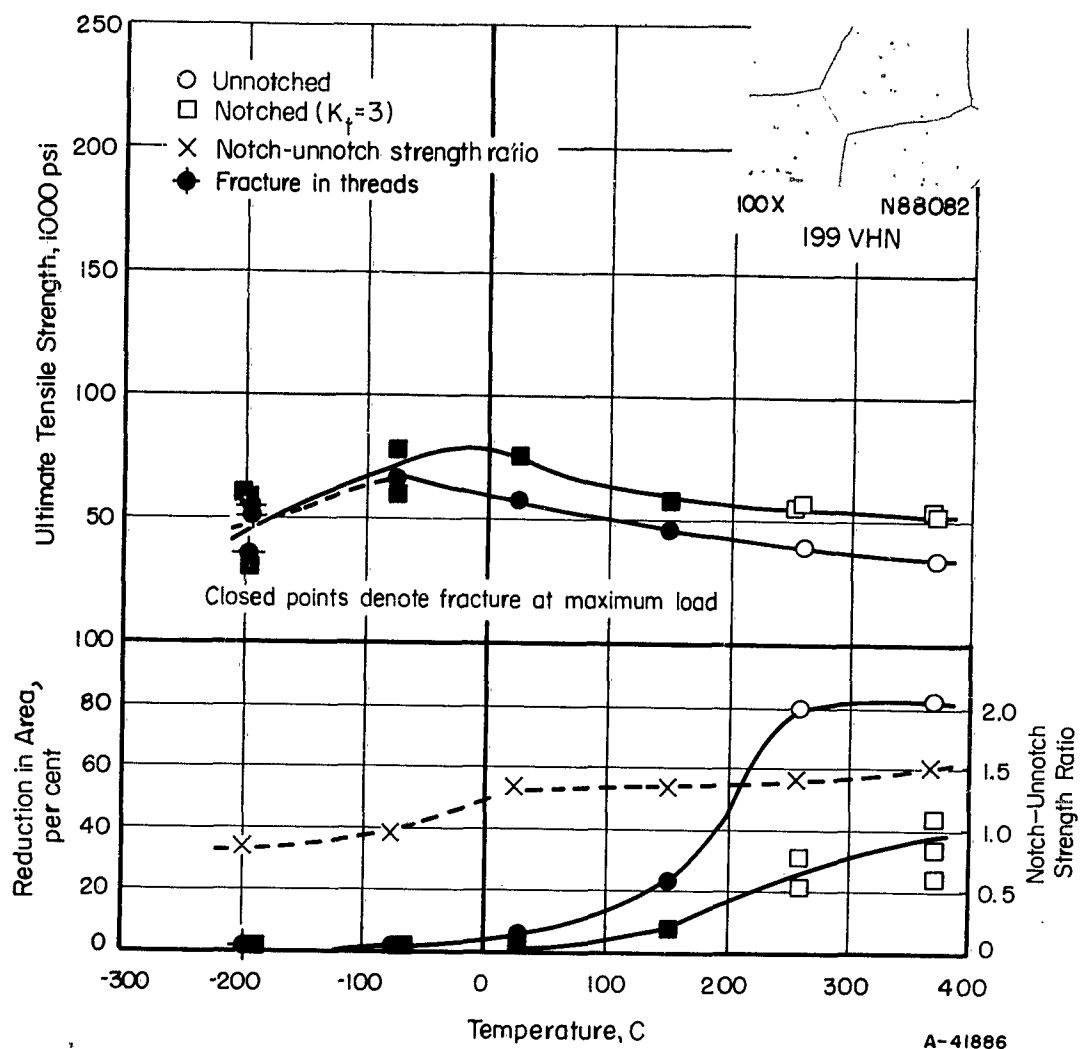


FIGURE 16. TENSILE AND NOTCH TENSILE PROPERTIES OF MEDIUM-GRAINED RECRYSTALLIZED (1/2 HR AT 1930 C) Mo-0.5Ti

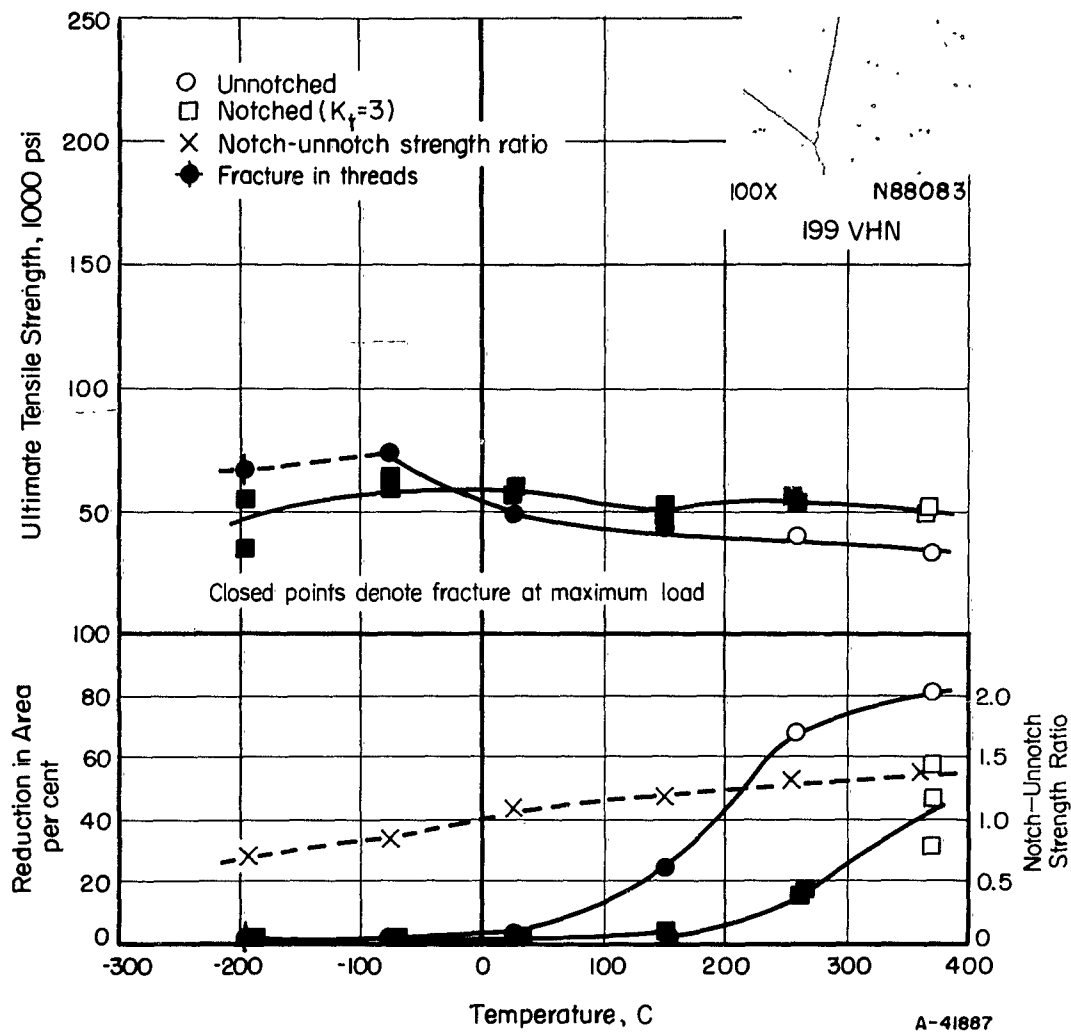
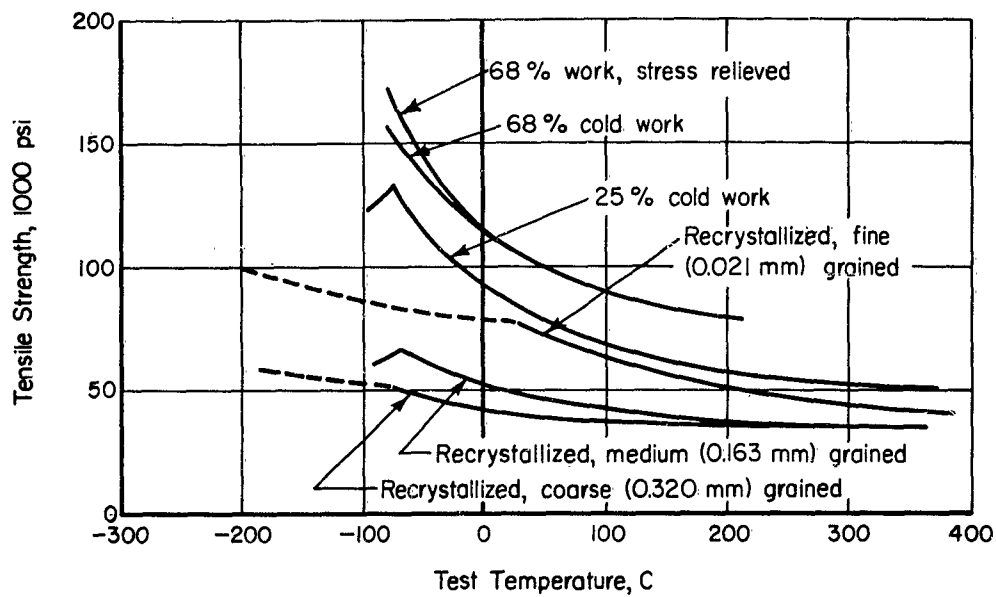
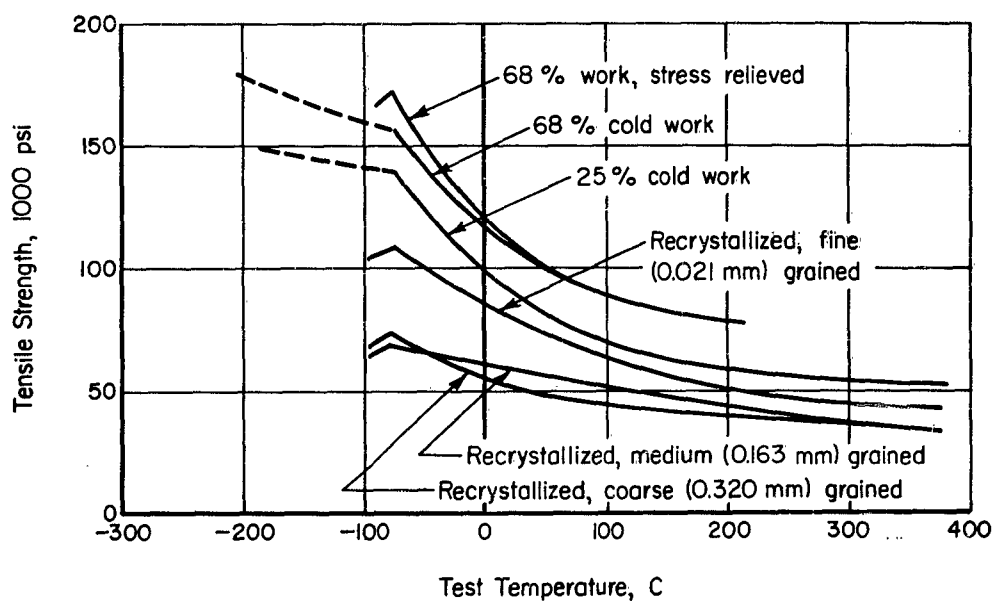


FIGURE 17. TENSILE AND NOTCH TENSILE PROPERTIES OF LARGE-GRAINED RECRYSTALLIZED (1/2 HR AT 2090 C) Mo-0.5Ti



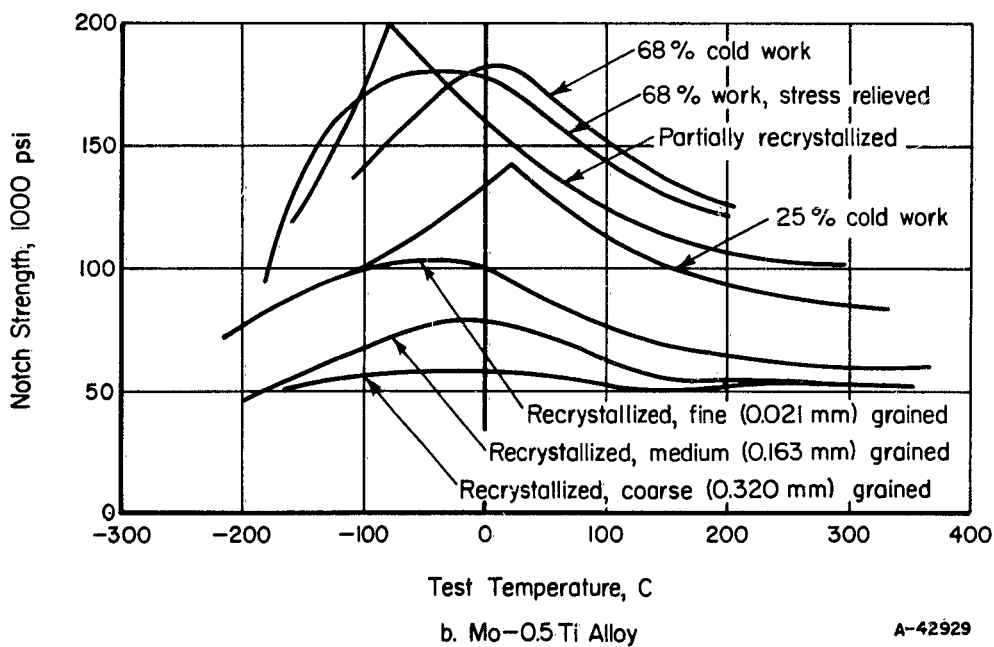
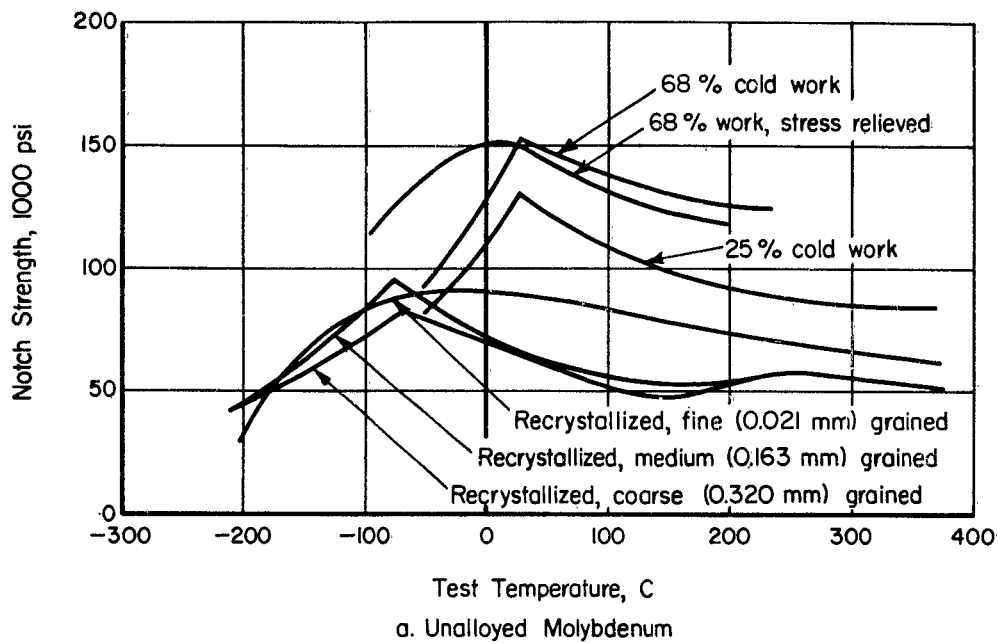
a. Unalloyed Molybdenum



b. Mo-0.5Ti Alloy

A-42928

FIGURE 18. EFFECTS OF STRUCTURE ON UNNOTCH TENSILE STRENGTH



A-42929

FIGURE 19. EFFECT OF STRUCTURE ON NOTCH TENSILE STRENGTH

to the fine-grained structure (single phase) resulted in notch properties that did not allow definition of specific peak temperatures, but rather, a broad range of temperature through which the notch strength gradually deteriorated was indicated. (Testing at closer temperature increments within the critical ranges might have improved definition of behavior.) Nevertheless, the parameters shown suggest that the thermal treatments lower the peak notch-strength temperature, with greater decreases effected by more severe heat-treatment conditions.

Properties of the medium- and coarse-grained molybdenum (which contained second-phase particles) again defined the characteristic sharp peak temperature, and this occurred at about -75 C. Thus, maximum temperatures for fracture instability in notched specimens varies with structural condition as follows:

Condition	Fracture Instability Temperature, C
Fibered	25
Stress relieved	10
Recrystallized, fine grain	-25
Recrystallized, coarse grain	-75

In the fibered condition, molybdenum becomes very sensitive to the effects of notches at temperatures lower than about 25 C, where behavior is unpredictable from the design standpoint. It is further apparent that, with increasing severity of heat treatment, the temperature for fracture instability of notched specimens more closely approaches that of smooth molybdenum specimens. Thus, notches exhibit severe effects at higher temperatures in wrought molybdenum than in recrystallized molybdenum. In fact, the unnotch strength and notch strength properties of recrystallized molybdenum indicate the initiation of fracture instability at about the same threshold temperature, and in either case, behavior at lower temperatures is unreliable. In this sense, it appears that recrystallized molybdenum is not sensitive to the effects of macroscopic mechanical notches. However, the generally lower rate of increase in tensile strength with decreasing temperature at temperatures above the peak-strength temperature for recrystallized structures (particularly the coarser grained structures) compared with fibered structures warns that a minor, noncatastrophic degree of fracture instability may be present. Thus, behavior of recrystallized structures may not be so predictable as indicated by comparison of notch vs unnotch properties.*

The notch strength parameters for Mo-0.5Ti also exhibit fairly sharp peaks for as-worked material. The temperature range over which notch strength deteriorated was very broad for stress relieved and all recrystallized structures, and no distinct threshold temperature for fracture instability could be defined. This, coupled with a gradual, continuous decline in the notch-unnotch strength ratio, made assessment of notch sensitivity of recrystallized Mo-0.5Ti uncertain. Perhaps most meaningful was the observation that full (theoretical) notch strengthening was not observed in any recrystallized Mo-0.5Ti structure below about 100 to 200 C, as shown in Figure 20. As illustrated, deviation from the expected notch strengthening factor of 1.5 increased as grain size increased. This behavior suggests a degree of fracture instability which may be aggravated by the presence of notches in recrystallized structures at all lower temperatures.

*This viewpoint is reinforced by prior investigations⁽¹⁾ which showed fine-grained recrystallized molybdenum to be very notch-sensitive at temperatures less than 60 C, compared with about 0 C in the present work.

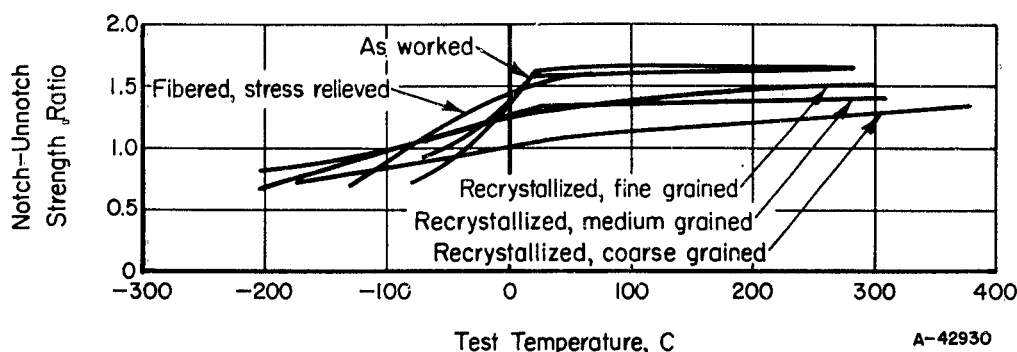


FIGURE 20. EFFECT OF STRUCTURE ON NOTCH-UNNOTCH STRENGTH RATIO OF Mo-0.5Ti ALLOY

The curve labelled "partially recrystallized" for the Mo-0.5Ti alloy in Figure 19b resulted when material identified as unalloyed molybdenum was annealed to produce a fine-grained recrystallized structure. The very unusual strength behavior, coupled with the observed microstructure (only a few equiaxed grains in a fibered matrix) demanded chemical analysis, whereupon it was determined that the material was actually Mo-0.5Ti. This bastard condition resulted in unusual stability and relatively high values for notch strength at temperatures down to -75 C, in which respect it was superior to either fully fibered or fully recrystallized structures.

The notch strength versus temperature curves of medium- and coarse-grained structures of both molybdenum and Mo-0.5Ti exhibited minima at 150 C. The reason for this consistent behavior was not determined.

Effects of structure on the low-temperature unnotch ductility behavior of both materials are shown in Figure 21. The fine-grained recrystallized structures displayed a quite well-defined step in the ductility versus temperature curve. Consideration of elongation data (Appendix I) associated with the reduction-in-area values indicates that, although the fine-grained structures are able to sustain appreciable uniform deformation at room temperature, their capacity for deformation under conditions involving triaxial stresses (necking) is inhibited at temperatures less than about 150 C. Thus, the lower plateau describes uniform reduction in area. Increases above this value result primarily from necking. Light degrees of working eliminated the step in the ductility curve without much effect on the range of temperature over which ductile-to-brittle transition occurred. The higher degree of working substantially lowered the upper threshold temperature for transition behavior, and stress-relief anneals exhibited slight additional benefits. Medium- and coarse-grained recrystallized structures exhibited relatively high transition-temperature ranges, but the upper threshold temperatures were not very different from that of the fine-grained recrystallized structure (no step was observed in their curves).

Notch ductility behavior, illustrated in Figure 22, reflected the same general effects of structure - properties of fine-grained (and lightly worked) structures were intermediate between the superior heavily worked and stress-relieved structures and

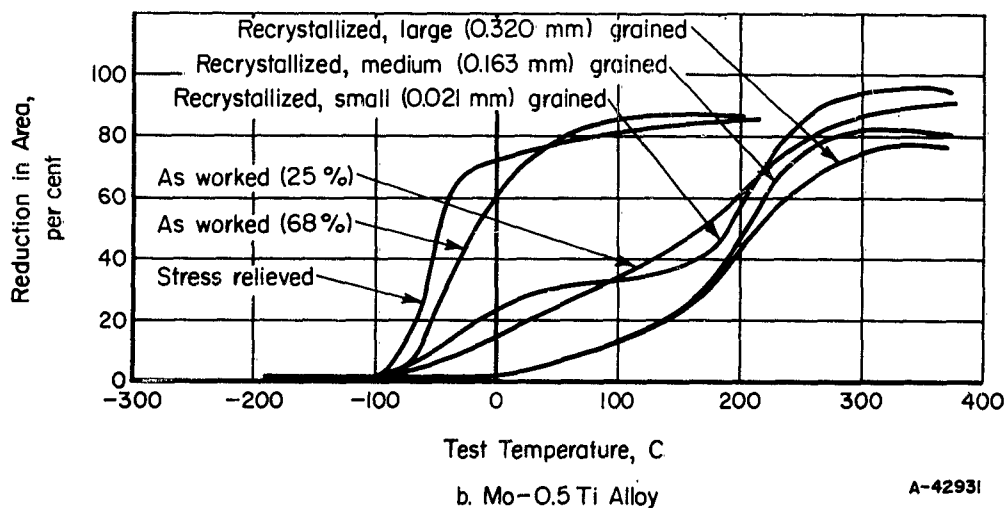
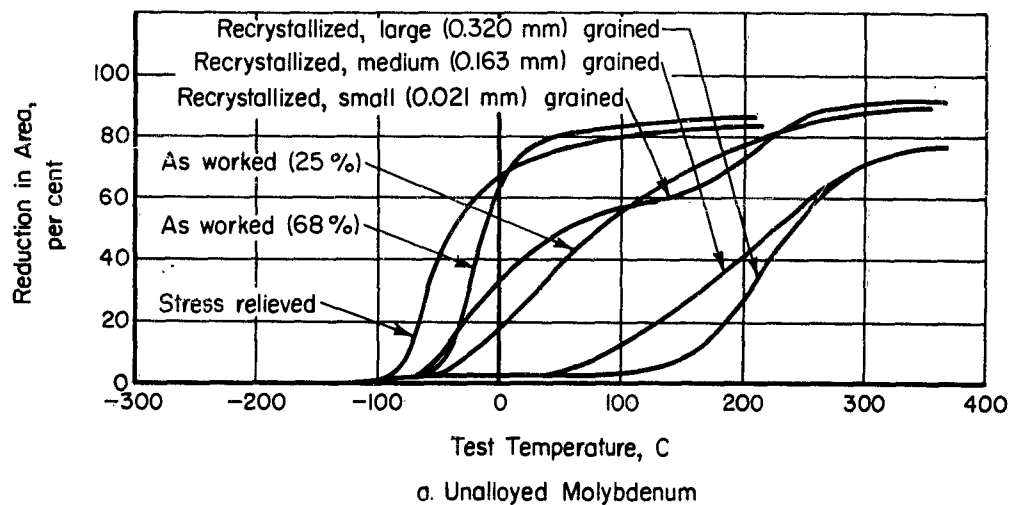
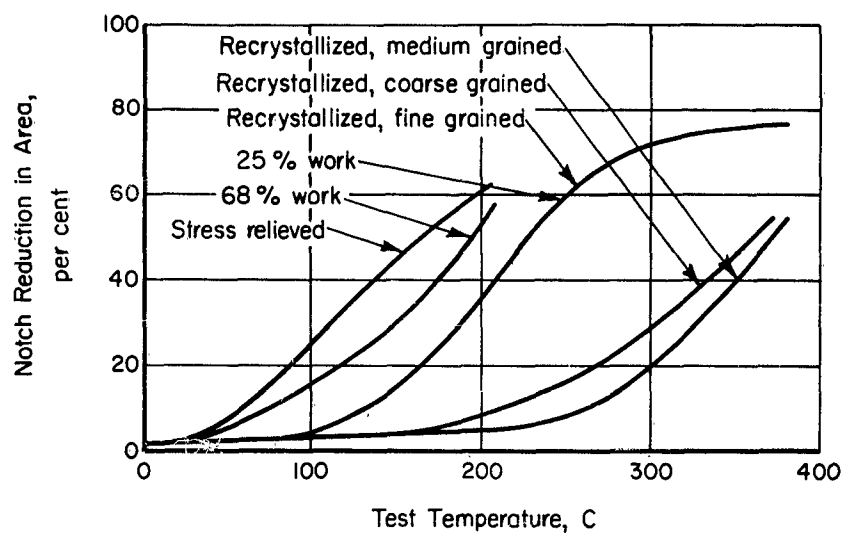
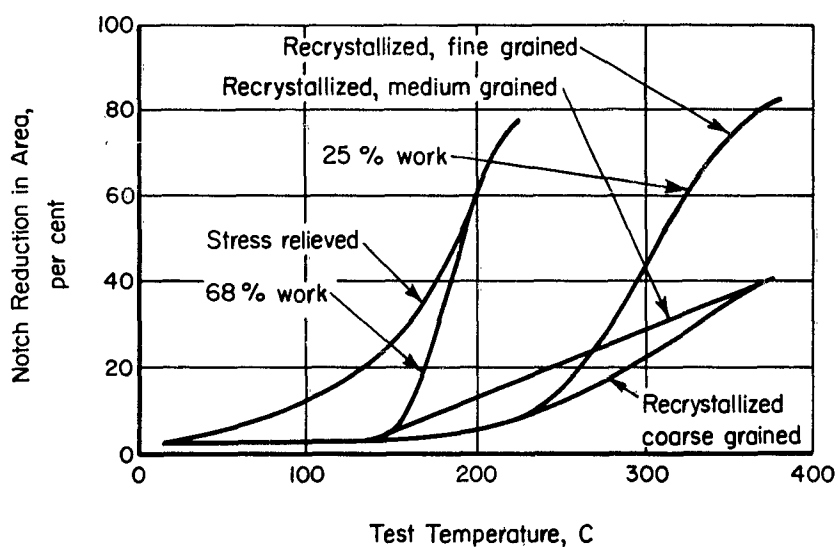


FIGURE 21. EFFECT OF STRUCTURE ON THE TRANSITION CHARACTERISTICS OF MOLYBDENUM AND Mo-0.5Ti



a. Unalloyed Molybdenum



b. Mo-0.5 Ti Alloy

A-42932

FIGURE 22. EFFECT OF STRUCTURE ON NOTCH DUCTILITY

the less desirable coarser grained recrystallized structures. The notch ductility curve for the fine-grained structure did not exhibit the step observed in the unnotch ductility curve (appreciable uniform elongation is impossible in notched specimens). The notch ductility curves were generally displaced to temperatures from 100 to 200 C higher than their respective unnotch ductility curves.

Effects of metallurgical structure upon ductile-to-brittle transition behavior, using as a general criterion the temperature at which reduction in area decreased to one-half of the maximum value, are summarized in Table 3. These data again demonstrate:

- (1) Beneficial effects of fibered structures
- (2) Additional benefits resulting from stress relief
- (3) Superiority of fine-grained relative to coarse-grained recrystallized structures.

The difference between notch and unnotch ductility transition temperatures is less for the recrystallized structures than is the general case for wrought structures. This substantiates the effects shown by the strength curves, where closer conformance of notch to unnotch properties in recrystallized material relative to fibered structures was indicated.

An additional observation pertinent to the effect of notches on low-temperature behavior is the maximum temperature at which fracture occurred at maximum load. This behavior (fracture at maximum load) is associated with loss of the ability to deform when the stress distribution in the area undergoing deformation changes from an essentially uniaxial to a multiaxial pattern. This, then, is the same type, but probably less intense, stress distribution existing at the root of a notch in notched specimens. Minimum temperatures at which necking (deformation under multiaxial stress) was observed during tensile testing are recorded below:

Condition	Minimum Temperature at Which Necking Was Observed, C			
	Mo		Mo-0.5Ti	
	Unnotched	Notched	Unnotched	Notched
25 per cent work	25	150	25	260
68 per cent work	-40	150	-40	150
68 per cent work, stress relieved	-40	25	-40	25
Recrystallized, fine grain	25	150	25	260
Recrystallized, medium grain	150	370	150	260
Recrystallized, coarse grain	260	370	260	260

Although the structures were altered in most cases by substantial uniform deformation prior to the onset of deformation instability (necking), definite effects attributable to initial metallurgical structure were retained. These data strongly indicate that the more heavily worked structures retain insensitivity to the effects of notches at lower temperatures than recrystallized (or lightly worked) structures. Coarse-grained recrystallized structures are particularly poor in this regard. Pre-existing notches

TABLE 3. EFFECT OF HEAT TREATMENT ON TRANSITION
TEMPERATURE AND NOTCH SENSITIVITY

Condition	Ductility Transition Temperature, C		Difference Between Notch and Unnotched Ductility Transition Temperature, $\Delta^{\circ}\text{C}$
	Unnotched	Notched ($K_t = 3$)	
<u>Molybdenum</u>			
As wrought (25%) (4) ^(a)	75	200	125
As wrought (68%) (5)	-25	175	200
Low temp, stress relieved (6)	-50	150	200
High temp, stress relieved (7)	-50	125	175
Recrystallized (small grain) (8)	50	200	150
Recrystallized (medium grain) (9)	200	325	125
Recrystallized (large grain) (10)	225	325	100
<u>Mo-0.5Ti</u>			
As wrought (25%) (11)	150	300	150
As wrought (68%) (12)	-25	175	200
Low temp, stress relieved (13)	-50	100	150
High temp, stress relieved (14)	-50	175	225
Recrystallized (small grain) (15)	50 ^(b)	200	150
Recrystallized (medium grain) (16)	200	325	125
Recrystallized (large grain) (17)	200	325	125

(a) Figures from which data were obtained.

(b) Approximate minimum of plateau.

appear to increase the "notch-sensitivity" temperature, although the significance of this observation is obscure.

Examination of all data shows that the temperatures at which the notch and unnotch strengths of heavily fibered (and stress relieved) structures begin to decrease coincide with the maximum temperatures at which completely brittle fractures are obtained. Thus, the onset of fracture instability is coincident with complete loss of ductility in both notched and unnotched specimens. Because notch transition temperatures are higher than unnotch transition temperatures, the occurrence of notch sensitivity at temperatures higher than those required for complete loss of unnotch ductility is axiomatic. Coarse-grained recrystallized structures, however, continue to display increases in strength, although slight, with decreasing temperatures well below the maximum temperature for nil ductility. This is true for both unnotched and notched specimens. Intermediate structures (lightly worked, fine grained and medium grained recrystallized) display intermediate effects - strengths continue to increase at temperatures somewhat below the maxima for nil ductility.

Examination of fracture surfaces of recrystallized specimens revealed that fracture generally originated at a grain boundary near the surface (or near the notch root in notched specimens), and thereafter propagated mainly by transgranular cleavage.

"River" markings on cleavage planes were traced back to the grain-boundary facet shown in the right side of Figure 23a. The dark, acicular tracings are probably second-phase particles in the grain boundary. Figure 23b illustrates the point of fracture initiation in a notched specimen. Clearly, fracture started at a point slightly removed from the notch root, probably at a precipitate particle in a grain boundary below the exposed cleavage plane.

It is apparent that grain boundaries are a strong controlling factor in the failure of recrystallized structures. The data show that grain boundaries initiate cleavage fractures at much lower stress levels than are required in the absence of the regular grain-boundary network, regardless of specimen design. In fibered specimens, notch sensitivity arises from inhibition of the propensity of the material to flow, resulting in cleavage fractures at high stress. Recrystallized specimens, with readily available cleavage-fracture initiation sites, do not require the stress pattern characteristic of notches to achieve the detrimental effects of cleavage fracture. Thus, machined notches might be expected to have a far less pronounced effect in recrystallized than in wrought material. This reasoning is supported by observations of the notch-unnotch strength ratio curves which reflect the more pronounced decrease in notch strength with wrought material, and show incomplete notch strengthening of recrystallized material.

Grain boundaries may also largely account for the difference in transition characteristics of wrought and recrystallized structures. Recrystallization introduces a regular grain-boundary network to act as favored sites for cleavage-fracture initiation. Therefore, cleavage fractures predominate at higher temperatures in recrystallized structures, resulting in lower ductilities and higher transition temperatures.

Thus, although working did not appear to improve the notch-sensitivity behavior of molybdenum or Mo-0.5Ti as judged by the notch-unnotch strength ratio curve, probably more important than the effects of notches are the apparent effects of grain boundaries, and their pre-emptive action on the effects of notches in recrystallized materials.



2000X

N90334

a.



200X

b.

FIGURE 23. BRITTLE FRACTURE SURFACE OF MOLYBDENUM SPECIMENS

Effect of Notch Acuity

Figures 8 and 15 for small-grained molybdenum and Mo-0.5Ti show no significant effect of notch acuity. This also may be attributed to the controlling effect grain boundaries have on fracture, masking any effects of increased notch severity.

Conclusions

Studies of the effects of metallurgical structure upon the low-temperature behavior of molybdenum and Mo-0.5Ti alloy resulted in the following conclusions:

- (1) Molybdenum and Mo-0.5Ti alloy exhibit similar low-temperature behavior.
- (2) The ductility transition temperature of fibered molybdenum or Mo-0.5Ti is roughly 200 C lower than that of recrystallized material. The transition temperature of coarse-grained material is about 100 C higher than that of fine-grained material.
- (3) Fibered (stress relieved) molybdenum and Mo-0.5Ti become markedly notch sensitive at temperatures lower than about 0 C.
- (4) The notch properties of recrystallized molybdenum and Mo-0.5Ti deteriorate gradually with decreasing temperature below about 300 C, but these materials are not markedly notch sensitive at temperatures as low as -75 C. However, several observations (lower-than-expected low-temperature strength, lack of necking at temperatures less than 150 C, etc.) suggest unreliable behavior in the recrystallized condition at temperatures lower than about 150 C.

FRACTURE-TOUGHNESS STUDIES*

The fracture-mechanics approach to measuring fracture toughness, as developed by G. R. Irwin, is closely related to the classical work of Griffith in 1920 on the fracture of glass.⁽³⁾ Basically, Griffith calculated two energy terms: (1) the stored elastic energy released by a body as a crack progressed, and (2) the energy required to form new surface area. When the rate (with respect to crack length) of the former exceeds that of the latter, the crack becomes unstable and spontaneous fracture occurs. Griffith's calculations of energy release were based upon an elastic stress analysis by Inglis⁽⁴⁾ for an infinitely wide plate of unit thickness containing a through crack of length 2a, normal to the applied tension, σ . The rate of release of stored elastic energy, U, with respect to crack length, 2a, was shown to be:

$$\frac{dU}{d(2a)} = \frac{\pi\sigma^2 a}{E} \quad , \quad (1)$$

*Authored by C. W. Marschall and F. C. Holden.

where E is Young's modulus. Since the area of new surface increases linearly with crack length, the rate at which total surface energy, H, changes with crack length is

$$\frac{dH}{d(2a)} = 2\gamma \text{ (for unit thickness) } , \quad (2)$$

where γ is the surface energy per unit area. Setting Equation (1) equal to Equation (2) then defines the stress beyond which spontaneous fracture will occur for any crack length, $2a$:

$$\sigma_f^2 = \frac{2\gamma E}{\pi a} . \quad (3)$$

Griffith's experiments on glass provided reasonable confirmation of Equation (3).

In attempting to apply Griffith's concepts to fracture of metals, two major difficulties are encountered. First, elastic stress analyses may no longer be rigorously applied, because of the plastic yielding associated with the high stresses near flaws. Second, the energy required to form new surfaces must now include the work of plastic deformation. In most cases, this term is sufficiently large that the surface energy term may be neglected. In Irwin's treatment of fracture mechanics, the first complication is sidestepped by assuming that an elastic stress analysis is adequate if the plastic deformation is restricted to a small region near the crack tip. Thus, Equation (1) remains applicable. Equation (2), however, is modified to take into account the energy of plastic deformation, P:

$$\frac{dP}{d(2a)} = 2p , \quad (4)$$

where p is the plastic deformation energy per unit area of new fracture surface. Combining Equations (1) and (4) gives a Griffith-type expression relating fracture stress, σ_f , and crack length:

$$\sigma_f^2 = \frac{2pE}{\pi a} . \quad (5)$$

Irwin designates the strain-energy release rate, $\frac{dU}{d(2a)}$, as G, and since this is set equal to $\frac{dP}{d(2a)}$ at crack instability, we can write

$$G_c = \text{critical strain-energy release rate} = 2p .$$

Equation (5) can now be rewritten as

$$\sigma_f^2 = \frac{G_c E}{\pi a} . \quad (6)$$

According to Equation (6), if G_c can be evaluated, then it should be possible to predict the fracture stress from knowledge of the crack length and Young's modulus. The method of evaluation is merely to perform a tension test on a flat specimen containing a central transverse crack, noting the stress and crack length at the moment of crack

instability. Inserting these values into Equation (6) yields a value for G_c . Experience has shown that G_c values obtained in this way are not constant for a given material, except where extreme brittleness is displayed. In materials displaying considerable ductility, as evidenced by shear-lip formation during fracture, G_c is found to vary with specimen thickness and ratio of crack length to specimen width. Hence, in reporting G_c results, it is necessary always to report these dimensions.

Recently, Irwin has modified Equation (6) to correct partially for plastic flow at the tip of the crack. As a first approximation, he assumes that the influence of the plastic zone is equivalent to an added crack length, r_y , the size of which may be estimated by knowledge of the applied tensile stress, the yield stress, and the stress distribution in the plane of the crack. From elastic-stress analysis, the variation in stress, σ , ahead of the crack as a function of distance, r , from the crack tip can be expressed as:

$$\sigma = \sqrt{\frac{G_c E}{2\pi r}} \quad (7)$$

When plastic flow occurs, σ equals the yield stress, σ_y , and, at crack instability, Equation (7) becomes:

$$r_y = \frac{G_c E}{2\pi\sigma_y^2} \quad (8)$$

By adding the additional crack length to a in Equation (6), we obtain:

$$\sigma_f^2 = \frac{G_c E}{\pi(a + r_y)} = \frac{G_c E}{\pi\left(a + \frac{G_c E}{2\pi\sigma_y^2}\right)}$$

Rearranging and solving for G_c , this becomes:

$$G_c = \frac{\pi\sigma_f^2 a}{E\left[1 - \frac{1}{2}\left(\frac{\sigma_f}{\sigma_y}\right)^2\right]} \quad (9)$$

Notice that if the fracture stress, σ_f , is a small fraction of the yield stress, σ_y , Equation (9) reduces to Equation (6).

Up to this point, the discussion has centered around the energy term, G_c , as a measure of fracture toughness of a material. More recently, the ASTM Committee on Fracture Testing of High Strength Materials has recommended use of the term K_{Ic} , called the critical-stress-intensity factor. It is equal to the square root of the product of G_c and Young's modulus. Hence, Equation (9) may be written as:

$$K_{Ic}^2 = \frac{\pi\sigma_f^2 a}{\left[1 - \frac{1}{2}\left(\frac{\sigma_f}{\sigma_y}\right)^2\right]} \quad (10)$$

In a flat center-cracked tension specimen, K increases in proportion to the applied stress and the square root of the half-crack length, reaching its critical value, K_C , at the onset of crack instability. If one assumes an infinitely wide specimen carrying a tensile stress equal to the yield stress, then the critical crack length, $2a_c$, is [from Equation (10)]:

$$2a_c = \frac{1}{\pi} \left(\frac{K_C}{\sigma_y} \right)^2 .$$

This is called the critical-crack index of the material and is useful for comparing different materials stressed to their yield strengths. Presumably, cracks larger than this will lead to failure at applied stresses below the yield strength. For specimens of finite width, W , Equation (10) may be modified to allow determination of K_C as follows:

$$K_C^2 = \frac{\sigma_f^2}{1 - 1/2 \left(\frac{\sigma_f}{\sigma_y} \right)^2} W \tan \left(\frac{\pi a}{W} \right) . \quad (11)$$

As mentioned earlier, G_C and K_C do not have single values for a given material. In general, K_C will decrease as specimen thickness is increased, until it reaches a minimum value when it is independent of further thickness increase. This variation in K_C is associated with a change in fracture mode from full shear to transverse. When the fracture is entirely in the transverse mode, K_C has its minimum value and is referred to as K_{IC} , the plane-strain fracture toughness. According to Irwin, K_{IC} governs the propagation of small elliptical surface cracks through a sheet or plate, since such cracks extend in a transverse mode. Once the crack extends through the thickness, K_C governs further crack growth. If K_C for the thickness in question is not much greater than K_{IC} , fracture should proceed with little increase in load. If, however, it is considerably greater than K_{IC} , due to an appreciable percentage of shear-lip formation, much higher loads should be required to cause complete fracturing.

Experimental determination of K_{IC} can, in principle, be done wherever fracture occurs in the transverse mode. Thus, flat tensile specimens containing surface cracks or cylindrical specimens containing circumferential cracks have frequently been employed. Recently, it has been observed that flat tensile specimens containing through-the-thickness central cracks (as are used to determine K_C) may also yield K_{IC} data if complete fracture is preceded by a small burst of crack growth under plane-strain conditions. All that is required is measurement of the load at which this "pop-in" occurs. Various means have been used to detect pop-in, including electrical resistance, compliance gage, and sound-detection techniques. There is mounting evidence that K_{IC} for a given material and test temperature does not vary with thickness or specimen geometry and thus may more closely approach a material property than does K_C .

In its present state of development, fracture mechanics has several limitations. First, it is based upon elastic-strain analysis and thus cannot be expected to apply rigorously where appreciable plastic deformation occurs prior to fracture. Second, although, in principle, fracture mechanics can predict the critical crack size for complete fracture at a given level of stress, it does not predict whether a smaller crack will grow to the critical size during loading.

Experimental Procedures

Specimen Preparation

Two types of specimens, smooth and notched, were used in this investigation. They are shown in Figure 24. Specimens of molybdenum were prepared with the axis of the applied stress parallel and perpendicular to the rolling direction. Other materials were tested parallel to the rolling direction only. The main purpose of testing the smooth specimens was to determine an approximate value for the yield strength at several different temperatures, to facilitate making the plastic-zone correction in K_C calculations as discussed previously. Accordingly, only three smooth specimens were made for each material condition.

The notched specimen is based upon recommendations of the ASTM Committee on Fracture Testing of High Strength Materials. Specifically, the ASTM Committee recommends this specimen for testing materials having strength-to-density ratios in excess of 700,000 psi per pound per cubic inch. Although the refractory metals do not fall within this category, it was felt that meaningful fracture-toughness data could be obtained with these specimens if testing was carried out within the ductile-brittle transition range of temperatures.

When testing at temperatures where specimens were ductile, it was necessary to clamp stiffening plates to the loading region of the specimen to better distribute the load and minimize plastic deformation in the vicinity of the loading pins.

Originally, it was planned to introduce central cracks in each of the materials by tension-tension fatigue loading of specimens which had previously been slotted with a jeweler's saw. This method was found to work very well for tantalum and columbium. By applying a maximum net-section stress of approximately 30,000 psi, fatigue cracks could be grown from the initial 0.6-inch saw cut to the desired length of 0.7 inch in about 5 to 10 minutes at a cycling speed of 1750 cycles per minute.

With molybdenum, fatigue cracks could frequently be initiated, but control of their growth was difficult. Repeated attempts with both longitudinal and transverse specimens revealed that the short cracks either remained stationary or traversed the specimen in one loading cycle. An attempt was made to improve the control of fatigue cracking in transverse molybdenum specimens by heating the specimen center section to 200 F during fatigue cycling. After 5000 cycles at 40,000 psi, no cracks were detected. After about 13,000 cycles, the specimen failed through the center section with evidence of only very slight fatigue cracking at the tips of the saw cut. No further attempts were made to produce fatigue cracks in molybdenum at elevated temperatures.

Attempts were also made to produce cracks in molybdenum by forcing a tapered punch into a drilled hole slotted at opposite ends of a diameter with a jeweler's saw. This produced cracks only in the surface of the sheet specimens.

Because of the lack of success in introducing central cracks in molybdenum specimens by cyclic loading, it was decided to prepare the notches mechanically. The procedure employed was as follows:

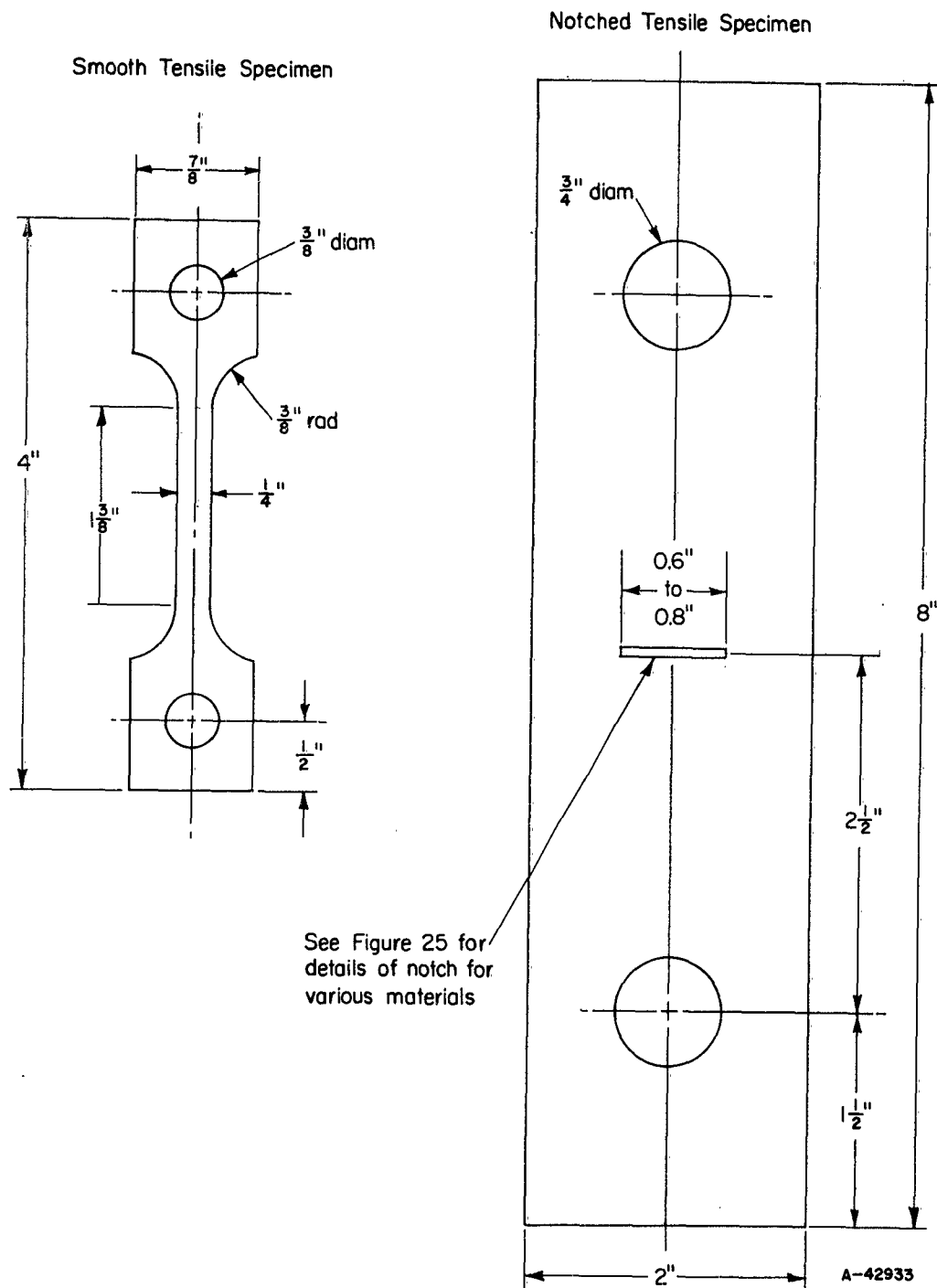


FIGURE 24. DESIGN OF SMOOTH AND NOTCHED TENSILE SPECIMENS

- (1) Drill several overlapping 1/16-inch-diameter holes to provide a slot large enough for a hacksaw blade.
- (2) Extend the slot equally from both sides of the drilled hole with a hacksaw blade to a length of approximately 0.7 inch.
- (3) Extend the slot at each end another few hundredths of an inch with a thin (0.005 to 0.009 inch) hardened steel file.
- (4) Sharpen the ends of the slot, first with a thin file that had been sharpened to a fine point, and finally with a razor blade.

Using this procedure, notch radii of less than 0.001 inch were obtained.

Because of the extreme brittleness of tungsten, no attempts were made to fatigue crack this material at room temperature. An attempt was made to fatigue crack a tungsten specimen at 45,000 psi maximum net-section stress with the central portion of the specimen heated to 400 F. Failure occurred in the grips on the first cycle of loading. Some thought was given to enclosing the entire specimen in a furnace during stress cycling to overcome the difficulty of failure in the grips. However, results by investigators at Southern Research Institute⁽⁵⁾ indicated that such procedures probably would not be rewarding. While stress cycling at 1000 F and 30,000 psi, they were unable to detect any fatigue cracking in tungsten after 280,000 cycles. An additional 60,000 cycles at 1300 F likewise revealed no cracking. On the basis of these results, no further attempts were made to introduce fatigue cracks into tungsten specimens.

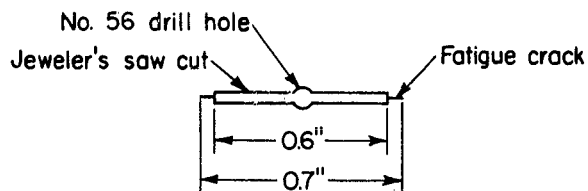
The method chosen for preparation of sharp central notches in tungsten specimens was electrical-discharge machining. The notch was diamond shaped, its long dimension being 0.75 inch and its short dimension, 0.15 inch. The radius at the notch tip varied between about 0.001 and 0.003 inch, which is somewhat less sharp than recommended by the ASTM Committee on Fracture Testing of High Strength Materials. Attempts to further sharpen the notch by use of sharpened files and razor blades were unsuccessful because of the high hardness of the tungsten.

The central-notch configurations employed for the various materials investigated are summarized in Figure 25.

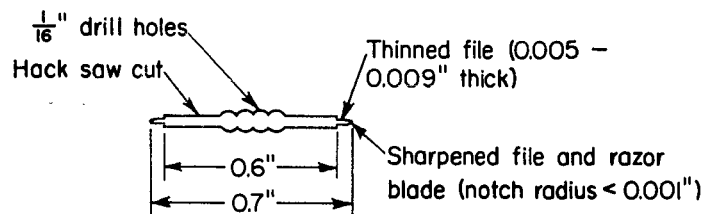
Mechanical Testing

All tests were conducted with a Baldwin-Southwark Universal Testing machine, at a constant head speed of approximately 0.02 inch per minute. For the smooth specimens, approximate values of yield strength were obtained from load versus load-movement curves.

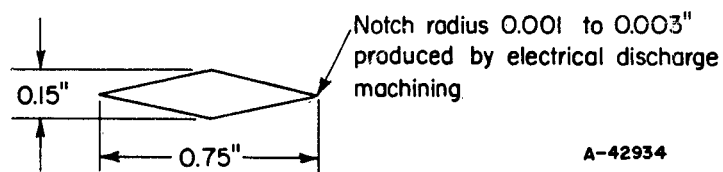
For the centrally notched specimens, a compliance gage was constructed for use at room temperature and lower temperatures to indicate the occurrence of notch "pop-in" and slow crack growth, as discussed previously. The compliance gage was a loop of beryllium-copper to which were cemented electric-resistance strain gages. The loop was precompressed between two posts attached to the specimen approximately 3/4 inch above and below the central notch. As load was applied, the specimen elongated, allowing the compliance gage to relax slightly, thereby straining the gages.



a. Tantalum and Columbium



b. Molybdenum



c. Tungsten

A-42934

FIGURE 25. CONFIGURATION OF CENTRAL NOTCH FOR EVALUATION OF FRACTURE TOUGHNESS FOR TANTALUM AND COLUMBIUM, MOLYBDENUM, AND TUNGSTEN

As long as the specimen remained elastic and no crack extension occurred, the load-strain curve was approximately linear. Deviations from the linear curve, resulting from a disproportionate increase in strain, were indicative of crack extension, plastic flow, or both. At elevated temperatures, load-versus-head travel curves were obtained with the centrally notched specimens. Although this was not as sensitive as the compliance gage for detecting notch pop-in or crack growth, it did serve to indicate the relative amount of crack growth and plastic flow prior to fracture. In addition, if the load-versus-head travel curve remained linear up to the fracture load, it indicated that notch pop-in and total fracture occurred simultaneously.

For testing at temperatures below room temperature, specimens were immersed in the appropriate coolant, allowed to soak for about 10 minutes, and then pulled to failure. Elevated-temperature testing was performed with the specimen and grips enclosed in a furnace. After the desired test temperature was reached, the specimen was allowed to soak for about 30 minutes prior to performing the test.

The following equation was used for the calculation of fracture toughness, K_C :

$$K_C^2 = \frac{\sigma_f^2}{1 - \frac{1}{2} \left(\frac{\sigma_f}{\sigma_Y} \right)^2} W \tan \left(\frac{\pi a}{W} \right),$$

where

σ_f is the observed fracture (or crack "pop-in") stress

σ_Y is the yield stress for the material

W is the specimen width

a is 1/2 the crack length.

In specimens in which slow crack growth occurred prior to fracture, K_C could not be calculated precisely because the extent of slow crack growth was not measured. In such cases, K_C was indicated as being greater than the calculated value based upon the original crack length. When no slow crack growth preceded fracture and fracture was entirely in the transverse mode, K_C was equal to K_{IC} and could be calculated from knowledge of the fracture stress and original crack length.

It should be recognized that some of the fracture-toughness data obtained in this study must be qualified because of difficulties in preparing specimens to the recommended configuration. This is particularly true in the case of tungsten. Had natural cracks been present in the tungsten specimens, rather than notches having radii from 0.001 to 0.003 inch, it is possible that fracture would have initiated and propagated at lower applied stresses, leading to smaller values of K_C and K_{IC} .

Experimental Results

Molybdenum

The results of tests with smooth and center-notched molybdenum-sheet tensile specimens are presented in Figures 26 through 29. Detailed test results are tabulated in Appendix II.

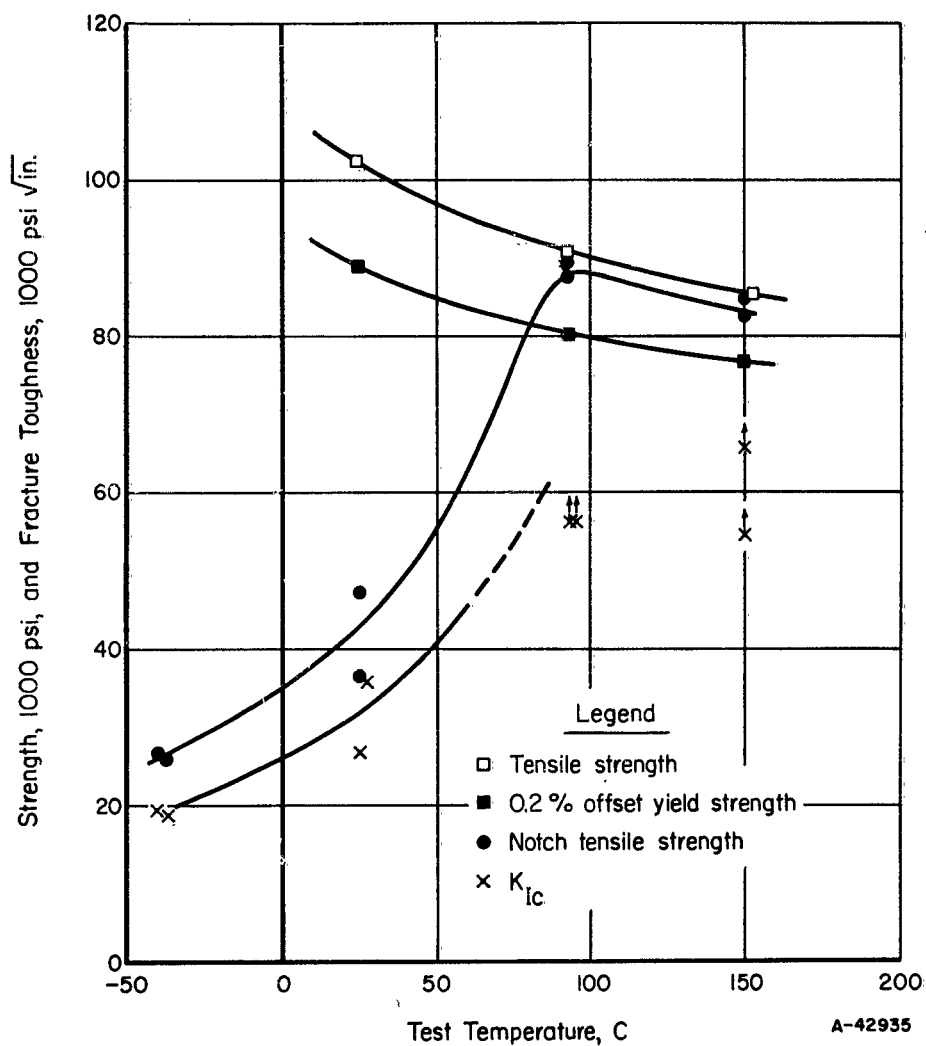


FIGURE 26. TENSILE STRENGTH AND FRACTURE TOUGHNESS OF WROUGHT, STRESS-RELIEVED MOLYBDENUM (LONGITUDINAL) AS A FUNCTION OF TEST TEMPERATURE

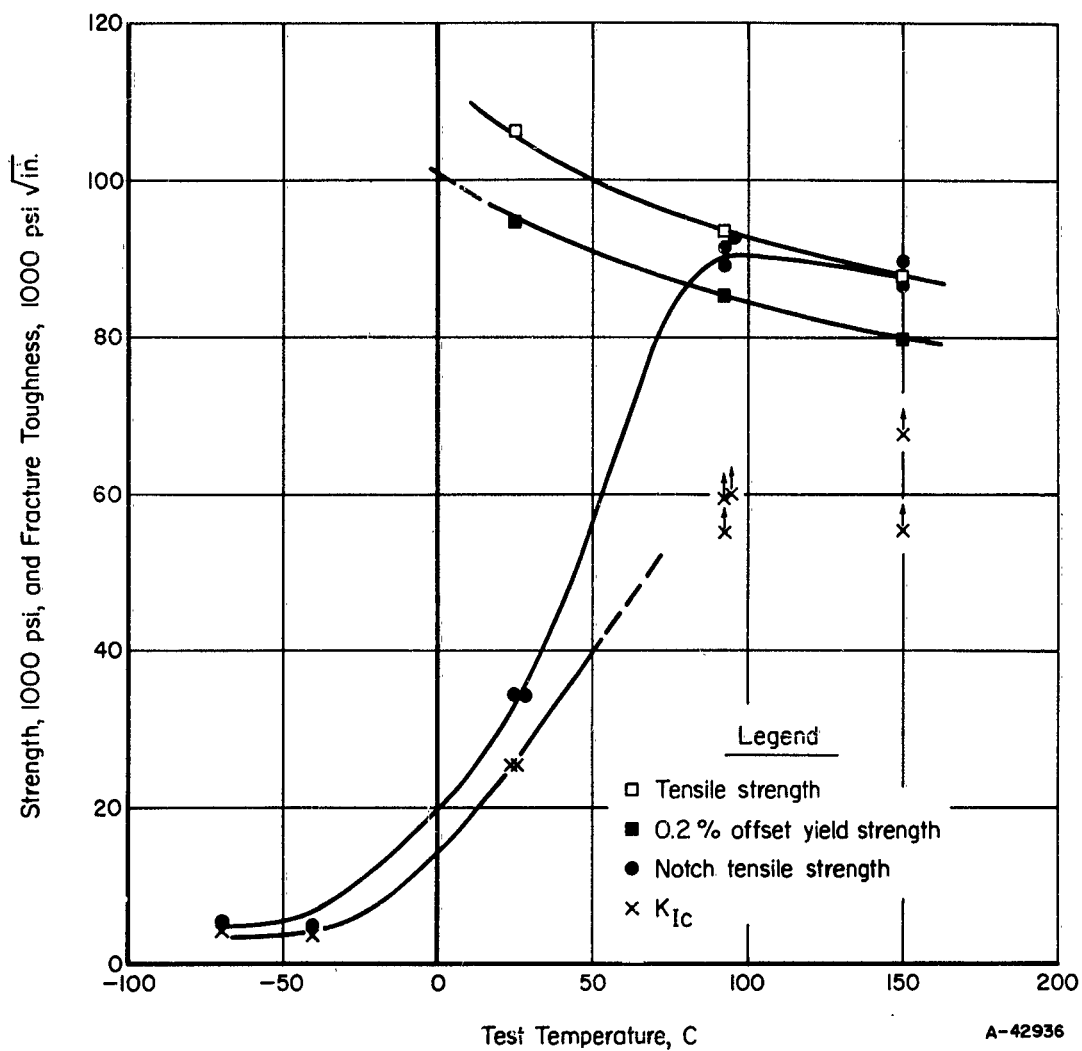


FIGURE 27. TENSILE STRENGTH AND FRACTURE TOUGHNESS OF WROUGHT, STRESS-RELIEVED MOLYBDENUM (TRANSVERSE) AS A FUNCTION OF TEST TEMPERATURE

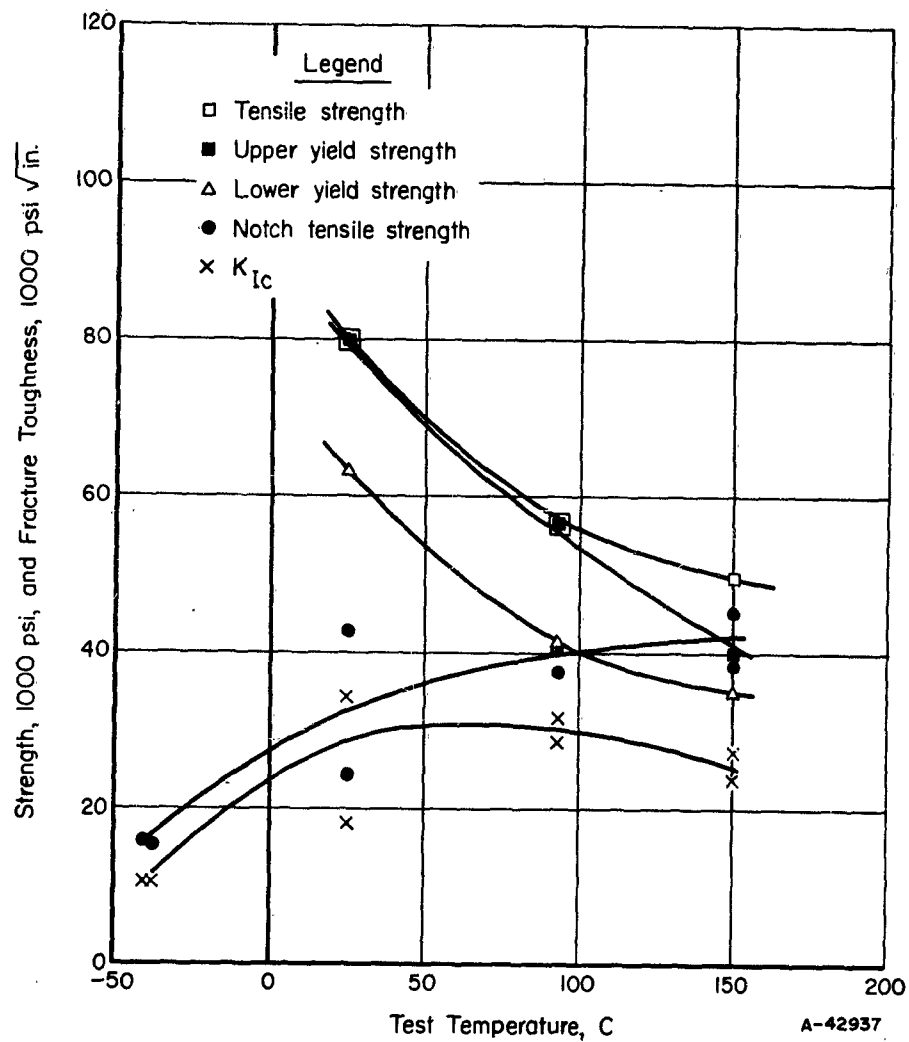


FIGURE 28. TENSILE STRENGTH AND FRACTURE TOUGHNESS OF RECRYSTALLIZED MOLYBDENUM (LONGITUDINAL) AS A FUNCTION OF TEST TEMPERATURE

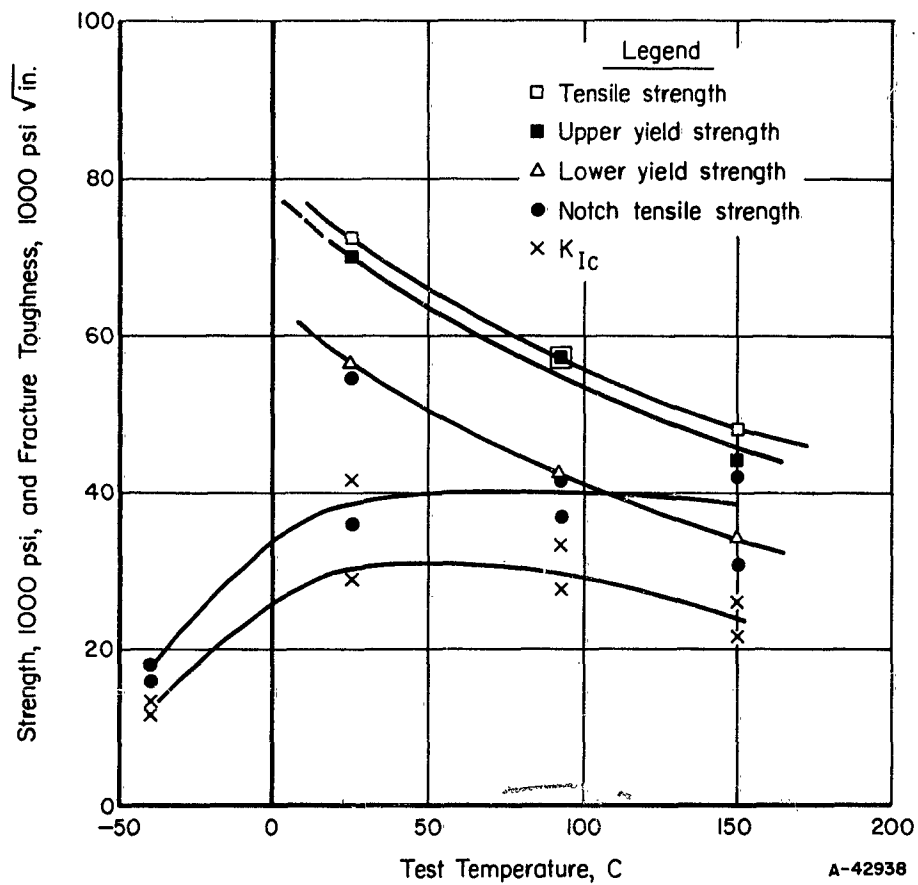


FIGURE 29. TENSILE STRENGTH AND FRACTURE TOUGHNESS OF RECRYSTALLIZED MOLYBDENUM (TRANSVERSE) AS A FUNCTION OF TEST TEMPERATURE

Stress Relieved. The stress-relieved condition (Figures 26 and 27) is characterized by a rather sudden change in fracture behavior as the temperature is lowered from 80 C to -50 C. Above about 80 C, the notch tensile strength equals or exceeds the yield strength and the plane-strain fracture toughness exceeds approximately 60,000 psi $\sqrt{\text{in.}}$. At these higher temperatures, cracks formed at the tips of the sharp central notches under the influence of the applied stress and grew slowly across the specimen. The appearance of the fracture surface in the region of slow-crack extension was quite different from that found in high-strength steel, where pronounced shear lips may develop. In molybdenum, no well-defined shear lip was evident, even when the specimens exhibited high fracture toughness. The fracture surface was essentially flat and perpendicular to the applied tensile stress. Closer examination, however, revealed that the regions of slow-crack extension were layered, with each layer appearing to develop a shear lip of its own. This provided resistance to crack extension, which accounts for the relatively high fracture toughness.

At room temperature and below, the notch tensile strength is considerably below the yield strength, and the fracture toughness drops below about 30,000 psi $\sqrt{\text{in.}}$. Near -50 C, the fracture toughness of the transverse molybdenum specimens is less than 5000 psi $\sqrt{\text{in.}}$, indicating an extremely small tolerance for pre-existing flaws at this temperature. At these temperatures, the fracture appearance was typically brittle. Fracture occurred without any slow-crack extension or shear-lip formation. Hence, K_{IC} is equal to K_{IC} at these temperatures.

In comparing transverse and longitudinal properties, little difference is noted, except near -50 C, where the transverse specimens have considerably lower fracture toughness than the longitudinal specimens.

Recrystallized. The recrystallized condition (Figures 28 and 29) is characterized by a gradual transition in fracture properties between -50 and +150 C. In general, the fracture toughness and notch tensile strength are lower than those for the wrought, stress-relieved condition. The largest value of plane-strain fracture toughness is about 30,000 to 40,000 psi $\sqrt{\text{in.}}$. This occurs near room temperature and drops off slightly at higher temperatures. Except in one instance, the notch tensile strength is less than the upper yield strength. However, it equals or exceeds the lower yield strength at temperatures above about 100 C.

The fracture surfaces at temperatures up to about 90 C were perpendicular to the applied tensile stress and showed no evidence of slow-crack extension or shear-lip formation. Specimens tested at 93 C exhibited small dimples at the notch tip, indicating that some plastic flow occurred prior to fracture. At 150 C, the fracture appearance varied from transverse* (preceded by dimpling and plastic flow) to full shear. This suggests that 150 C may be within the transition range in which the plane-stress fracture toughness, K_{IC} , is increasing rapidly.

The results indicate that there are no major differences in fracture-toughness properties between transverse and longitudinal specimens of recrystallized molybdenum.

*The term transverse fracture is used to describe fracture surfaces that are essentially flat and perpendicular to the applied tensile stress, without evidence of slow-crack growth.

Tungsten

The results of tests with smooth and center-notched tungsten-sheet tensile specimens are presented in Figures 30 and 31, with detailed tabulations being presented in Appendix II. It should be noted that the notch radii of the central notches varied from 0.001 to 0.003 inch. Had sharper notches been used, it is possible that lower values of fracture toughness would have been obtained.

Stress Relieved. In the stress-relieved condition, tungsten undergoes a very sharp transition in fracture toughness as the temperature is lowered from about 250 C (Figure 30). Above this temperature, the notch tensile strength equals or exceeds the yield strength and the plane-strain fracture toughness reaches values in excess of 70,000 psi $\sqrt{\text{in}}$. At test temperatures of 260 C, the fracture mode varies from completely transverse to partial shear. For example, Specimen WS-13, tested at 260 C, exhibited a transverse fracture with little evidence of plastic flow, while Specimen WS-20, also tested at 260 C, exhibited slow-crack extension to a total crack length of about 1-1/8 inches prior to failing in the transverse mode. At temperatures above 260 C, fractures occurred by shear. As discussed previously for molybdenum specimens, no well-defined shear lip was evident. However, the fracture surface appeared to consist of many thin layers, each having its own shear lip.

At temperatures below about 250 C, fractures were entirely transverse, with no macroscopic evidence of plastic flow at the notch tip. The notch tensile strength falls far below the yield strength and fracture toughness drops rapidly to values of 10,000 to 20,000 psi $\sqrt{\text{in}}$.

Recrystallized. In the recrystallized condition, the fracture toughness of tungsten sheet is extremely low, even at elevated temperatures (Figure 31). The transition in fracture properties is much more gradual than is the case for wrought, stress-relieved tungsten. From room temperature to 260 C, fractures were completely transverse with no macroscopic evidence of plastic flow. Notch tensile strength is about 10,000 to 15,000 psi and K_{IC} is about 10,000 psi $\sqrt{\text{in}}$. At 400 C, cracking and dimpling was detected at the tip of the notch prior to complete transverse fracture. Likewise, the notch tensile strength and fracture toughness are slightly greater than at lower temperatures. At 538 C, cracks formed at the ends of the notch and grew slowly by shear, indicating increased resistance to plane-stress fracturing.

Tantalum and Columbium

Experimental results for tantalum and columbium are presented in Figure 32 (see Appendix II for detailed results). It is apparent from these results that neither tantalum nor columbium is weakened by a pre-existing crack at temperatures down to -196 C. This is true for the recrystallized as well as the stress-relieved condition. Use of a compliance gage revealed no sudden change of compliance corresponding to crack movement, but only a gradual change corresponding to extension of the plastically deformed zone across the specimen width. In the recrystallized condition, a pronounced yield point occurred at room temperature for both tantalum and columbium. At -196 C, only tantalum displayed a yield point. These yield points were observed in the center-cracked specimens as well as in the smooth specimens. In general, fracture occurred beyond the maximum load.

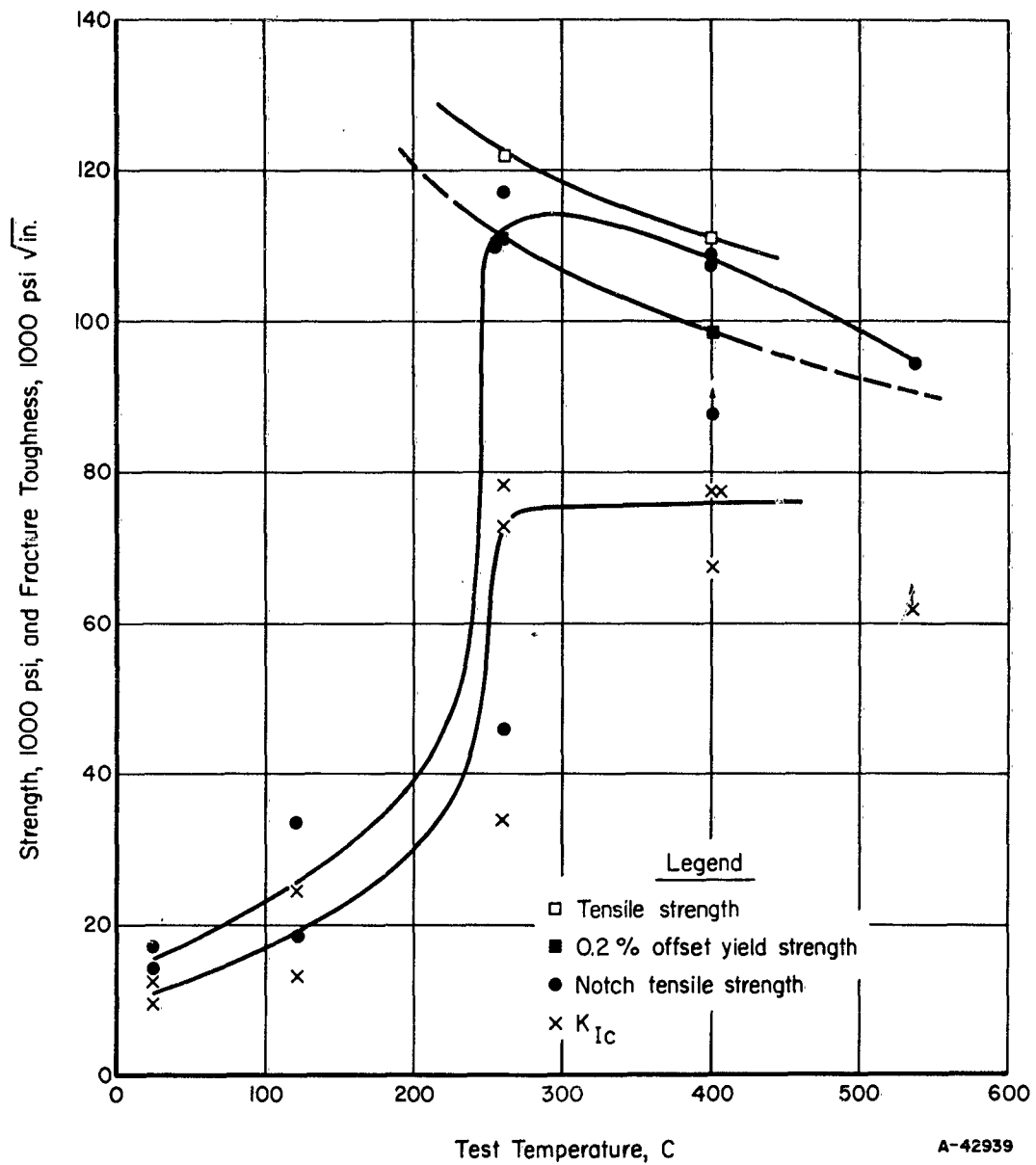


FIGURE 30. TENSILE STRENGTH AND FRACTURE TOUGHNESS OF WROUGHT, STRESS-RELIEVED TUNGSTEN AS A FUNCTION OF TEST TEMPERATURE

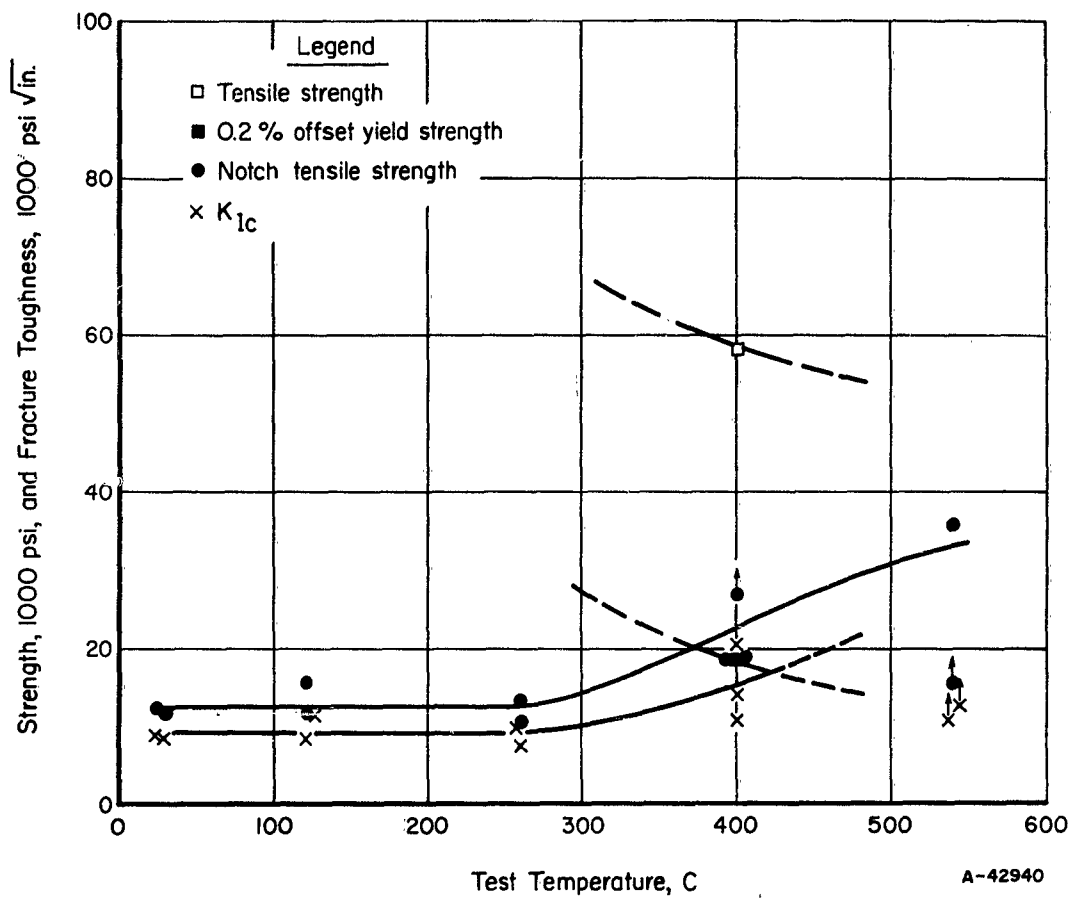


FIGURE 31. TENSILE STRENGTH AND FRACTURE TOUGHNESS OF RECRYSTALLIZED TUNGSTEN AS A FUNCTION OF TEST TEMPERATURE

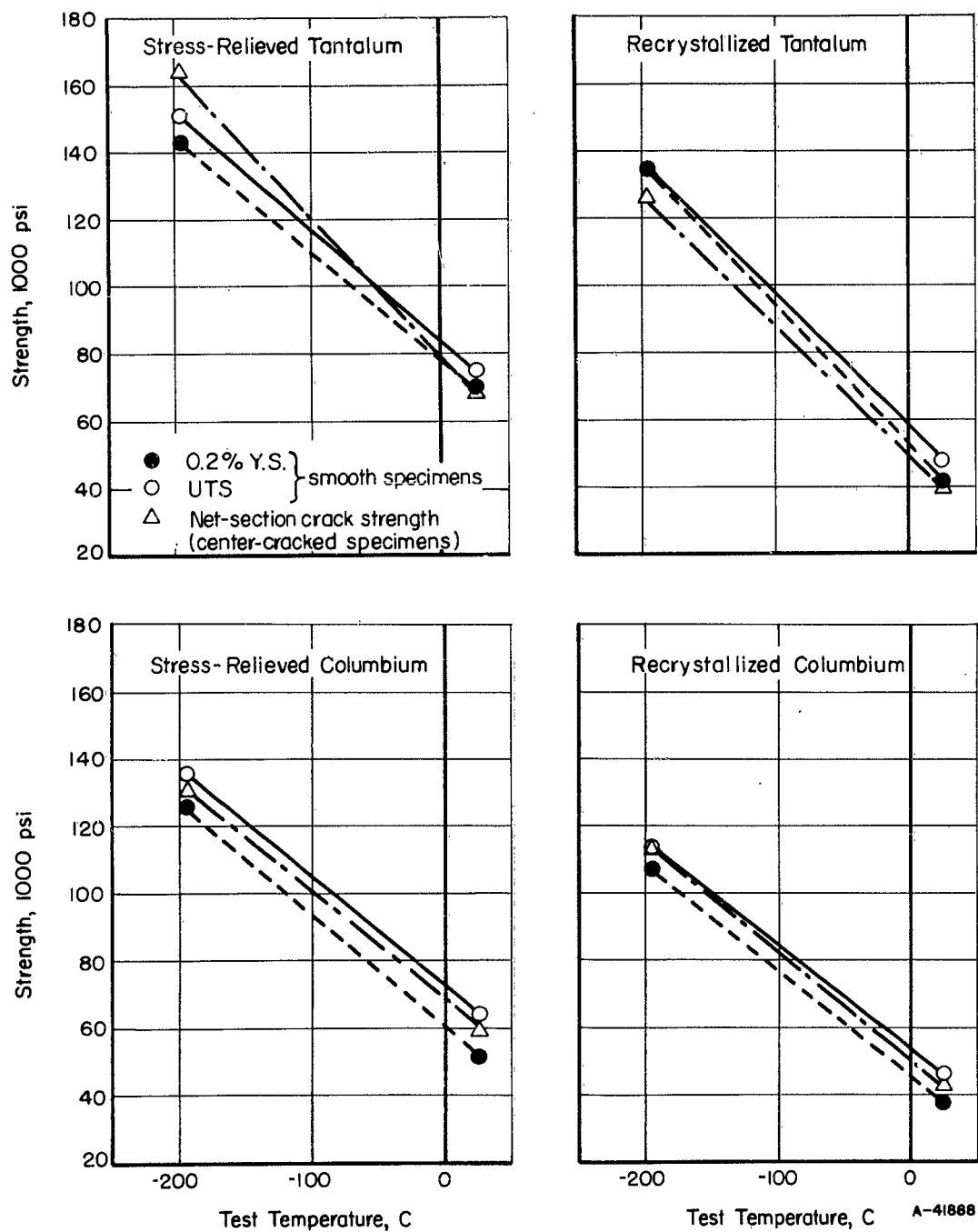


FIGURE 32. EFFECT OF TEST TEMPERATURE ON STRENGTH OF SMOOTH AND CENTER-CRACKED SHEET SPECIMENS OF TANTALUM AND COLUMBIUM

Inasmuch as no notch pop-in was detected and gross yielding occurred prior to crack propagation, calculations of K_{IC} and K_C were not justified. The results demonstrate that tantalum and columbium in the form of 50-mil sheet can be expected to perform reliably at -196 C, even in the presence of through-cracks.

Practical Implication of Fracture-Toughness Results

As discussed previously, the objective of fracture mechanics is to make it possible to predict the approximate failure stress from knowledge of the size of the largest flaw and the fracture toughness. Conversely, one can decide upon a design stress level and calculate the limiting flaw size from knowledge of the fracture toughness. Figure 33 illustrates the relationship between crack length, fracture toughness, and predicted fracture strength. As an example, suppose it is necessary to operate at a stress level of 75,000 psi with a material possessing a fracture toughness of 15,000 psi $\sqrt{\text{in.}}$. From Figure 33, the maximum flaw should not exceed about 0.025 inch if integrity is to be maintained. However, if the fracture toughness is 60,000 psi $\sqrt{\text{in.}}$, flaws exceeding 0.3 inch may be safely tolerated. This, of course, is a highly idealized picture of how the results of fracture-toughness studies can be applied. The limitations of fracture mechanics in its present state of development, discussed in an earlier section of this report, must always be borne in mind.

Despite the limitations of fracture mechanics and the uncertainties connected with some of the data reported herein, the results show quite clearly why commercially available unalloyed molybdenum and tungsten are such unreliable structural materials when subjected to stress near room temperature. At room temperature, tungsten has a K_C value of about 10,000 psi $\sqrt{\text{in.}}$, while molybdenum has approximately the same value at temperatures near -40 C. From Figure 33, this suggests that, even at applied stresses of only 25,000 psi, the maximum flaw size must be something less than about 0.1 inch. Flaws of this size in structures are extremely hard to detect. On the other hand, at somewhat higher temperatures, where K_C has a value of 30,000 psi $\sqrt{\text{in.}}$ or greater, cracks of the order of 1.0 inch can be tolerated at applied stresses of 25,000 psi. To improve the reliability of structures made from molybdenum or tungsten, it would be highly desirable to lower the transition temperatures of these materials, perhaps by suitable alloying, to provide higher values of K_C near room temperature. Likewise, reducing the pre-existing flaw size by improved fabrication techniques should improve reliability.

Conclusions

The following conclusions are based upon tests conducted on 50-mil sheet of commercially available unalloyed refractory metals.

- (1) Wrought, stress-relieved molybdenum sheet tested in tension in the presence of extremely sharp central notches undergoes a sharp transition in fracture properties near 80 C. In longitudinal specimens, the plane-strain fracture toughness, K_{IC} , increases from 20,000 to >60,000 psi $\sqrt{\text{in.}}$ as the temperature is raised from -40 to 100 C. Over the same range of temperature, K_{IC} for transverse

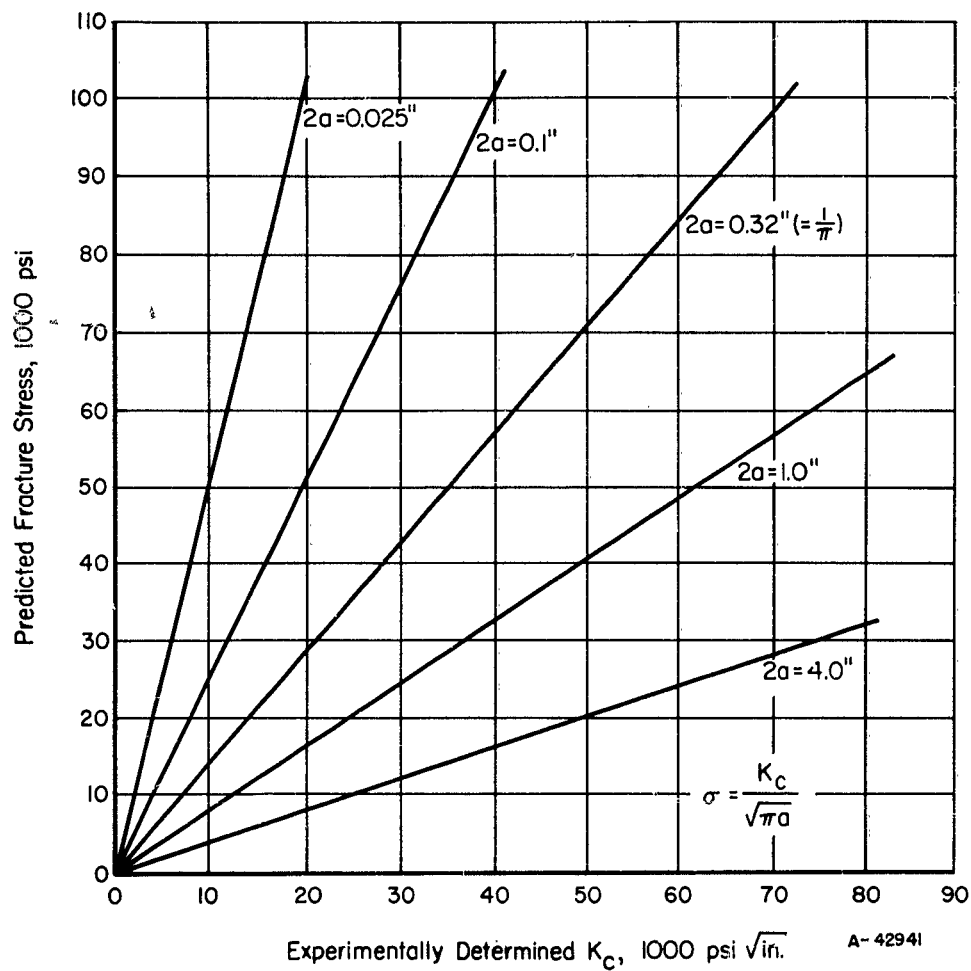


FIGURE 33. DEPENDENCE OF FRACTURE STRESS ON FRACTURE TOUGHNESS FOR VARIOUS CRACK LENGTHS ($2a \ll W$), AS PREDICTED BY FRACTURE-MECHANICS THEORY (ASSUMING NO SLOW-CRACK EXTENSION)

specimens increases from 5000 to $>60,000 \text{ psi} \sqrt{\text{in.}}$. Above 90 C, K_C becomes greater than K_{IC} , irrespective of orientation.

- (2) Recrystallized molybdenum sheet undergoes a gradual transition in fracture properties as temperature is varied. K_{IC} increases from 10,000 to 30,000 $\text{psi} \sqrt{\text{in.}}$ as the temperature is raised from -40 to +25 C. As temperature is increased further, K_{IC} appears to drop slightly to about 25,000 $\text{psi} \sqrt{\text{in.}}$. Little difference in fracture toughness is noted between transverse and longitudinal specimens. Above about 150 C, K_C becomes greater than K_{IC} .
- (3) The results of fracture-toughness tests on tungsten are less conclusive than those for molybdenum, because the notch radius was not as sharp as would be desirable. Had sharper notches been employed, it is likely that lower values of K_{IC} would have been measured than are reported herein. For wrought, stress-relieved tungsten sheet, K_{IC} was found to increase sharply from 10,000 to $>70,000 \text{ psi} \sqrt{\text{in.}}$ as the temperature was raised from 25 to 260 C. K_C exceeded K_{IC} above approximately 260 C. For recrystallized tungsten sheet, K_{IC} rose gradually from 10 to 15,000 $\text{psi} \sqrt{\text{in.}}$ as the temperature was raised from 25 to 400 C. The temperature above which K_C exceeded K_{IC} was approximately 400 C.
- (4) In tantalum and columbium sheet, whether stress relieved or recrystallized, the presence of natural cracks does not give rise to brittle failure at temperatures as low as -196 C. Calculations of fracture toughness were not warranted because gross yielding occurred prior to fracture.

MECHANISM OF NOTCH EMBRITTLEMENT*

Development and Application of Model Relating to Crack Propagation in Refractory Metals

This section examines the material properties governing the response of metals to sharp notches, especially moving cracks - the problem of crack-propagation resistance. Crack propagation in metals capable of plastic flow is an unusually complex phenomenon. Its analysis must draw on three disciplines, each presenting problems difficult in their own right. These are:

- (1) Continuum Mechanics. The problems of formulating for a sharp notch an elastic-plastic stress-and-strain field solution responsive to the extent of plastic relaxation at the notch root.
- (2) Plasticity. The problems of formulating plastic relaxation in terms of measurable parameters.

*Authored by G. T. Hahn and A. Gilbert.

- (3) **Fracture.** The problems of formulating the fracture strength on the macroscopic scale in terms of metallurgical parameters, and as a function of strain, strain rate, and temperature.

Efforts by Orowan⁽⁶⁾, Irwin⁽⁷⁾, and their followers, which largely circumvent these problems by couching crack propagation in terms of a quasi-brittle Griffith energy balance, fall short of providing all the needed insights. To be sure, the Orowan-Irwin approach does provide in a single parameter, such as either K_C or G_C , a useful relative measure of crack-propagation resistance. However, the separate contributions of stress intensity, plastic relaxation, and fracture strength, and the relative importance of these factors are not resolved. While the direct approach, a complete and rigorous solution in terms of stress and strain, plasticity, and fracture, is not yet tractable, some progress in this direction is possible. Recent studies by Gilman and Johnston⁽⁸⁾ have laid the groundwork for formulating the plastic relaxation rate in quantitative terms. Such a formulation, together with a simplified mechanics treatment of the elastic-plastic problem evolved at Battelle⁽⁹⁾, provides a model of a propagating crack useful for evaluating relevant materials properties. This model is here developed in more detail and applied to the refractory metals. Results are also included of dislocation-parameter measurements performed on molybdenum and described in a later section, Determination of Dislocation Parameters for Molybdenum Relevant to the Crack-Propagation Model.

Model of a Partially Relaxed Crack

The crack model⁽⁹⁾ adopted for the calculations is illustrated in Figure 34. It consists of a sharp crack of length $2a$ preceded by a zone of plastic relaxation. It is assumed that the extent of the plastic zone can be described simply by the radius r , that the stresses within the zone are substantially relaxed, and that conditions of plane stress prevail. The crack-plastic zone complex can then be treated as an elliptical hole of semimajor axis a , and root radius r (as indicated in Figure 34 by the broken line), the point $x = a$ (see Figure 34 representing one point on the elastic-plastic boundary). The stress-concentration factor, α , in advance of such an elliptical hole in a large plate for the condition $x > a$, $y = 0$ (see Figure 34) is given by the following expression in curvilinear coordinates^(4,10):

$$\alpha_{(y=0)} = 1 + \frac{\cosh \theta_0}{2 \sinh^2 \theta} \left[e^{\theta_0} (e^{2\theta_0} - 3) (1 + 1/2 \coth \theta) e^{-2\theta} + \cosh \theta_0 \coth \theta \right], \quad (12)$$

where

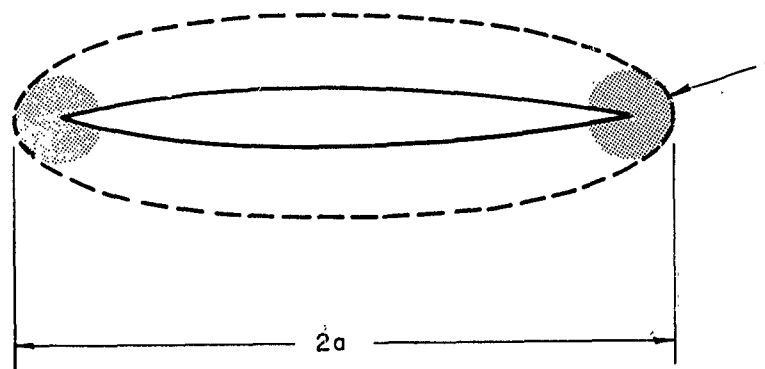
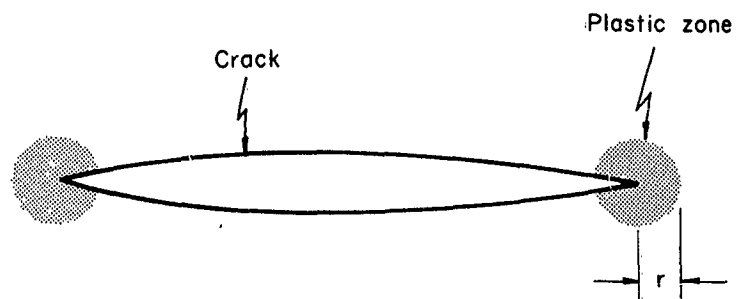
$$\theta_0 = \text{arc coth } \sqrt{\frac{a}{r}}, \quad (12a)$$

and

$$\theta = \text{arc cosh } \frac{x \cosh \theta_0}{a}. \quad (12b)$$

The maximum stress concentration α^* occurs at the elastic-plastic boundary (the base of the elliptical hole, $x = a$, $y = 0$) and is:

$$\alpha^* = 1 + 2 \sqrt{\frac{a}{r}}. \quad (13)$$



A-41890

FIGURE 34. THE MODEL OF A PARTIALLY RELAXED CRACK

Calculated values of the stress-concentration factor α as a function of distance x and a/r , the hole geometry, are summarized in Table 4 and illustrated in Figure 35. The important feature is the steep gradient of the stress-concentration factor close to the elliptical hole.

Rate of Plastic Relaxation

Gilman and Johnston's⁽⁸⁾ analysis, as recently amplified by Hahn⁽¹¹⁾ and Johnston⁽¹²⁾, offers a means of characterizing the plastic relaxation rate in terms of basic dislocation parameters:

$$\frac{d\epsilon_p}{dt} \equiv \dot{\epsilon}_p = 0.5 b L \bar{v} , \quad (14)$$

where ϵ_p is the plastic strain, $\dot{\epsilon}_p$ the plastic-strain rate, b the Burgers vector, L the total length of dislocations in motion, and \bar{v} the average velocity of the dislocations. The quantity L depends on both ρ_0 (the number of dislocations initially mobile) and the number of free dislocations produced by multiplication. The ρ_0 values appropriate for the different refractory metals are not well known, since a large fraction of the dislocations present after annealing are probably "locked" by interstitial atoms. For the purposes of the present calculations and as a first approximation, the values $\rho_0 = 10^3/\text{cm}^2$ and $\rho_0 = 10^7/\text{cm}^2$ are assumed to be characteristic of metals substantially "locked" and substantially "unlocked", respectively.

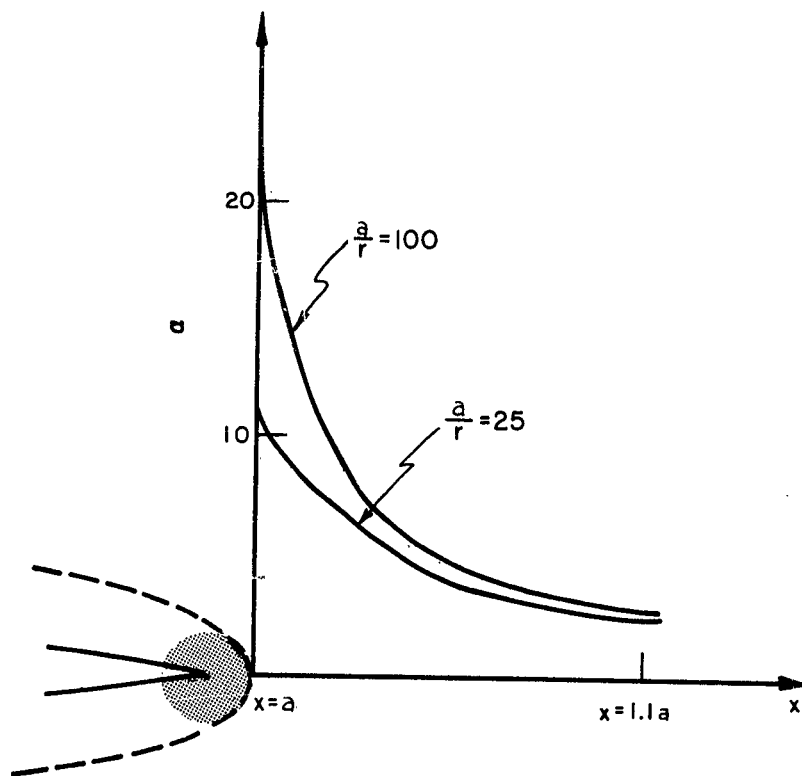
Results for LiF⁽⁸⁾, iron⁽¹³⁾, and tantalum⁽¹⁴⁾ show that ρ , the total dislocation density, in the range $0.005 < \epsilon_p < 0.10$ can be described by a relation of the form:⁽¹¹⁾

$$\rho = \rho'_0 + C \epsilon_p^\beta , \quad (15)$$

where ρ'_0 is the initial dislocation density including the dislocations that are locked and C and β are empirical constants. Existing data for the refractory metals are summarized in Table 5. It should be noted that the values quoted for tungsten and columbium are based on only one or two determinations each and are not well documented.

In order to describe the number of mobile dislocations, the following approximations are made:

- (1) Equation (15) is valid for refractory metals for plastic strains $0 < \epsilon_p < 0.10$. The validity of this assumption for small strains, $\epsilon_p < 0.005$, has not been tested, and this assumption must be regarded as a first approximation.
- (2) The parameters C and β are independent of strain rate, stress, or dislocation velocity. While work recently completed at Battelle⁽¹⁸⁾ does show this to be true to a good approximation for mild steel tested in the strain-rate range 10^{-5} to 10^{-2} per second, it has not been tested at high strain rates.
- (3) The number of mobile dislocations is a fixed fraction f of the total dislocation density, where $f \approx 0.1$. This is regarded as a useful first approximation.



A-41891

FIGURE 35. CALCULATED STRESS CONCENTRATION α FOR AN ELLIPTICAL CRACK, LENGTH $2a$ AND ROOT RADIUS r , AS A FUNCTION OF DISTANCE

TABLE 4. CALCULATED VALUES OF THE STRESS-CONCENTRATION FACTOR α AS A FUNCTION OF DISTANCE x AND HOLE GEOMETRY a/r ^(a)

Stress-Concentration Factor α				
x	$\frac{a}{r}$			
	4	25	10^2	10^4
a	5.00	11.0	21.0	201
1.00001 a	--	--	--	169
1.0001 a	4.99	10.9	20.5	77.5
1.001 a	4.95	10.5	17.5	22.9
1.01 a	4.58	7.37	7.90	7.14
1.1 a	3.09	2.56	2.44	2.40
2.0 a	1.17	--	--	--

(a) For $y = 0$, $x > a$ (see Figure 34), where $2a$ is the major axis and r is the root radius of the ellipse.

TABLE 5. VALUES OF THE DISLOCATION MULTIPLICATION PARAMETERS, C AND β , FOR THE REFRACTORY METALS

Material	Method	Strain Rate, sec ⁻¹	C		β	Reference
			Per Cm ²	Per 1%		
Ta	T.E.M. (a)	3×10^{-4}	1.7×10^{10}		1	Hull and McIvor ⁽¹⁴⁾
Cb	T.E.M.	2×10^{-4}	2×10^{10}		<1	Gregory ⁽¹⁵⁾
Mo	T.E.M.	2×10^{-4}	8×10^8		~1	Benson, Thomas, and Washburn ⁽¹⁶⁾
Mo	T.E.M.	2×10^{-5}	7.2×10^8		--	Present investigation, see page 80
W	E.P. (b)	--	2×10^7		--	Schadler and Low ⁽¹⁷⁾

(a) Transmission electron microscopy.

(b) Etch pitting.

Accordingly, since $\beta \approx 1$, the quantity L can be expressed as follows:

$$L = [\rho_0 + fC\epsilon_p] \quad (16)$$

Direct measurements of the average dislocation velocity by means of the etch-pitting technique⁽⁸⁾ have been performed by Stein and Low⁽¹⁹⁾ on Fe-3.25Si crystals, and by Schadler and Low⁽¹⁷⁾ on tungsten crystals. These studies show that in the range 10^{-5} to 10^{-1} centimeters per second, the average dislocation velocity can be described by an expression of the form:

$$\bar{v} = \left(\frac{\sigma}{\sigma_0} \right)^n, \quad (17)$$

where n is a constant at a given temperature, and σ_0 the stress corresponding to unit dislocation velocity, can be regarded as a friction stress. There is some evidence that the value of n decreases systematically at high velocities, e.g., 10^3 to 10^5 centimeters per second.^(8,20) However, for the purposes of the present calculations, Equation (17) and the constancy of n are assumed over the entire range of dislocation velocity. On the basis of this assumption and those outlined in the preceding section on dislocation multiplication, four indirect methods of calculating n from mechanical-test data can be derived. These are described more fully in a later section and include:

- a. The dependence of the yield stress, σ_y , on the strain rate $\dot{\epsilon}_p$:

$$n = \frac{d \log \dot{\epsilon}_p}{d \log \sigma_y} \quad (18)$$

- b. The dependence of the delay time for yielding, t_d , on stress, σ :

$$n = - \frac{d \log t_d}{d \log \sigma} \quad (19)$$

- c. The dependence of the Lüders' band front velocity, μ , on yield stress:

$$n = \frac{d \log \mu}{d \log \sigma_y} \quad (20)$$

- d. The stress dependence of the rate of stress relaxation, $\frac{d\sigma}{dt}$, by plastic creep under fixed grip conditions:

$$n = \frac{d \log \frac{d\sigma}{dt}}{d \log \sigma} \quad (21)$$

Available information on the value of n for the different refractory metals derived from etch-pit experiments, and calculated from mechanical-test data, is summarized in Table 6. Values determined for molybdenum in two grain-size conditions are given later in Table 10. Agreements among the various experimental methods are not good in all cases, and only in the case of tungsten where a reliable value has been obtained by the direct etch-pitting method⁽¹⁷⁾ can the parameter n be regarded as well established.

TABLE 6. VALUES OF THE DISLOCATION-VELOCITY PARAMETER,
n, FOR THE REFRACTORY METALS(a)

Material	Type of Measurement	Strain-Rate Range, sec ⁻¹	n	Reference
Cb	Strain-rate sensitivity of yield stress	10 ⁻⁴ - 10 ⁻¹	15	Tankins and Maddin(21)
Cr	Strain-rate sensitivity of yield stress	10 ⁻⁴ - 10 ⁻¹	11	Marcinkowski(22)
Cr ^(b)	Strain-rate sensitivity of flow stress	10 ⁻⁴ - 10 ⁻³	7	Reid, Gilbert, and Hahn(23)
Mo	Strain-rate sensitivity of upper yield stress	10 ⁻⁴ - 10 ⁻¹	13	Bechtold(24)
Mo	Strain-rate sensitivity of upper yield stress	10 ⁻⁵ - 10 ⁻²	14	Carreker and Guard(25)
Mo	Strain-rate sensitivity of lower yield stress	10 ⁻⁵ - 10 ⁻²	17	Carreker and Guard(25)
Mo	Stress dependence of the delay time for yielding	10 ⁻⁴ - 10	10 15	Hendrickson, Wood, and Clark(26)
W	(250 C) Strain-rate sensitivity of upper yield stress	10 ⁻⁵ - 10 ⁻²	7	Bechtold(27)
W	(250 C) Strain-rate sensitivity of flow stress at 3 per cent strain	10 ⁻⁵ - 10 ⁻²	14	Bechtold(27)
W ^(b)	(250 C) Strain-rate cycling	10 ⁻⁴ - 10 ⁻³	41	Schadler and Low(17)
W ^(b)	(-196 C) Strain-rate cycling	10 ⁻⁴ - 10 ⁻³	71	Schadler and Low(17)
W ^(b)	(25 C) Dislocation etch- pit displacement	10 ⁻⁵ - 10 ^{-2(c)}	5	Schadler and Low(17)
W ^(b)	(-196 C) Dislocation etch-pit displacement	10 ⁻⁵ - 10 ^{-1(c)}	11	Schadler and Low(17)

(a) Data refer to polycrystalline material tested at room temperature, except where otherwise noted.

(b) Single crystals.

(c) Dislocation-velocity range.

Current best estimates of the values of ρ_0 , c , and n for refractory metals are listed in Table 7. The compilation points up significant differences in both the ease of multiplication and the stress dependence of dislocation velocity among the different refractory metals. It is interesting to note that the more ductile metals, i. e., tantalum and columbium, possess the highest multiplication rates, and that the more brittle metals, i. e., chromium and tungsten, are the most rate sensitive (exhibit small n values).

TABLE 7. ESTIMATES OF THE DISLOCATION PARAMETERS ρ_0 , C , AND n APPROPRIATE FOR THE REFRACTORY METALS

Metal	ρ_0	C	n
Cb	10^3	10^{10}	15
Ta	10^3	10^{10}	--
Cr	10^3	--	7
Mo	10^3	10^9	12
W	10^3	10^7	5

The influence of work hardening can be introduced as follows⁽¹¹⁾:

$$\bar{v} = (\sigma_0)^{-n} (\sigma - q\epsilon_p)^n \dots, \quad (22)$$

where q is the rate of linear work hardening.

Together, Equations (14), (16), and (22) provide a simplified but relatively accurate expression of the plastic response of metals^(11,12):

$$\dot{\epsilon}_p = 0.5 b (\rho_0 + fC\epsilon_p^\beta) (\sigma_0)^{-n} (\sigma - q\epsilon_p)^n. \quad (23)$$

For the purposes of the present calculations which involve small plastic strains, i. e., less than 1 per cent, the term β and the work-hardening contribution $q\epsilon_p$ is neglected:

$$\dot{\epsilon}_p = 0.5 b (\rho_0 + fC\epsilon_p) (\sigma_0)^{-n} \sigma^n. \quad (23a)$$

Equation (23a) taken together with the crack model already described can now be used to treat crack propagation quantitatively.

Crack-Propagation Model

The plastic zone size, r , and the maximum stress, σ^* , consistent with the crack model and the rate of plastic relaxation specified by Equation (23a), can now be calculated by noting the following. The stress, σ , acting on an element, dV , a distance $(x-a)$ in front of the elastic-plastic boundary (see Figure 36) is $\sigma_{nom} \cdot \alpha$, the nominal stress multiplied by the stress-concentration factor, where α is strongly dependent on x . Rewriting Equation (23a) we obtain:

$$\frac{d\epsilon_p}{dt} = 0.5 b \sigma_o^{-n} (\rho_o + fC\epsilon_p) \alpha^n \sigma_{nom}^n \quad , \quad (24)$$

or

$$\int_0^{\epsilon_p} \frac{d\epsilon_p}{0.5 b \sigma_o^{-n} (\rho_o + fC\epsilon_p)} = \int_0^t \alpha^n \sigma_{nom}^n dt \quad . \quad (25)$$

On integrating the left-hand side of Equation (25), the strain history of an element, dV , is described, and on integrating the right-hand side, the stress history. The integral at the right, however, is with respect to time, while the stress-concentration factor, α , is known only with respect to distance in front of the crack. If we now assume a constant linear crack velocity, u , the limits of the integral may be converted to distance and Equation (25) becomes:

$$\int_0^{\epsilon_p} \frac{d\epsilon_p}{0.5 b \sigma_o^{-n} (\rho_o + fC\epsilon_p)} = \frac{\sigma_{nom}^n}{u} \int_a^{x \gg a} \alpha^n dx \quad , \quad (26)$$

and on integrating:

$$\left(\frac{\sigma_o}{\sigma_{nom}} \right)^n \frac{u \log_e \left(1 + \frac{fC\epsilon_p^*}{\rho_o} \right)}{0.5 b fC} = I \quad , \quad (27)$$

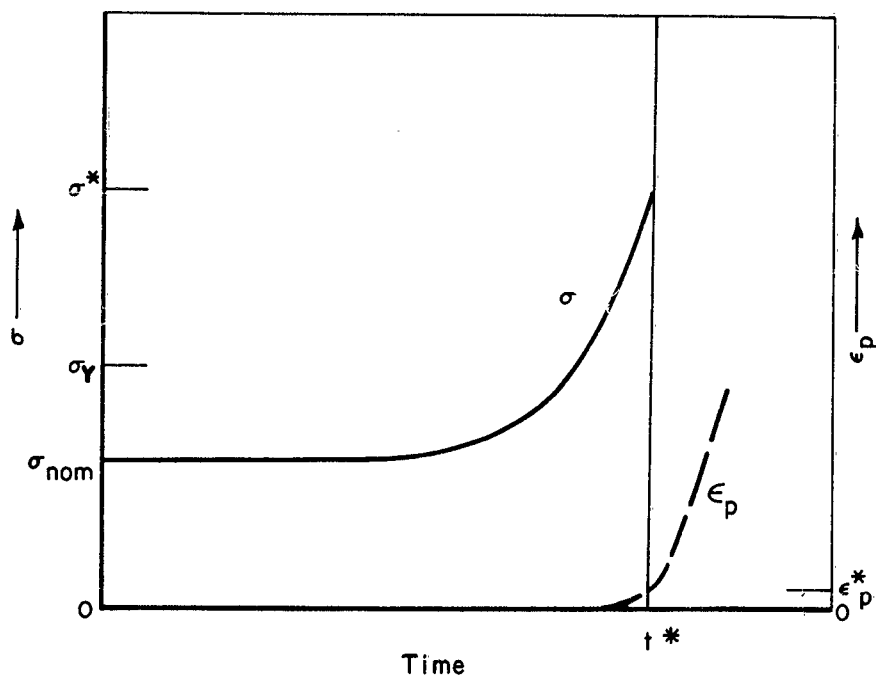
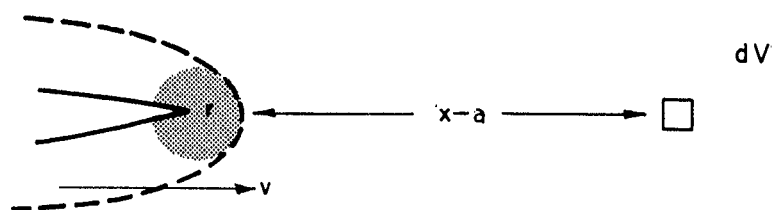
where

$$I \equiv \int_a^{x \gg a} \alpha^n dx \quad , \quad (27a)$$

and ϵ_p^* is the plastic strain at the elastic-plastic boundary, i.e., $\epsilon_p^* = 0.1$ per cent as a first approximation. Finally, by combining Equation (27) with Equation (23a), the term σ_o can be replaced by σ_y , the lower yield stress measured in an ordinary tensile test:

$$\left(\frac{\sigma_y}{\sigma_{nom}} \right)^n \frac{u (\rho_o + fC\epsilon_y) \log_e \left(1 + \frac{fC\epsilon_p^*}{\rho_o} \right)}{\dot{\epsilon}_p fC} = I \quad , \quad (28)$$

where $\epsilon_y \approx 0.1$ per cent is the value of the plastic strain corresponding to the σ_y , and $\dot{\epsilon}_p$ is the plastic-strain rate employed in the tensile test, e.g., 10^{-3} per sec.



A-41892

FIGURE 36. SCHEMATIC PRESENTATION OF STRESS AND STRAIN AHEAD OF A MOVING CRACK

For a given set of parameters, the left-hand side of Equations (27) and (28) reduces to a constant. The integral I on the right-hand side can be evaluated as a function of a/r for appropriate values of n via Equation (12). Results of such calculations are summarized in Table 8 and Figure 37, and the integral I is plotted against a/r in Figure 38. The quantity I for which the equality of Equation (25) or (26) is satisfied thus determines, through Figure 38, the crack-plastic zone geometry a/r consistent with the conditions imposed. The quantity a/r , in turn, fixes the maximum stress concentration α^* [see Equation (13) and Figure 39], and the maximum stress σ^* :

$$\sigma^* = \alpha^* \sigma_{\text{nom}} \quad (29)$$

Finally, by choosing a value for the crack length a , the plastic-zone size r can be calculated. A schematic presentation of the calculation is given in Figure 36 which shows that, before the volume element dV yields in front of the advancing crack, it is subjected to a magnified stress σ greater than the nominal applied stress σ_{nom} and the static yield stress σ_y . The maximum stress σ^* attained at time t^* when the elastic-plastic boundary just reaches the volume element decides whether or not the material continues to fracture.

TABLE 8. VALUE OF THE INTEGRAL I AS A FUNCTION OF A CRACK GEOMETRY a/r AND STRAIN-RATE-SENSITIVITY EXPONENT n

a/r	I, units of crack length, for Value of n Indicated			
	5	10	15	20
4	1.3×10^2	1.2×10^5	2.5×10^8	5.5×10^{11}
25	8.7×10^2	5.9×10^7	6.6×10^{12}	7.6×10^{17}
10^2	5.1×10^3	8.5×10^9	2.4×10^{16}	6.5×10^{22}
10^4	4.6×10^6	6.5×10^{17}	1.4×10^{29}	3.0×10^{40}
10^6	4.5×10^9	2.9×10^{25}	1.3×10^{42}	2.9×10^{58}

Results and Discussion

Values of α^* , σ^* , and the plastic-zone size calculated from Equation (27) as a function of crack length and crack velocity for various values of the dislocation parameters n , C , and ρ_0 are shown in Figures 40 through 43. The calculations were made for the case $\sigma_{\text{nom}} = 1/2 \sigma_y$. The main predictions of the crack-propagation model are summarized in the following paragraphs.

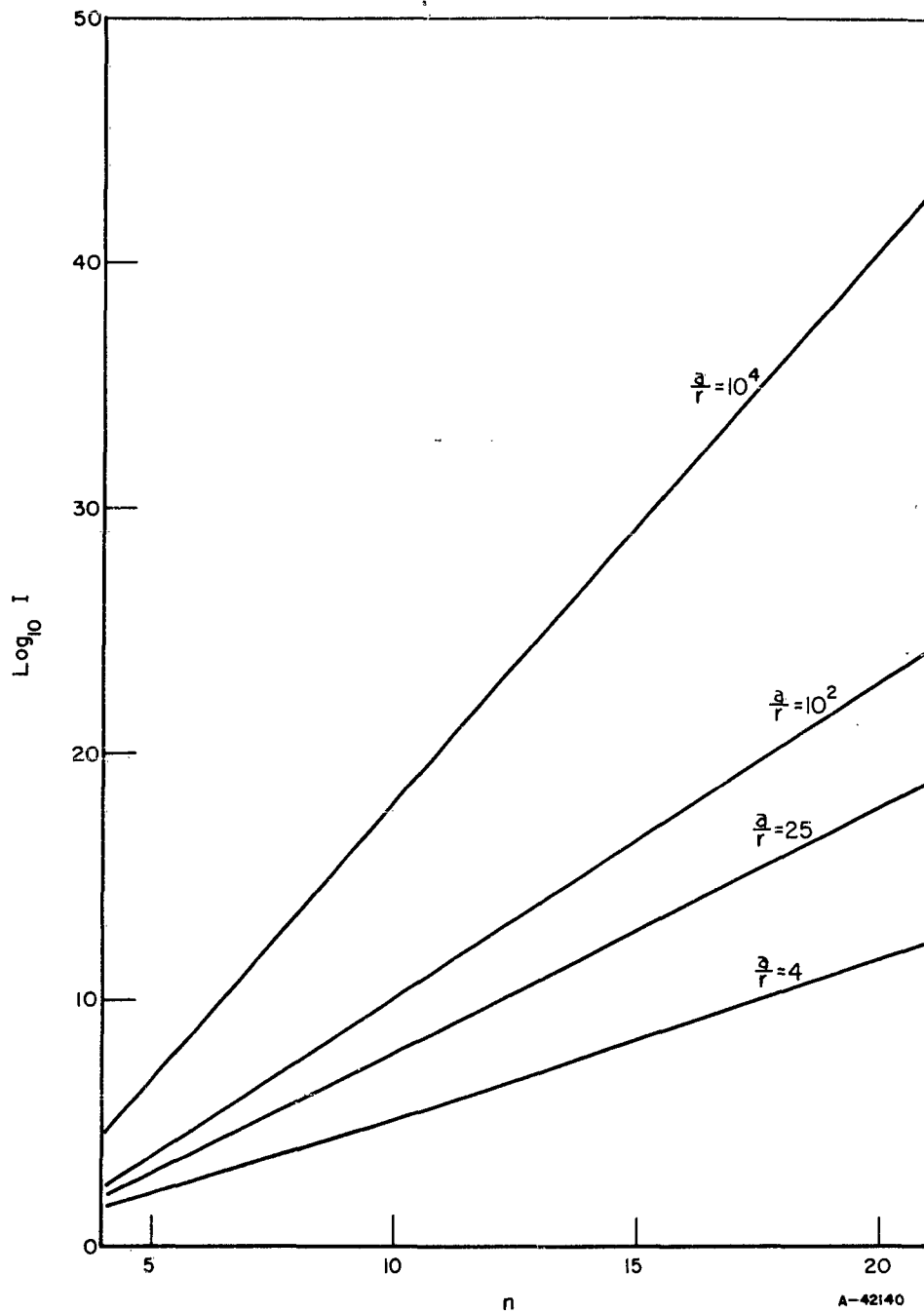


FIGURE 37. THE VALUE OF THE INTEGRAL I AS A FUNCTION OF THE DISLOCATION-VELOCITY PARAMETER n FOR DIFFERENT VALUES OF a/r , THE CRACK-PLASTIC ZONE GEOMETRY

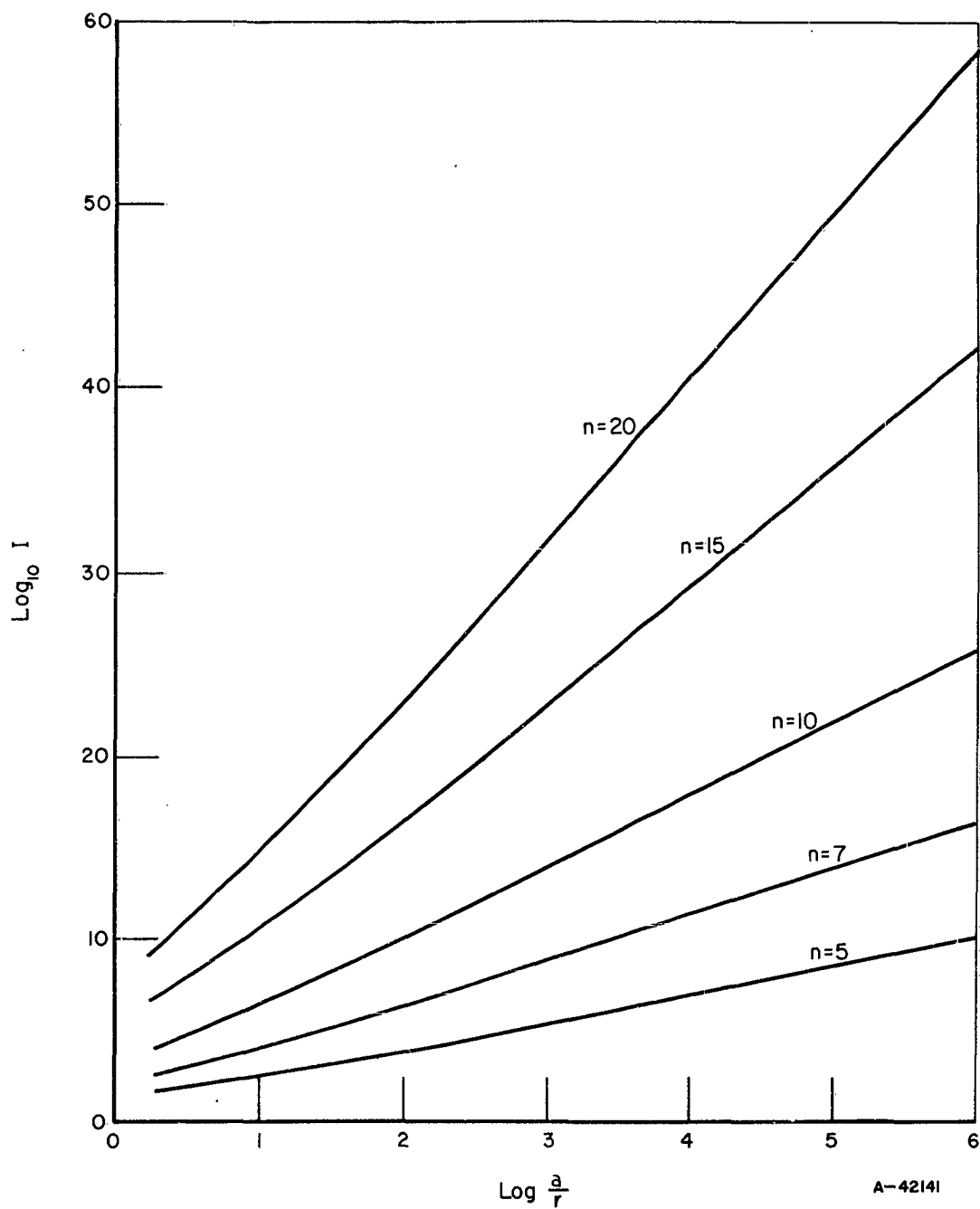


FIGURE 38. THE VALUE OF THE INTEGRAL I AS A FUNCTION OF a/r , THE CRACK-PLASTIC ZONE GEOMETRY, FOR DIFFERENT VALUES OF THE DISLOCATION VELOCITY PARAMETER n

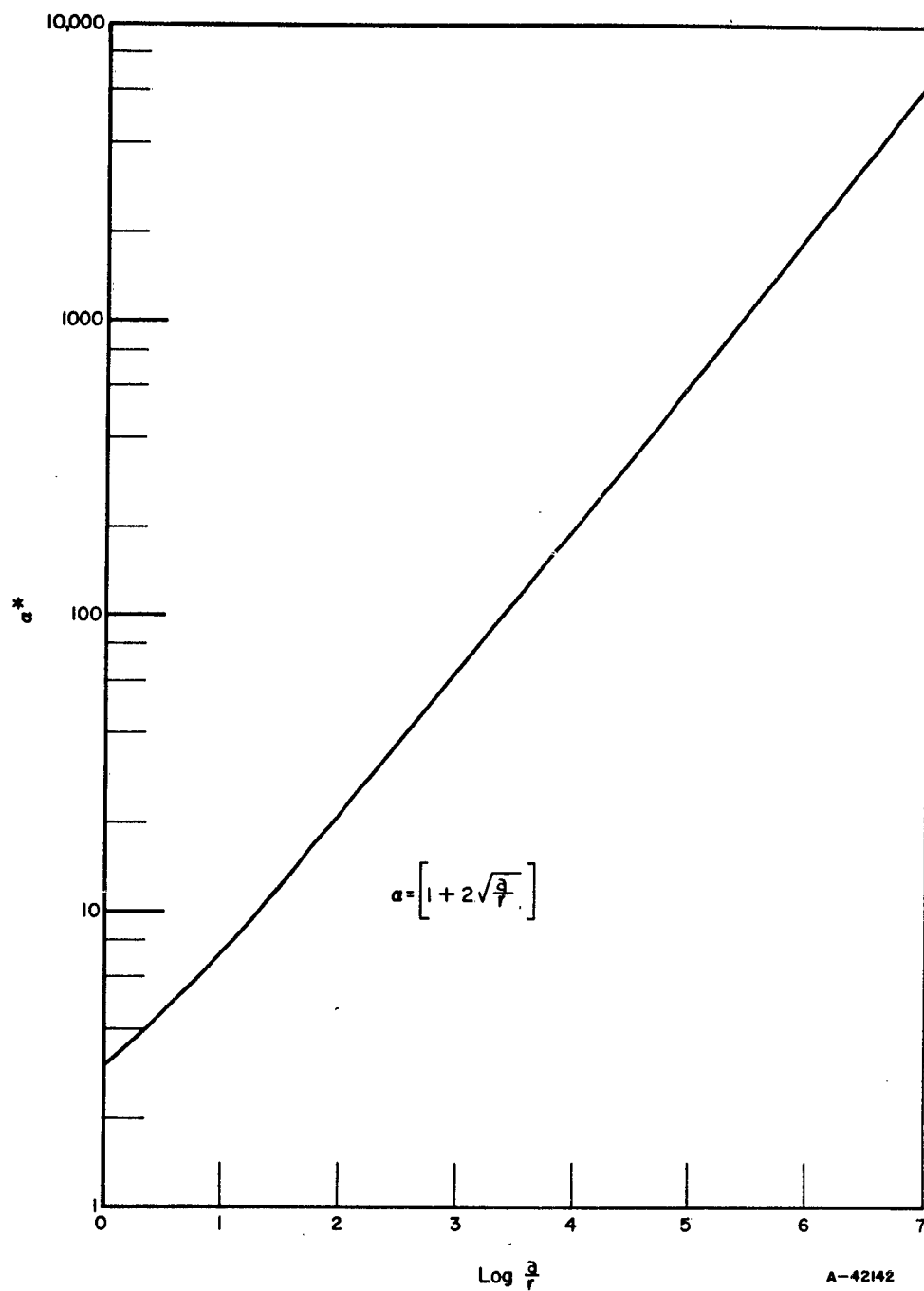


FIGURE 39. THE RELATION BETWEEN α^* , THE MAXIMUM STRESS CONCENTRATION AT THE ELASTIC PLASTIC BOUNDARY AND a/r , THE CRACK-PLASTIC ZONE

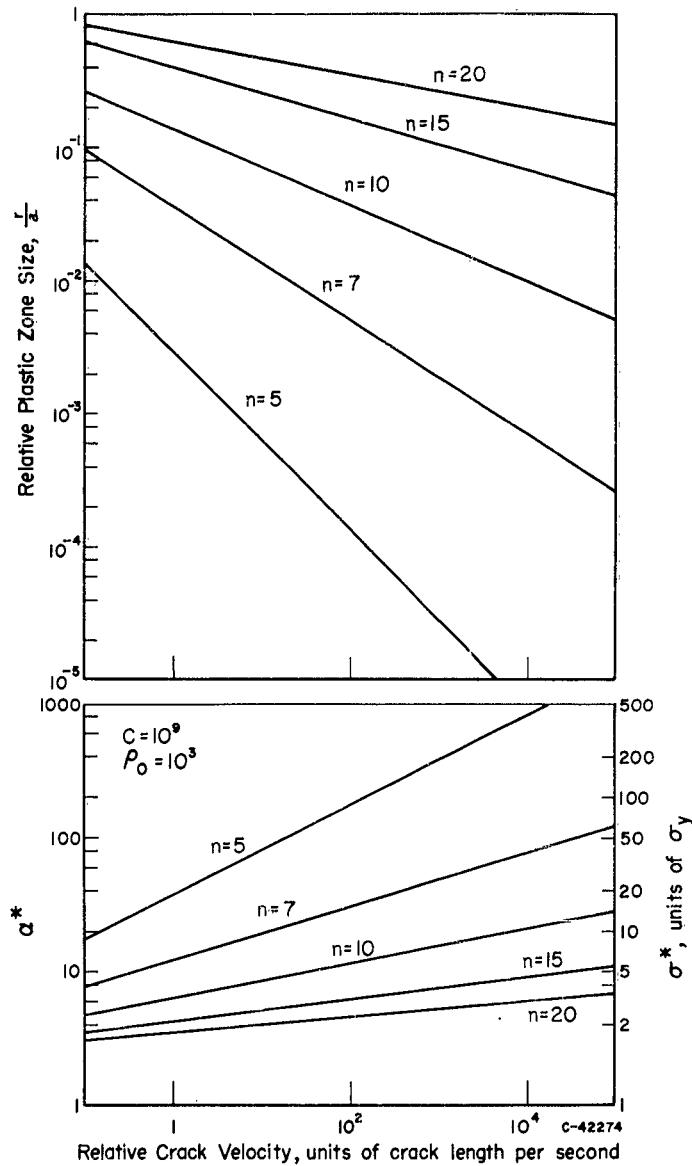


FIGURE 40. THE INFLUENCE OF THE DISLOCATION PARAMETER n ON THE RELATIVE PLASTIC ZONE SIZE a/r , THE MAXIMUM STRESS-CONCENTRATION FACTOR α^* , AND THE MAXIMUM STRESS σ^* IN ADVANCE OF A MOVING CRACK ACCORDING TO EQUATION (26) ($\sigma_y/\sigma_{nom} = 2$, $\rho_0 = 10^3$, $C = 10^9$, $f = 0.1$, $\epsilon_y = 10^{-3}$, $\epsilon_p^* = 10^{-3}$, $\dot{\epsilon}_p = 10^{-3}/\text{sec}$)

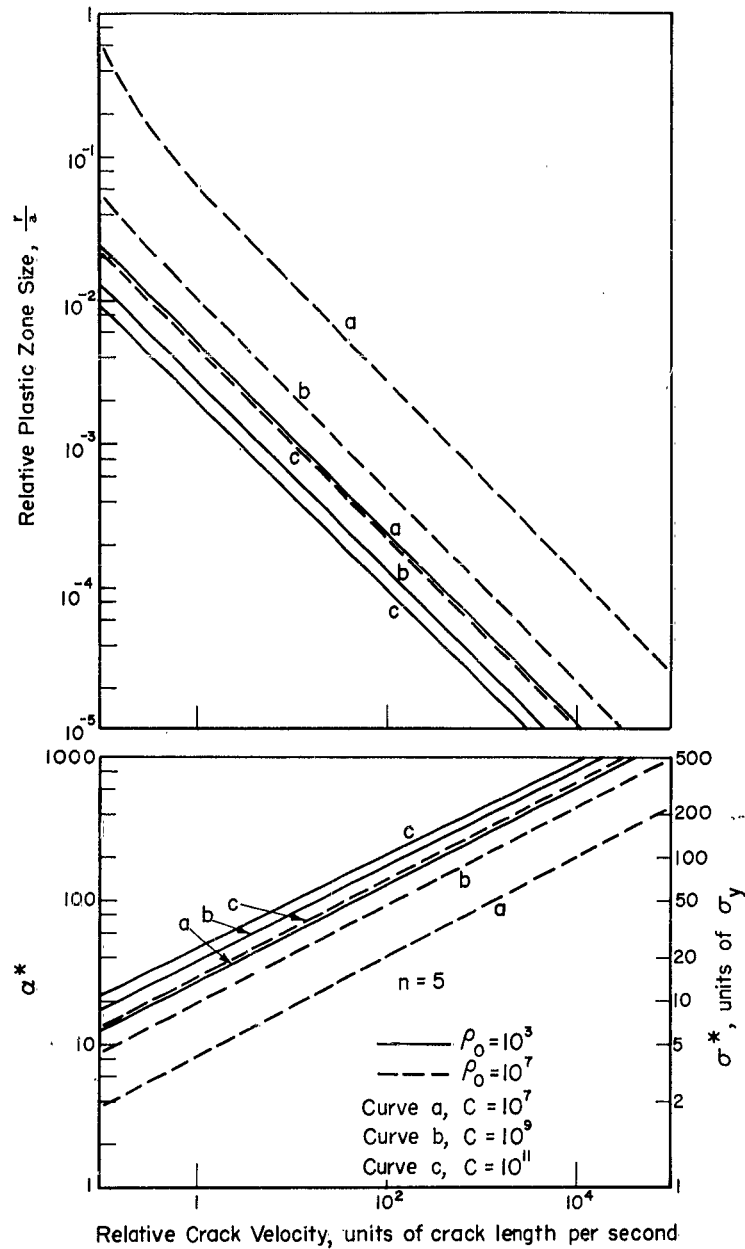


FIGURE 41. INFLUENCE OF THE MULTIPLICATION RATE C AND INITIAL MOBILE DISLOCATION DENSITY ρ_0 ON THE RELATIVE PLASTIC-ZONE SIZE a/r , THE MAXIMUM STRESS-CONCENTRATION FACTOR α^* , AND THE MAXIMUM STRESS σ^* IN ADVANCE OF A MOVING CRACK ACCORDING TO EQUATION (26) ($\sigma_y/\sigma_{nom} = 2$, $n = 5$, $f = 0.1$, $\epsilon_y = 10^{-3}$, $\epsilon_p^* = 10^{-3}$, $\dot{\epsilon}_p = 10^{-3}/\text{sec}$)

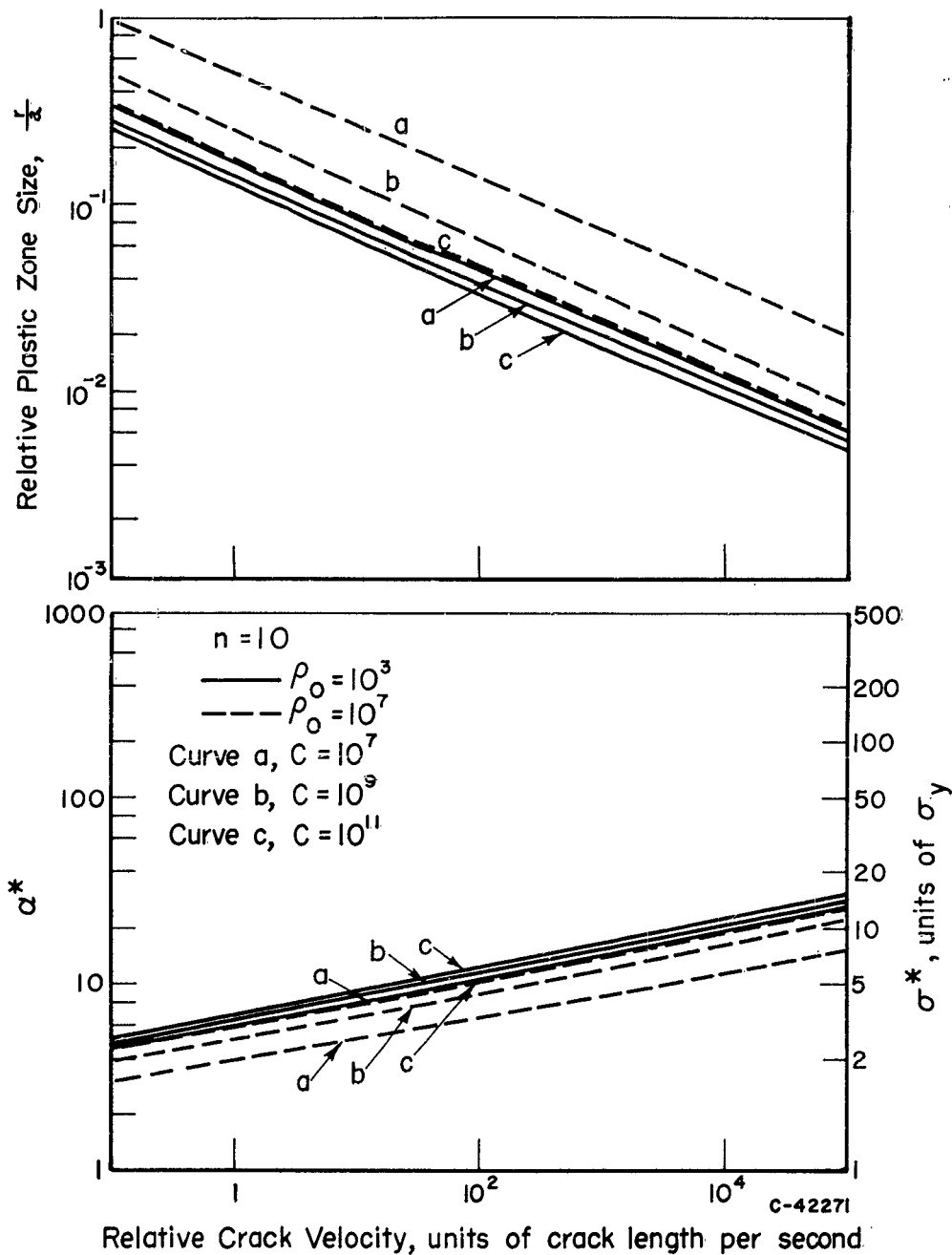


FIGURE 42. INFLUENCE OF THE MULTIPLICATION RATE C AND THE INITIAL MOBILE DISLOCATION DENSITY ρ_0 ON THE RELATIVE PLASTIC-ZONE SIZE a/r , THE MAXIMUM STRESS-CONCENTRATION FACTOR α^* , AND THE MAXIMUM STRESS σ^* IN ADVANCE OF A MOVING CRACK ACCORDING TO EQUATION (26) ($\sigma_y/\sigma_{nom} = 2$, $n = 10$, $f = 0.1$, $\epsilon_y = 10^{-3}$, $\epsilon_p^* = 10^{-3}$, $\dot{\epsilon}_p = 10^{-3}/\text{sec}$)

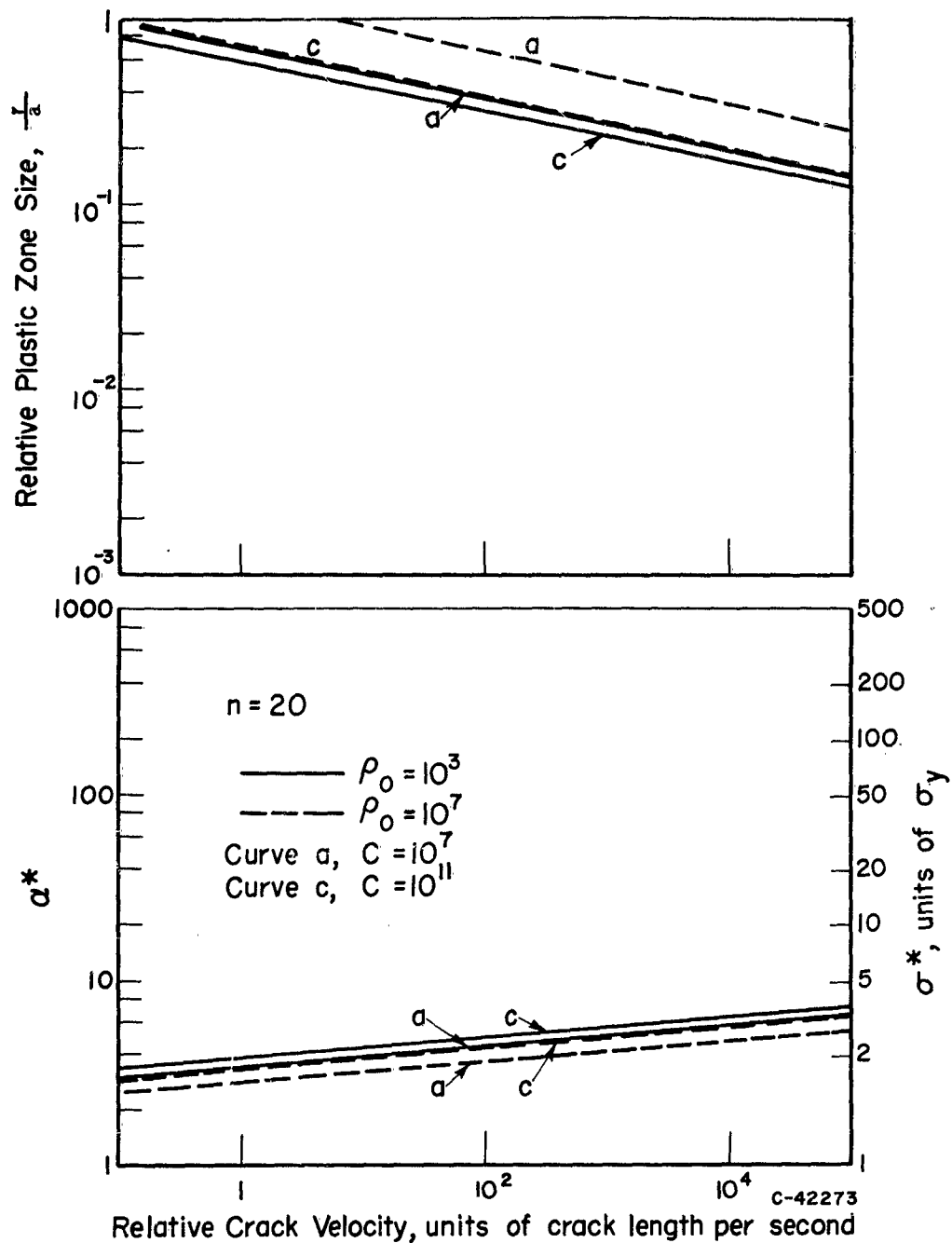


FIGURE 43. INFLUENCE OF THE MULTIPLICATION RATE C AND THE INITIAL MOBILE DISLOCATION DENSITY ρ_0 ON THE RELATIVE PLASTIC-ZONE a/r ON THE MAXIMUM STRESS-CONCENTRATION FACTOR α^* , AND THE MAXIMUM STRESS σ^* IN ADVANCE OF A MOVING CRACK ACCORDING TO EQUATION (26) ($\sigma_y/\sigma_{nom} = 2$, $n = 20$, $f = 0.1$, $\epsilon_y = 10^{-3}$, $\epsilon_p^* = 10^{-3}$, $\dot{\epsilon}_p = 10^{-3}/\text{sec}$)

- (1) Crack Velocity. The model predicts a progressively smaller plastic zone and larger values of σ^* with increasing crack velocity. In effect, higher crack speeds reduce the time available for plastic relaxation, and, consequently, the amount of relaxation preceding fracture. Since the "blunting" of the crack is thereby reduced, the maximum stress σ^* in advance of the crack increases with crack speed. This is shown in Figures 38 through 41.
- (2) Crack Length. Figures 40 through 43, which describe plastic-zone size in terms of the relative crack velocity, imply that increasing the crack length at a given absolute crack velocity is equivalent to reducing the relative crack velocity. Accordingly, larger cracks possess disproportionately larger plastic zones and are less effective stress concentrators. This result is simply a manifestation of the crack-stress field geometry prescribed by the Inglis solution - that the extent of the stress field is proportional to the crack length.
- (3) Dislocation-Velocity Characteristics. Both the increase in σ^* and the reduction in plastic-zone size effected by increasing crack speed become more marked as the value of n decreases. This is illustrated in Figure 38. Particularly dramatic effects are evident when the value of n is in the range 5 to 7. In this case, σ^* , the maximum stress in advance of a fast-moving, 1-cm crack, i. e., $u = 10^3$ to 10^4 cm/sec, is of the order of $100 \sigma_y$, and the predicted plastic-zone size, less than 10^{-3} cm, is smaller than the grain diameter. On the other hand, when n is 15 to 20, σ^* is only 3 to $4 \sigma_y$, and the radius of the plastic zone is about 100 times the grain diameter. The model thus points up, in quantitative terms, that rate-sensitive materials (those characterized by small values of n) although capable of plastic flow: (1) do not relax as quickly, (2) are, therefore, subjected to higher stresses by a moving crack, and (3) are potentially more notch sensitive.
- (4) Initial Dislocation Density. Figures 41 to 43 show the effect on plastic-zone size and stress of two values of ρ_0 , $\rho_0 = 10^3$ and $\rho_0 = 10^7$, believed appropriate for the case when the dislocations present initially are substantially locked and unlocked, respectively. The model shows that a small value of ρ_0 , e. g., locking, tends to retard plastic relaxation and leads to smaller plastic zones and higher stresses. This result is entirely consistent with the oft stated view that dislocation locking enhances brittleness. However, the model also shows that these effects of locking depend on the other dislocation parameters, and are much more pronounced when n and C are small. For example, the increase in σ^* accompanying locking (reduction of ρ_0 from 10^7 to 10^3) is 300 per cent when $n = 5$ and $C = 10^7$, but only 15 per cent when $n = 20$ and $C = 10^9$.
- (5) Dislocation Multiplication. The curves presented in Figures 41 to 43 show that plastic relaxation is progressively retarded when the rate of dislocation multiplication C increases. This result is surprising and requires further comment. The source of the effect resides in the

selection of the fixed ratio $\frac{\sigma_y}{\sigma_{nom}} = 2$, to define the nominal stress imposed on the model in all the calculations. Examination of Equation (23a) actually shows the expected result, namely, that increasing the multiplication rate C should enhance the relaxation rate when the ratio $\frac{\sigma_0}{\sigma_{nom}}$ is kept constant. Since σ_y is inversely related to C [see Equation (23a)], increasing values of C for a constant ratio of $\frac{\sigma_y}{\sigma_{nom}}$ thus imply a decrease in the value of σ_{nom} . It is this reduction in σ_{nom} that is, in fact, responsible for the decrease in plastic-zone size and the higher stress values shown by the results.

- (6) Mechanism of Propagation. According to the model, when $n < 7$ the maximum stress generated at the tip of a fast-moving crack can exceed the theoretical strength, i. e., about $100 \sigma_y$ for polycrystalline metals. In this case crack propagation can proceed in a continuous manner simply by the separation of atoms close to the crack tip. However, when $n > 10$, σ^* is about $10 \sigma_y$ or less, and crack propagation can proceed only if an additional stress-concentrating device, such as a slip band or twin, is operative. Under these conditions, propagation probably occurs by the repeated initiation of cracks ahead of the main fracture.

Predictions specific to the refractory metals, tungsten, molybdenum, and columbium, calculated for the dislocation parameters given in Table 5 are summarized in Figure 44. In this form, the predictions cannot readily be tested. However, they can be used to estimate the limiting temperatures for the penetration of a brittle crack of specified length and velocity, i. e., a transition temperature, which then can be compared with the results of notch tests. For this purpose, it is assumed (1) that the brittle fracture stress σ_F valid for material in advance of a moving crack is the same as the brittle fracture stress displayed by bulk samples, e. g., the brittle fracture stress at low temperatures, and (2) that σ_F is relatively insensitive to temperature. The limiting condition for crack penetration then, is:

$$\sigma_F = \sigma^* = \sigma_y(T) \frac{\alpha^*}{2}, \quad (30)$$

where $\sigma_y(T)$ is the lower yield stress at the transition temperature (the factor 2 is a consequence of the condition $\frac{\sigma_y}{\sigma_{nom}} = 2$ adopted for the present calculations). The quantity $\sigma_y(T)$ calculated directly from Equation (30) for a specific crack length and velocity condition, then identifies the transition temperature, provided the temperature dependence of σ_y is known. Results of such calculations for a 1-cm crack propagating at two extremes of crack velocity, $u = 1$ cm/sec and $u = 10^4$ cm/sec, for the data shown in Figure 44 and fracture and yield stress values in the literature are summarized in Table 9. In the same table, the model predictions for columbium, molybdenum, and tungsten are compared with the fracture appearance transition temperatures derived from precracked specimens in the fracture toughness studies. Table 9 shows that the model not only predicts the transition temperatures in the correct order, but that the values calculated for a 1 cm-1 cm/sec crack criterion are in excellent agreement with the actual measurements. The agreement is not unreasonable since the 1 cm-1 cm/sec

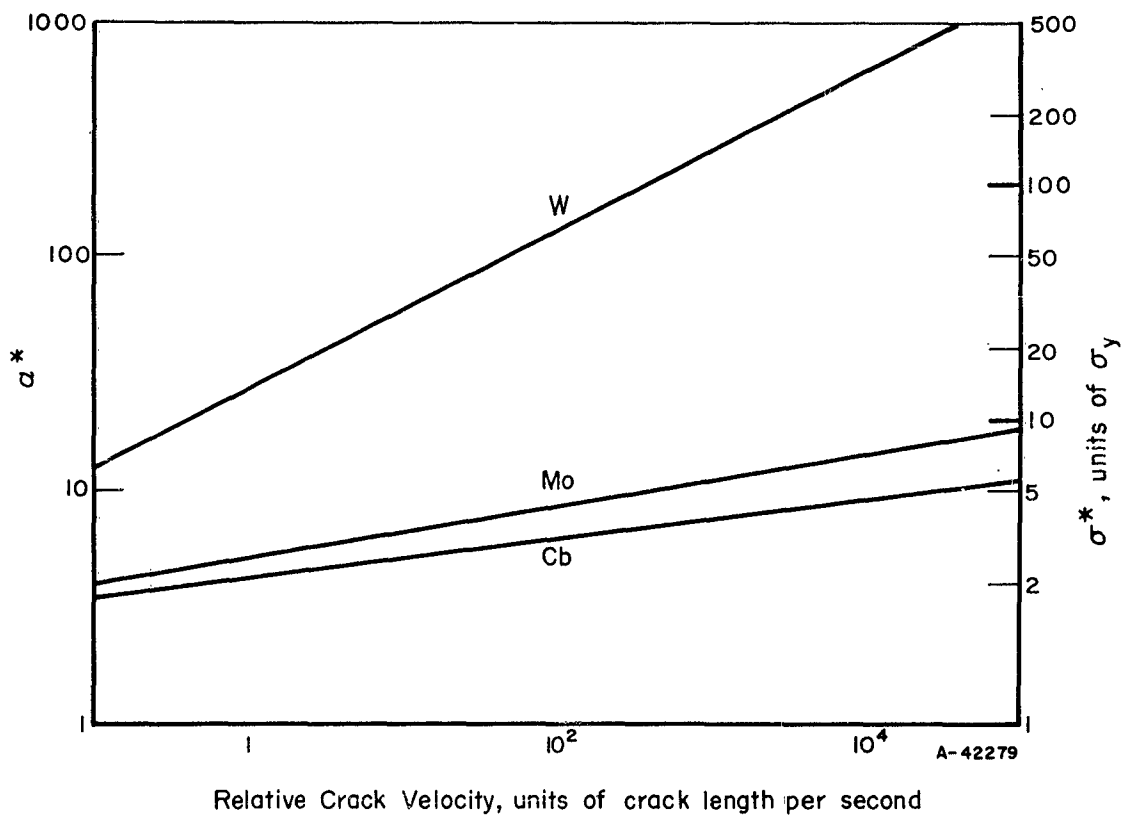


FIGURE 44. MAXIMUM STRESS CONCENTRATION FACTOR α^* AND MAXIMUM STRESS IN ADVANCE OF A MOVING CRACK PREDICTED BY EQUATION (26) FOR TUNGSTEN, MOLYBDENUM, AND COLUMBIUM FOR THE DISLOCATION PARAMETERS GIVEN IN TABLE 5 ($\sigma_y/\sigma_{nom} = 2$, $f = 0.1$, $\epsilon_y = 10^{-3}$, $\epsilon_p^* = 10^{-3}$, $\dot{\epsilon}_p^* = 10^{-3}/\text{sec}$)

criterion probably approximates the conditions preceding crack instability in tests of precracked specimens. The $1 \text{ cm}-10^4 \text{ cm/sec}$ criterion is believed to be appropriate for experiments where brittle cracks are injected at high speeds into the test material, such as in the drop-weight or in Robertson-type tests. It should be noted that calculations of the type presented in Table 5 must employ values of the dislocation parameters, n , C , ρ_0 , etc., valid at the transition temperature. Since the present calculations rely on values known to be valid only at room temperature, predicted transition temperatures differing significantly from the ambient may be in error.

TABLE 9. BRITTLE-CRACK-PENETRATION TRANSITION TEMPERATURES PREDICTED FOR SLOW AND FAST-MOVING CRACKS AND MEASURED FOR PRECRACKED TENSILE SPECIMENS

Metal	σ_F , psi	Crack Velocity $\mu = 1 \text{ cm/sec}$			Crack Velocity $\mu = 10^4 \text{ cm/sec}$			Fracture-Appearance Transition Temperature ^(a) , C
		a^*	$\sigma_y(T)$, psi	Temp, C	a^*	$\sigma_y(T)$, psi	Temp, C	
Columbium(28)	100,000	4.4	45,000	-100	9	22,000	40	<-196
Molybdenum(29)	100,000	5.0	40,000	130	14	14,000	400-500	150
Tungsten(30)	120,000	26	7,700	450	600	400	>1000	400-500

(a) See section entitled Fracture-Toughness Studies.

Strictly speaking, the present treatment of crack propagation examines the properties of a relatively simple model. The model simulates: (1) a stress environment similar to the one existing in advance of a crack and (2) rates of plastic relaxation similar to those of metals. Insight to the interplay of stress and plasticity given by the model, in all likelihood, is qualitatively sound. For example, the cited agreement with experiment supports the finding that properties governing rate of relaxation, particularly the value of n , have an important bearing on crack-propagation resistance. However, predictions specific in quantitative terms must be treated with caution for several reasons. First, the shape of the plastic zone and other assumptions implicit in the mechanics treatment are untested. Plane-stress conditions are likely to be met only while the plastic-zone size is comparable to the plate thickness. Relativistic effects at high crack velocity have so far been neglected. The formulation of plastic flow also involves simplifying assumptions and uncertain extrapolations. In nearly all cases, the important dislocation parameters are as yet poorly defined. Finally, very little is known about the requirements for fracture at the crack tip. More information must be gathered before predictions that are really meaningful can be made and tested.

Determination of Dislocation Parameters for Molybdenum Relevant to the Crack-Propagation Model

In order to apply the concepts of crack propagation developed in this section, a knowledge of the relevant dislocation-multiplication and dislocation-velocity parameters is required. Three parameters are obtainable by experiment. The parameters C and β characterizing dislocation multiplication in the formula

$$\rho = (\rho_0 + C\epsilon_p^\beta) \text{ [see Equation (15)]}$$

are obtainable by transmission electron microscopy. The parameter n in the formula

$$\bar{v} = \left(\frac{\sigma}{\sigma_0} \right)^n \text{ [see Equation (17)]}$$

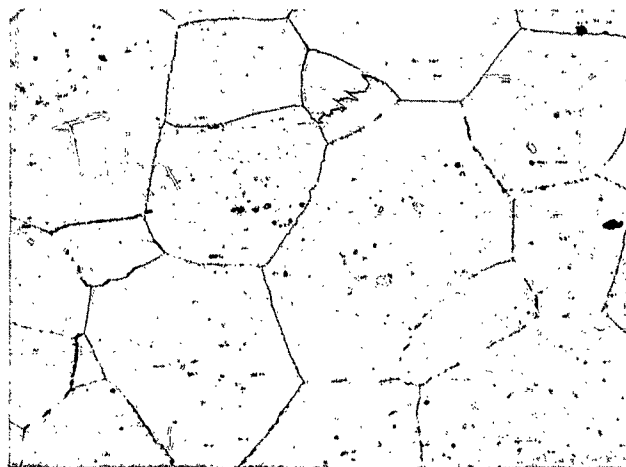
can be obtained either directly by etch pitting or indirectly by a number of techniques.

In order to completely derive the parameters for one material, and to compare the predictions of the model with experiments performed in the metallurgical-variables and fracture-toughness studies, experimental work in this phase was restricted to the molybdenum bar stock described in Table 1. The work was performed on two grain sizes, 0.02 mm and 0.16 mm mean linear intercept. The heat treatments used to produce these grain sizes are described in Table 2.

Dislocation-Density Measurements

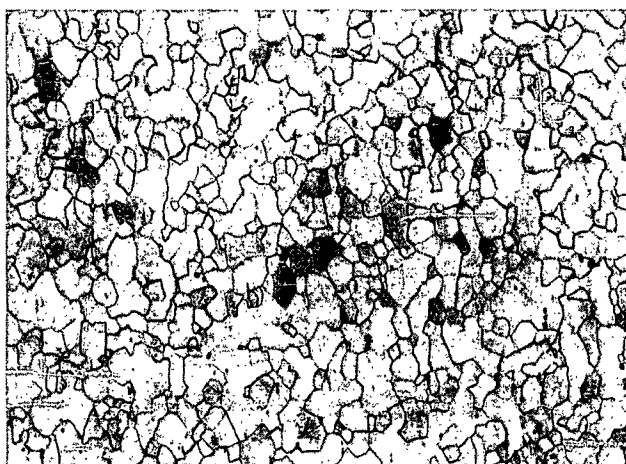
In order to determine the variation of dislocation density with strain, coarse-grained samples were strained 1/2, 2-1/2, and 7 per cent in an Instron testing machine at a strain rate of 2×10^{-5} /sec. Foils for transmission microscopy were prepared from these and also from annealed material by the following technique: specimens in the form of disks about 30 mils thick were cut from a tensile specimen perpendicular to its axis. This was done either using a cutoff wheel or more recently by use of an electrolytic jet of liquid constrained to the shape of a fan, thus acting as a cutting blade. These disks of about 1/8-inch diameter were then electrolytically jet indented on both faces, using a solution of 10 per cent nitric acid in water. With this solution and 1/16-inch-diameter jet, an applied voltage of 120 produced a current of 0.6 ampere. This technique left the foils with a thicker rim which had sufficient mechanical rigidity to permit subsequent handling of the foil without the introduction of fresh dislocations. The 4-mil-thick center section was then electrolytically thinned, using a solution of sulfuric acid to methyl alcohol in the ratio 1:3. This last step was carried out under a binocular microscope, the foil being illuminated from below. With this arrangement it was possible to detect the appearance of the first hole at an early stage, and to stop the attack before the thinned regions surrounding the hole were also polished away. The foil was then ready for examination in the electron microscope. The dislocation-density determinations were made by the lineal count method⁽³¹⁾ carried out on electron-transmission photographs. Up to 20 individual photographs were taken for any given strain, and on each photograph at least six counts were made. Polished and etched samples were also examined metallographically, in both the fine- and coarse-grained condition. Samples were prepared with a flat electropolished surface which was then chemically etched using a 1:1 mixture of 30 per cent potassium ferricyanide and 10 per cent sodium hydroxide for about 10 seconds.

Typical light micrographs of both grain sizes are presented in Figure 45. It is apparent that the coarse-grained material has a much greater density of intragranular inclusions (presumably carbide), than has the fine-grained, and that the inclusions are generally larger. Figure 46 is a similar area at greater magnification. In the etch-pitting studies, the regions surrounding inclusions in the coarse-grained material showed evidence of having a higher density of etch pits than had the matrix generally,



130X

a. Coarse Grained



130X

b. Fine Grained

FIGURE 45. TYPICAL MICROSTRUCTURES OF THE COARSE- AND FINE-GRAINED MATERIAL



650X



650X

FIGURE 46. MICROSTRUCTURES SHOWING THE DIFFERENCE IN PRECIPITATE DISTRIBUTION IN THE COARSE- AND FINE-GRAINED MOLYBDENUM

suggesting that the inclusions act as sources of dislocations. In the fine-grained material, there was little evidence of such an effect. Typical micrographs of this etch-pitting work are presented in Figure 47.

Electron-transmission studies on the areas surrounding inclusions confirmed the role of inclusions in the generation of free dislocations. This effect was most apparent in the annealed condition, and the inclusion distribution in the fine- and coarse-grain sizes offers an interesting comparison. The fine-grain size material, shown in Figure 48, contained only small inclusions, and these generally were located at grain boundaries where they seemed to have little or no effect as sources of dislocations, or as precipitates along dislocation lines. In the coarse-grained material however, the precipitates were much larger and were frequently surrounded by dislocations, the density of which was much higher than in the matrix areas free of inclusions. Examples of these areas are presented in Figure 49.

Figure 50 presents typical dislocation densities at the various strains, and the results of the density measurements are presented in Figure 51. Included in the same diagram are the results of Benson, Thomas, and Washburn⁽¹⁶⁾, published since the inauguration of this work, for comparison. The agreement is good, and a line drawn through all the points gives rise to the following values of the parameters:

$$\rho_0' = 4 \times 10^8$$

$$\beta = 1$$

$$C = 7.2 \times 10^8 .$$

Measurements of Stress Dependence of Velocity

In this first year's work it was intended to correlate various indirect methods of determining n with the direct method, which is by stressing and etch pitting. The direct method however is the most difficult to accomplish experimentally and so far no determination of n has been made by this means. The main experimental difficulty is the presence of large amounts of precipitate, even in a zone-refined single crystal. It is hoped in the continuation of this work to obtain a more pure starting material and, by zone refining, to produce a crystal with a much lower ρ_0' than is possible with the present material. This section is therefore concerned with the various indirect techniques for deriving n , and the results are summarized in Table 6.

The Strain-Rate Dependence of the Lower Yield Stress. Referring to Equation (23a) in the earlier part of this report, the strain-rate dependence of the stress at zero plastic strain, i. e., the yield stress, can be expressed by:

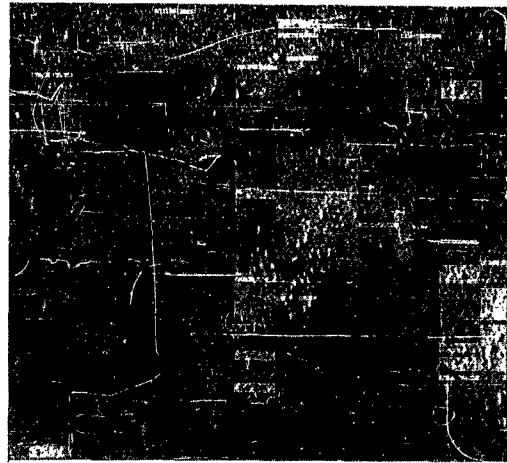
$$\sigma_y = \sigma_0 \left[\frac{\dot{\epsilon}_p}{0.5 \text{ bf } \rho_0} \right]^{\frac{1}{n}} \quad (31)$$

or

$$\ln \sigma_y = \ln A + \frac{1}{n} \ln \dot{\epsilon} , \quad (32)$$



1000X



1000X

a. Etch Pits Surrounding Inclusions in the Coarse-Grained Molybdenum



1000X

b. Random Etch Pits in Fine-Grained Molybdenum

FIGURE 47. TYPICAL ETCH-PITTING RESULTS

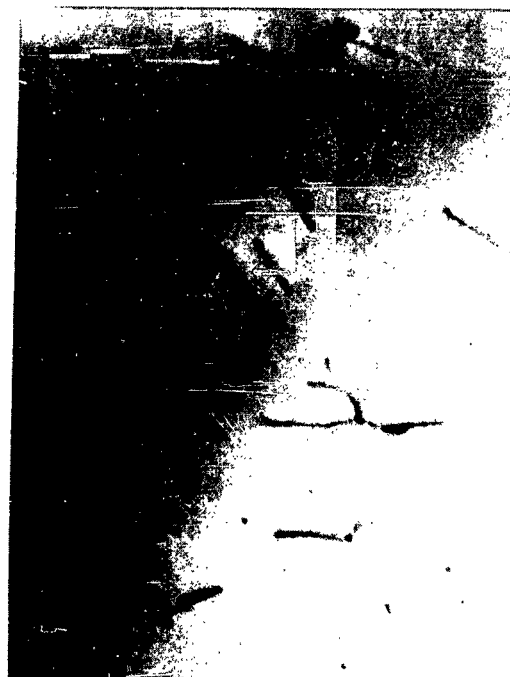
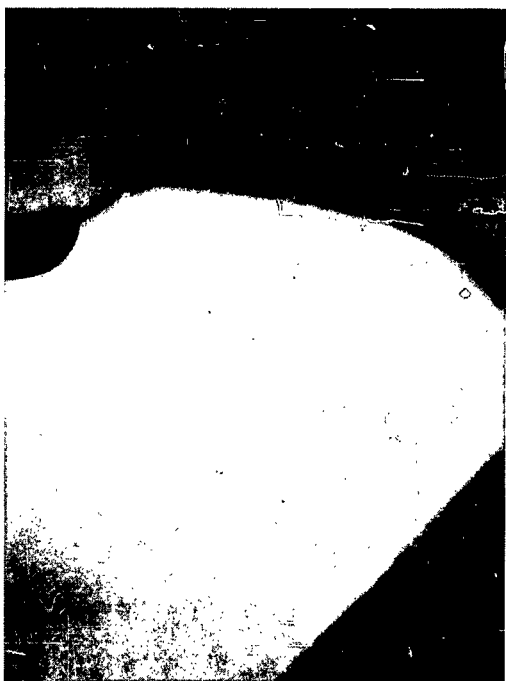
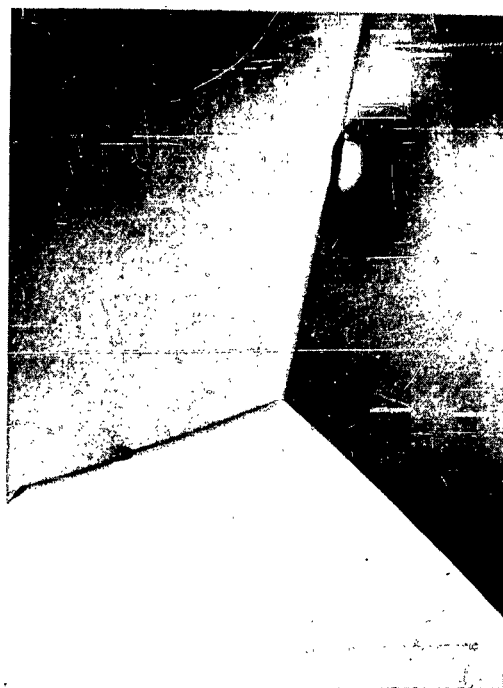


FIGURE 48. TRANSMISSION ELECTRON MICROGRAPHS OF FINE-GRAINED MOLYBDENUM IN THE ANNEALED CONDITION

Magnification 24,000X

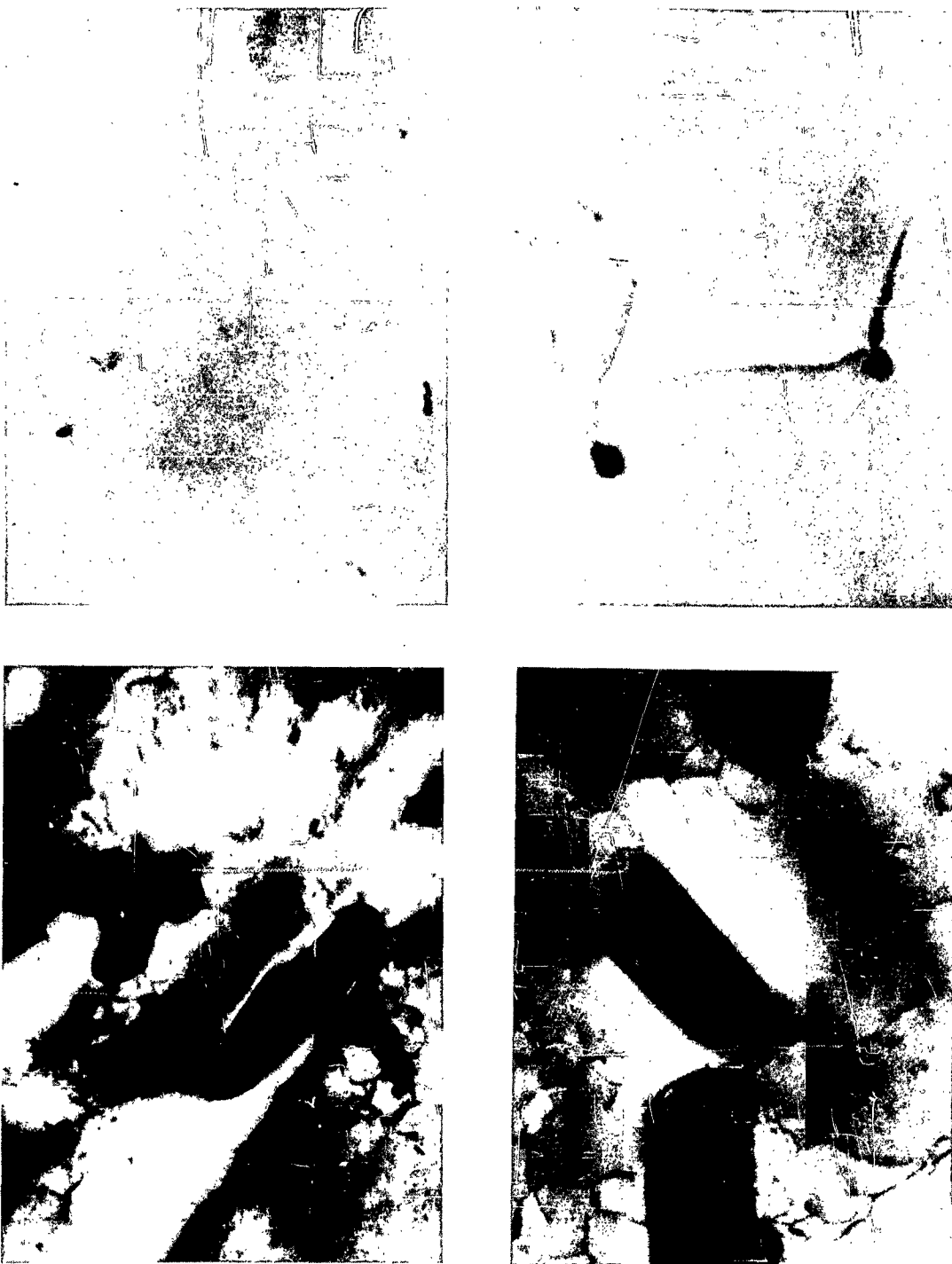
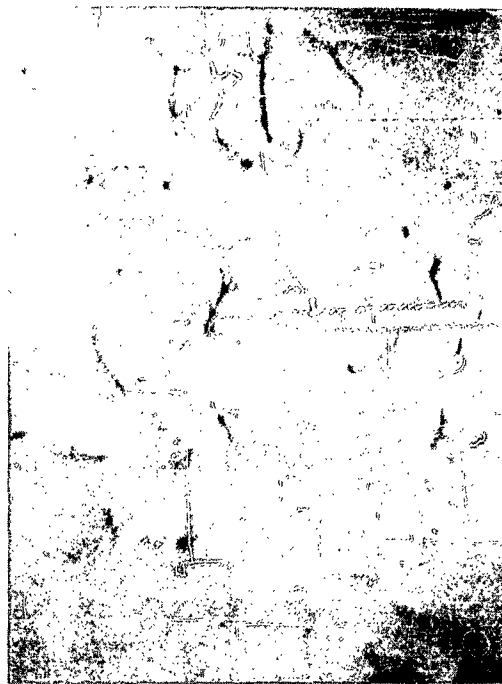


FIGURE 49. TRANSMISSION ELECTRON MICROGRAPHS OF COARSE-GRAINED MOLYBDENUM IN THE ANNEALED CONDITION, SHOWING THE EFFECT OF INCLUSIONS

Magnification 24,000X



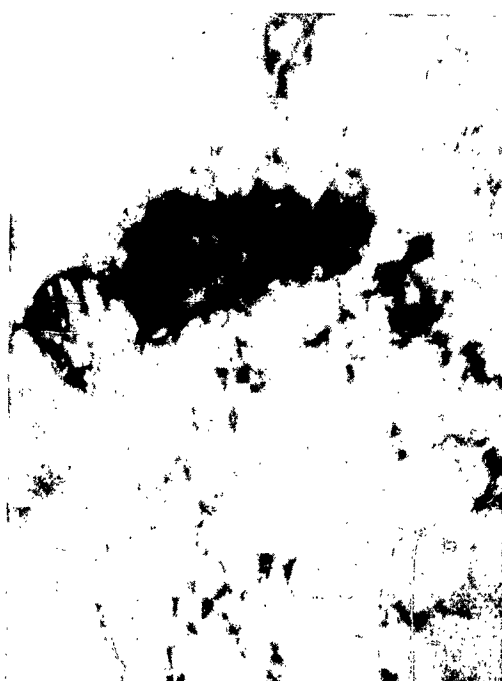
a. 0 Per Cent Strain



b. 1/2 Per Cent Strain



c. 2-1/2 Per Cent Strain



d. 7 Per Cent Strain

FIGURE 50. TYPICAL DISLOCATION DENSITIES IN COARSE-GRAINED MOLYBDENUM AT VARIOUS STRAINS

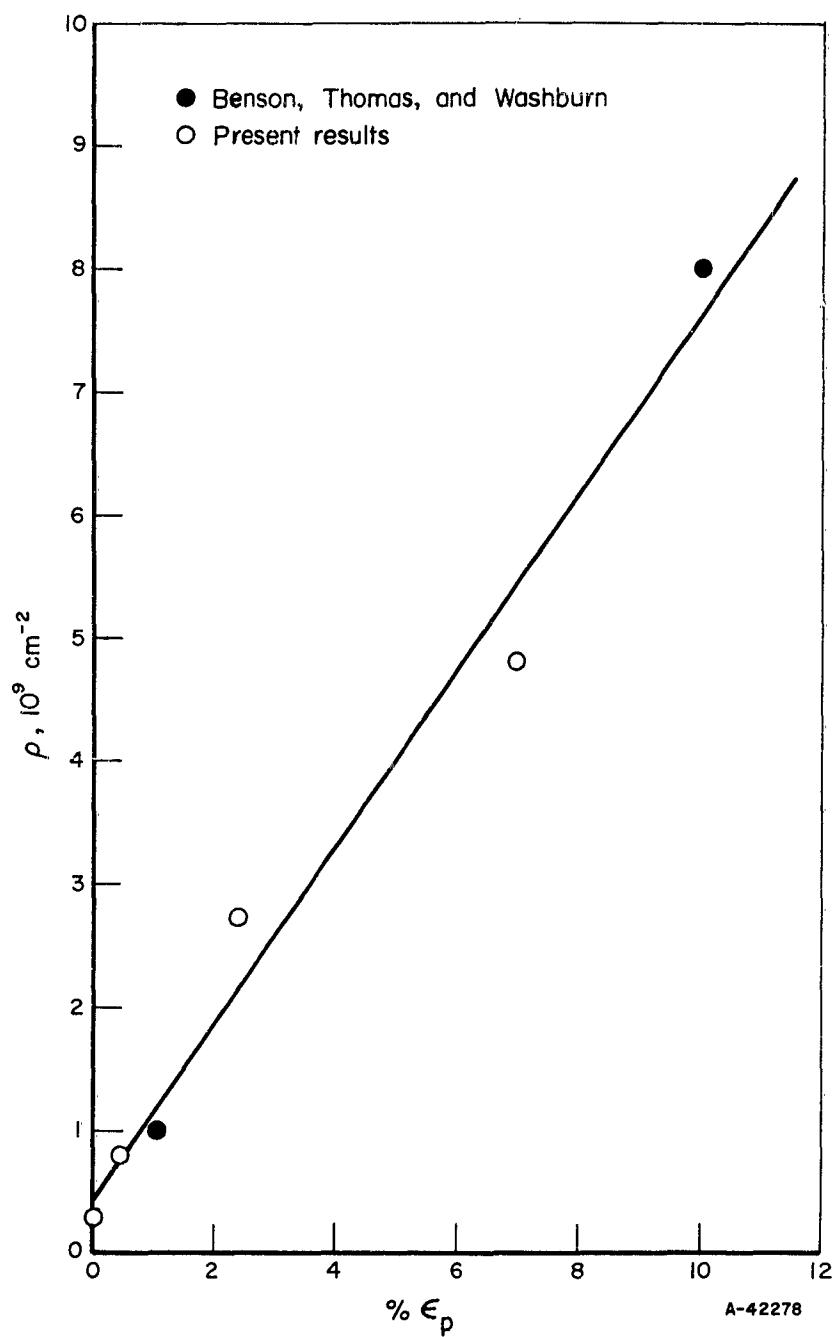


FIGURE 51. VARIATION OF DISLOCATION DENSITY WITH STRAIN IN COARSE-GRAINED MOLYBDENUM

where $A = \sigma_0 (0.5 b \rho_0)^{-\frac{1}{n}}$.

Thus:

$$n = \frac{d(\ln \dot{\epsilon}_p)}{d(\ln \sigma_y)} \quad (33)$$

Experimentally this means that if we plot the variation of yield stress with strain rate on a log-log scale, the results should lie on a straight line of gradient n . To avoid confusion, let us call the slope of the line m . If the assumptions of the model are correct, then m should equal n .

Tensile tests were performed on an Instron testing machine which permitted a range of crosshead speeds and autographically recorded the resultant stress-strain history of the specimen. The strain-rate dependence of the yield stress was determined for both grain sizes over the range .002 to 2 inch per minute crosshead speed.

Tensile specimens were machined after annealing in order to remove any contaminated surface layer, and before testing, at least 5 mils was removed from the ground surface by electropolishing. The design of the tensile specimens was as illustrated in Figure 52.

The experimental results are presented in Figures 53 and 54. Each line refers to specimens from the same batch heat treatment, and the number at the side of each point specifies the test concerned. It is apparent that specimens heat-treated under slightly different conditions had different strengths. In Figure 54, the lowest line refers to coarse-grained material, the other lines at the higher stress levels are for fine-grained material. The inverse slopes of the lines, m , are summarized on the same diagram and it is apparent that, for one heat treatment, although a straight line has been drawn through the points, the points actually tend to lie on a curve which would be convex upwards. In other words, for higher strain rates, m (the reciprocal slope) increases over its value at lower strain rates. Also, at the higher stress levels the average value of m increases. In the model, the basic assumption was made that there existed a unique value of n , and so the fact that m is not constant merits some discussion. Two possible explanations exist for the discrepancy. Either there is not a unique value n or the number of dislocations moving, as well as being a function of strain, may also be a function of strain rate. There is evidence to suggest that the second alternative may be the answer. Returning to the basic equation of flow,

$$\dot{\epsilon}_p \approx b \rho v \approx b \rho \sigma^n$$

$$\log \dot{\epsilon}_p \approx \log \rho + n \log \sigma + \log b \quad (34)$$

or

$$d \log \dot{\epsilon}_p \approx d \log \rho + n d \log \sigma ; \quad (35)$$

thus if ρ does not change with strain rate,

$$n = \frac{d \log \dot{\epsilon}_p}{d \log \sigma}$$

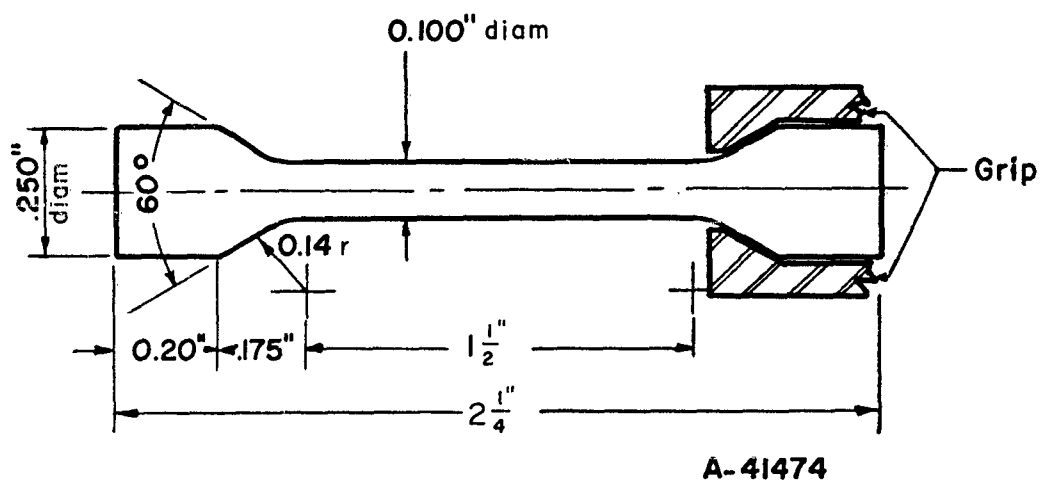


FIGURE 52. DESIGN OF TEST BAR

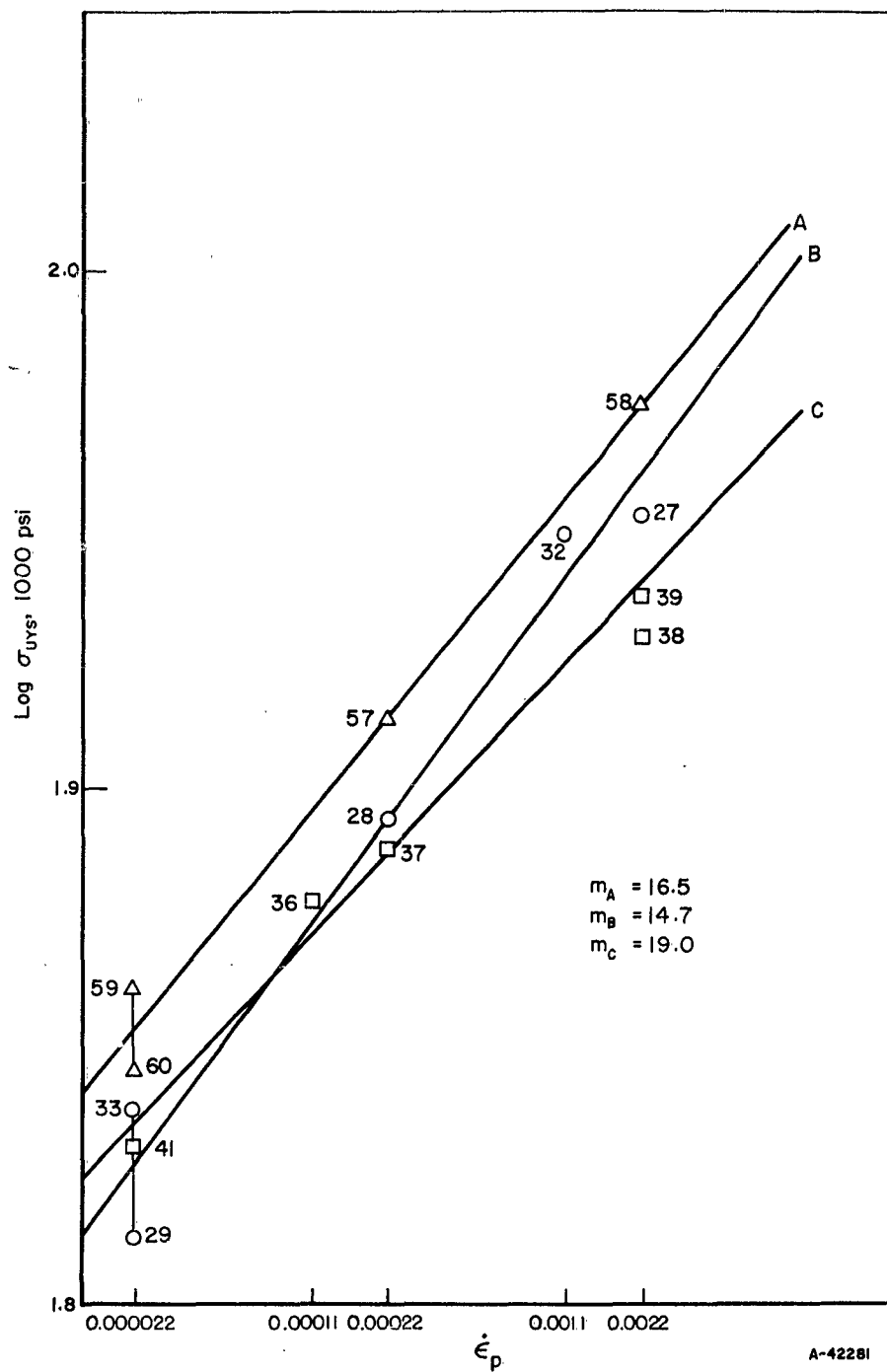


FIGURE 53. VARIATION OF UPPER YIELD STRESS WITH STRAIN RATE IN MOLYBDENUM

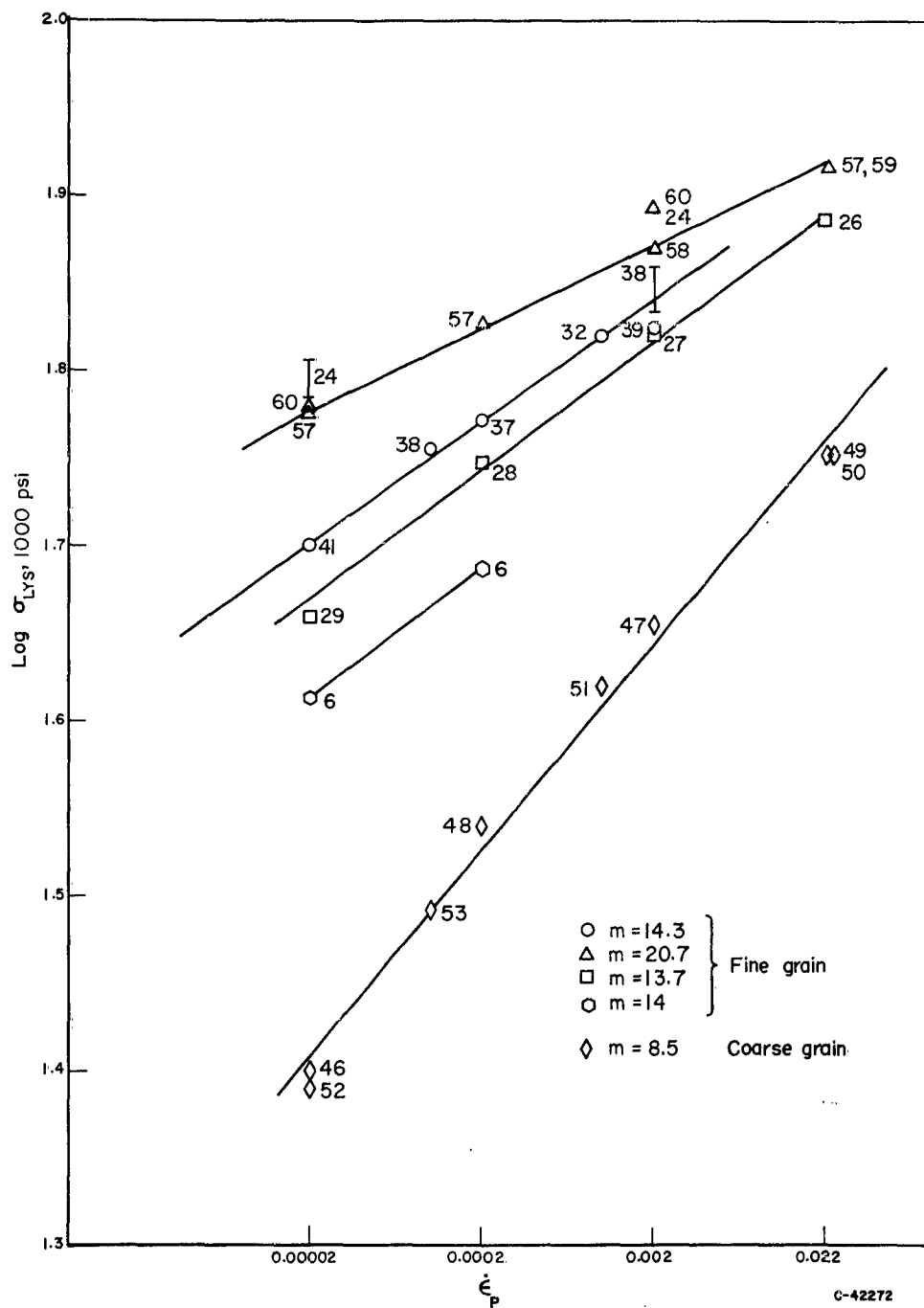


FIGURE 54. VARIATION OF LOWER YIELD STRESS WITH STRAIN RATE IN FINE-GRAIN MOLYBDENUM

However, if ρ is not constant with strain rate, then

$$1 = n \frac{d \log \sigma}{d \log \dot{\epsilon}_p} + \frac{d \log \rho}{d \log \dot{\epsilon}_p} \quad (36)$$

$$1 = \frac{n}{m} + \frac{d \log \rho}{d \log \dot{\epsilon}_p} \quad (37)$$

Since it is found experimentally that m increases with strain rate, then $\frac{n}{m}$ becomes <1 , which means $\frac{d \log \rho}{d \log \dot{\epsilon}_p}$ must be positive. In other words, for a given strain, the dislocation density will be higher, the higher the strain rate used to produce the strain. Evidence of such an effect in steel has been obtained by the present authors. The dislocation density at any strain was found to be about a factor of two greater for tests carried out at 2 inches per minute than for tests at .002 inch per minute. It thus seems entirely plausible that the same situation occurs in molybdenum, explaining the change of m over this range of strain rate.

The equation may also be rewritten(28):

$$\frac{d \log \dot{\epsilon}_p}{d \log \sigma} \approx \frac{d \log \rho}{d \log \sigma} + n, \quad (38)$$

that is,

$$(m - n) = \frac{d \log \rho}{d \log \sigma} \quad (39)$$

Thus the difference between m and n is equal to the dependence of the dislocation density on stress. As was pointed out by Guard(32) it is reasonable to assume that higher stresses cause an increase in the number of moving dislocations, perhaps by "unsticking" dislocations.

Measurement of Lüders' Band-Front Velocity. If we assume that the Lüders' band-front velocity μ is related to the dislocation velocity at the lower yield, then

$$\mu = kv(\sigma = \sigma_y) = k (\sigma_0)^{-n} \sigma_y^n, \quad (40)$$

where k is a constant, assumed to be of order unity.

Thus,

$$n = \frac{d \ln \mu}{d \ln \sigma_y} \quad (41)$$

Again, the experimental approach to this technique is to determine the Lüders' band velocity μ , and plot $\log - \log$ against the band propagation stress.

In principle, if only one band is formed, it should be possible to determine the velocity of the band from tensile test data. In these experiments however, it was very rare that only one band was in motion, and thus it was necessary to take motion pictures of the band during its propagation, and then subsequently determine the band-front

velocity from the film. It was found that if several bands were in motion nominally at the same time, the bands moved discontinuously, and only by filming was it possible to determine the velocity of an individual band during the time it was actually in motion. Even by this technique however, quite a large scatter in the results was unavoidable, and this made the approach difficult to apply. The most satisfactory type of specimen for these filming experiments was found to be a specimen with a ground "flat" on one side, which was then illuminated obliquely by a focused light source. By modifying the position of the light, a good contrast could be obtained at the Lüders' band front.

Figure 55 shows a stress-strain curve typically produced during this type of experiment. The test was started at the strain rate of .002 inch per minute, and the strain rate kept constant until the yield drop had occurred and a Lüders' band had been propagated for some distance along the specimen. The strain rate was then increased by a factor of 10, causing the stress level to rise by the amount necessary to increase the dislocation velocity by a factor of 10. (The small rise preceding this larger one in Figure 55 is due to one band front stopping as it reached the specimen shoulder so causing the dislocation velocity to rise by a factor of two over that necessary for Lüders' propagation by two band fronts.) Before the band had covered the specimen, the strain rate was reduced to the original in order to get a duplicate value. Photographs of the Lüders' bands taken during this propagation are presented in Figure 56.

The results of the method are summarized in Figure 57. In spite of the range of the experimentally determined points, the same trend is apparent in these values of m as in the strain-rate dependence of the yield stress - that is, m is found to be greater at the higher stress levels.

The plastic behavior of the molybdenum was such that the coarse-grained material did not deform by propagation of an obvious Lüders' band, but the fine-grained material did. Thus it was possible to determine the stress dependence of the Lüders' band-front velocity only in the fine-grained material.

Stress Dependence of Delay Time. The delay time t_d , the time taken for the plastic strain to reach the limit of detection ϵ_0 , at a constant stress can be calculated from the model of plastic flow

$$\int_0^{\epsilon_0} \frac{d\epsilon}{L} = \int_0^{t_d} 0.5 b (\sigma_0)^{-n} (\sigma - q\epsilon_p)^n dt . \quad (42)$$

At small strains

$$t_d = \frac{\int \frac{d\epsilon}{L} (\sigma_0)^n}{0.5 b} \cdot \sigma^{-n} , \quad (43)$$

assuming L is independent of stress, or

$$\ln t_d = \ln \gamma - n \ln \sigma , \quad (44)$$

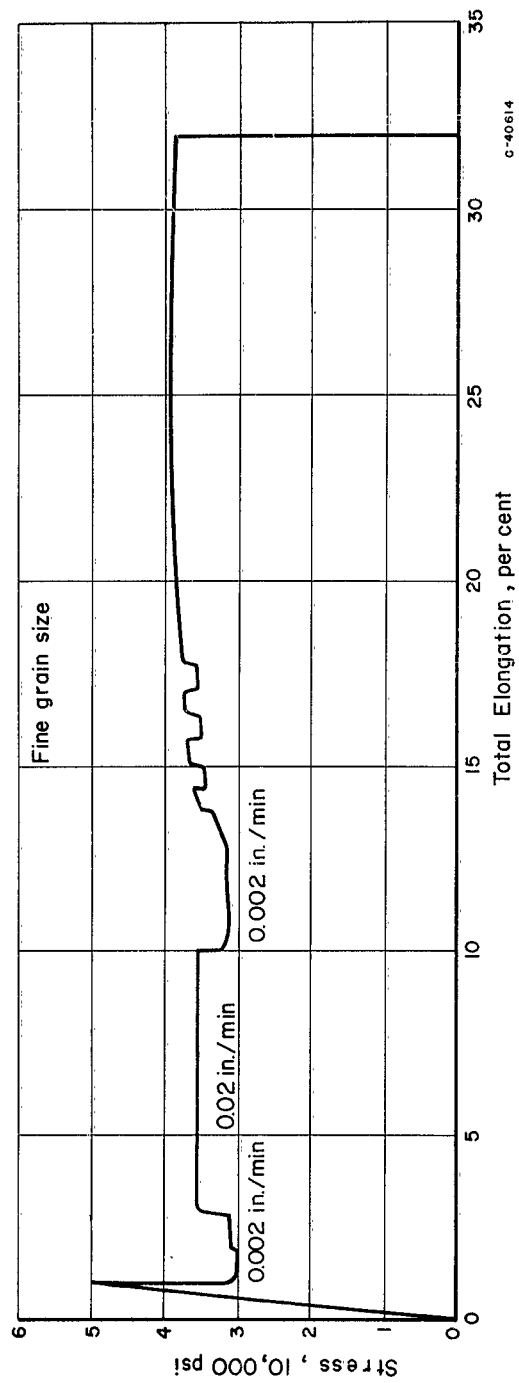


FIGURE 55. TYPICAL STRESS-STRAIN CURVE SHOWING A STRAIN RATE CHANGE DURING LÜDERS' PROPAGATION

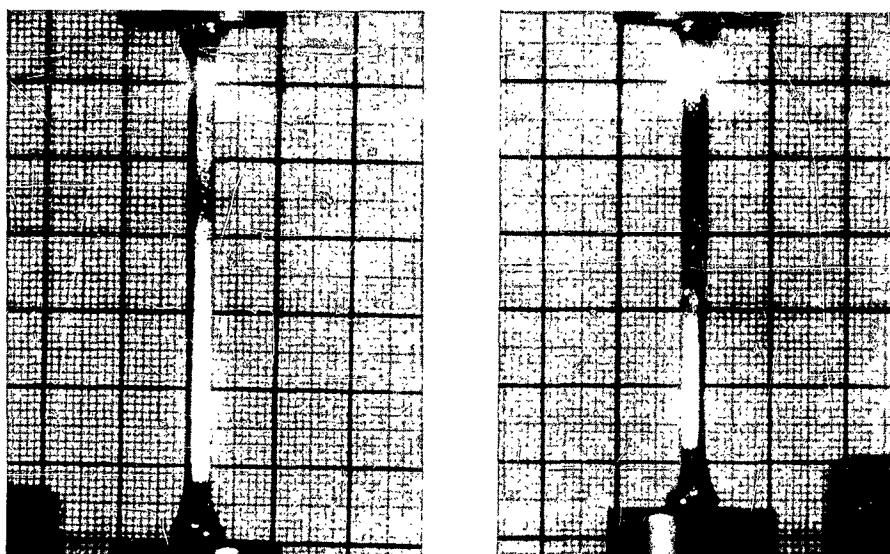
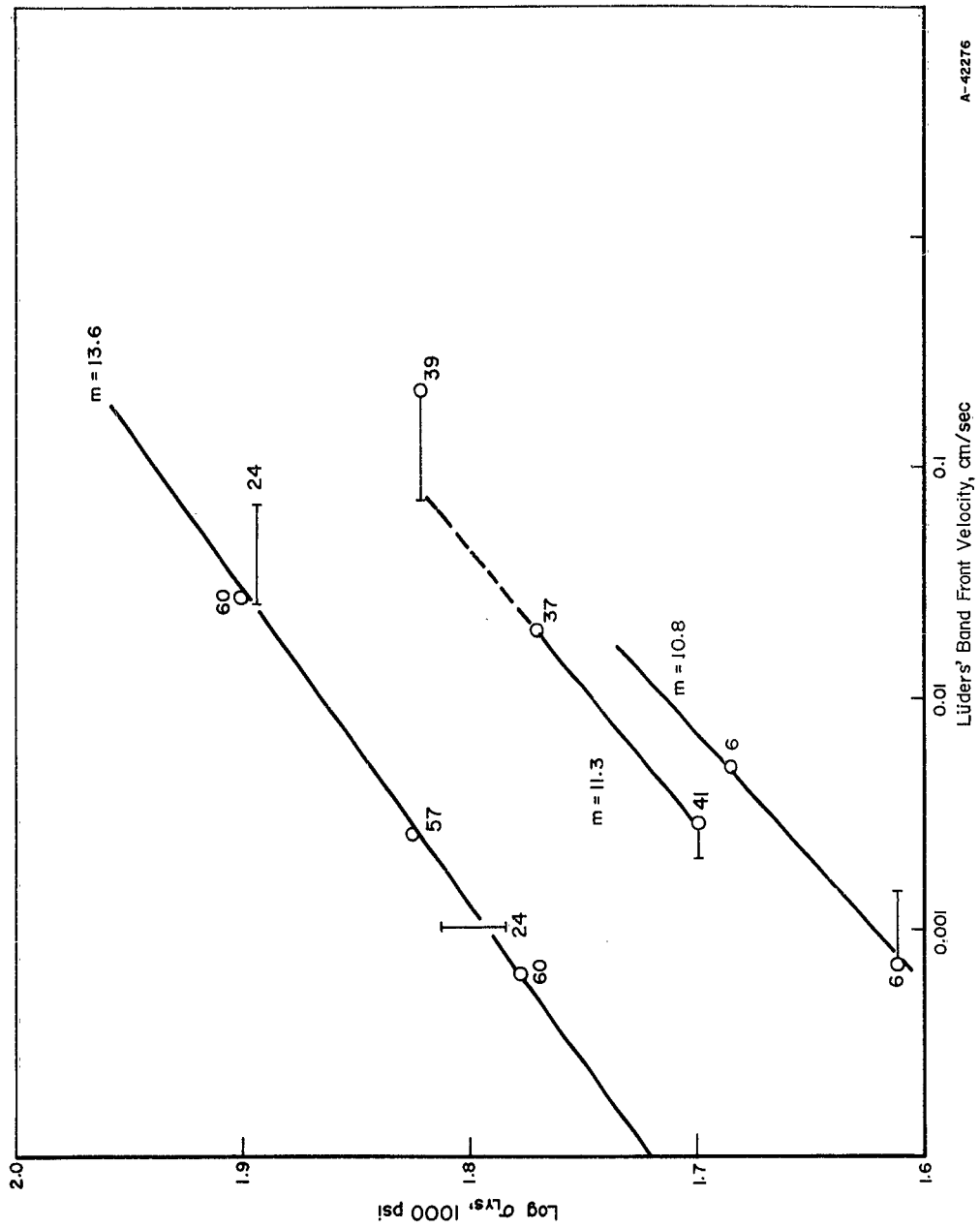


FIGURE 56. LÜDERS' BANDS IN FINE-GRAINED MOLYBDENUM, SHOWING
TYPICAL CONTRAST AT THE BAND FRONT



A-42276

FIGURE 57. STRESS DEPENDENCE OF LÜDERS' BAND-FRONT VELOCITY

where

$$\gamma = \frac{\int \frac{d\epsilon}{L} (\sigma_o)^n}{0.5 b} \quad (45)$$

Thus

$$n = - \frac{d \ln t_d}{d \ln \sigma} \quad (46)$$

No experimental determinations of delay time were made, but values obtained from the literature and substituted in the above equation are used to derive the values of n included in Table 10.

TABLE 10. VALUES OF n OBTAINED FROM THE LITERATURE FOR FINE- AND COARSE-GRAINED MOLYBDENUM

Method	Previous Work		Present Work	
	n	Reference	n	
			Coarse Grain	Fine Grain
Strain-Rate Dependence of Upper Yield Stress	13	20	8.5	14 - 19
	14	21		
Strain-Rate Dependence of Lower Yield Stress	17	21	8.5	13.7 - 20.7
Stress Dependence of Lüders' Band Velocity	--	--	--	10.8 - 13.6
Delay Time	10, 15	22	--	--
Stress Relaxation	--	--	8.6 at lower yield 12.1 at $\epsilon_p = .02$	17.3 Lüders' plateau, 28 at $\epsilon_p = .08$

Stress-Relaxation Method. If a tensile specimen is strained in a testing machine, and at some point subsequent to the initiation of plasticity the straining is stopped, the specimen will relax. That is, elastic strain in the machine will be exchanged for plastic strain in the specimen, and the stress will fall. Since this plastic flow is derived at the expense of elastic strain, then the rate of fall of stress is proportional to the rate of plastic flow. This therefore introduces a further way to derive a value of n :

$$n = \frac{d \ln (d \sigma / dt)}{d \ln \sigma} \quad (48)$$

Experimentally this means that the gradient of the relaxation curve is plotted log-log against the stress at the corresponding point. This method, as well as giving a value for n , has the additional advantage that it gives some idea of the stress range

over which a power law apparently holds. This method was applied to three samples molybdenum, and the extent to which the results lie on a straight line can be seen from Figures 58 and 59 together with the values of n derived, and the strains at which they were derived.

Discussion

Experiments designed to determine values of two parameters, n and c , assumed by the simple plastic model to be single valued, have been presented in the above section. The results (see Table 10) show that the experimentally determined values of the parameter n depend on grain size. The value of n for the coarse-grain size lies in the range 8.5 to 12 and that for the fine-grain size ranges from 13 to 20. For a given grain size (particularly the coarse) the agreement is quite good, and such variation as exists may be explained by considerations already discussed above, namely a dependence of dislocation density on stress or strain rate. In order to determine the most appropriate value of n for molybdenum, the direct method - of straining and etch pitting - will have to be successfully developed. At this time though, it should be worth while to critically review the values of n determined by the indirect means.

In order to derive the relationship $\frac{d \log \sigma}{d \log \dot{\epsilon}_p} = n$, the assumption must be made that no appreciable plastic flow has taken place. In the coarse-grain material which deforms without a noticeable Lüders' plateau, the yield strain may be small enough that this condition is approximately fulfilled and the value of n determined may have real meaning. In the fine-grain material, however, the yield drop is associated with the formation of a localized region of deformation within which the strain may be as high as 10 per cent. Values from the literature, summarized in Table 6, and from the results of relaxation tests done on the coarse-grain material (mean linear intercept of 0.16 mm) show that n increases with strain. In this case, it seems likely that the conditions are sufficiently different from the assumption that the values of n derived by this method may have lost their meaning. For the fine-grain material, therefore, the value of n based on Lüders' band-front velocity measurements may be closest to the truth. The Lüders' band velocity measurements are consistent with estimated values of dislocation velocity associated with the band front, as can be seen by comparing the dislocation velocity calculated from the formula $\dot{\epsilon}_p = 0.5 b f \rho v$ to that determined from Lüders' band experiments. Substituting $b = 2.5 \times 10^{-8}$, $f = 0.1$, and $\rho = 10^8$ (the estimated dislocation density at the front of the Lüders' band):

$$\dot{\epsilon}_p = \frac{0.5 \times 2.5 \times 0.1 \times 10^8}{10^8} \times v = 0.125 v$$

or

$$8 \dot{\epsilon}_p = v$$

At a crosshead speed of 2 inches per minute, the strain rate in a 1-1/2-inch gage length specimen is $\left(\frac{2}{60} \times \frac{2}{3}\right) = \frac{1}{45} = .022/\text{second}$

and

$$8 \dot{\epsilon}_p = 0.176 \text{ centimeters per second}$$

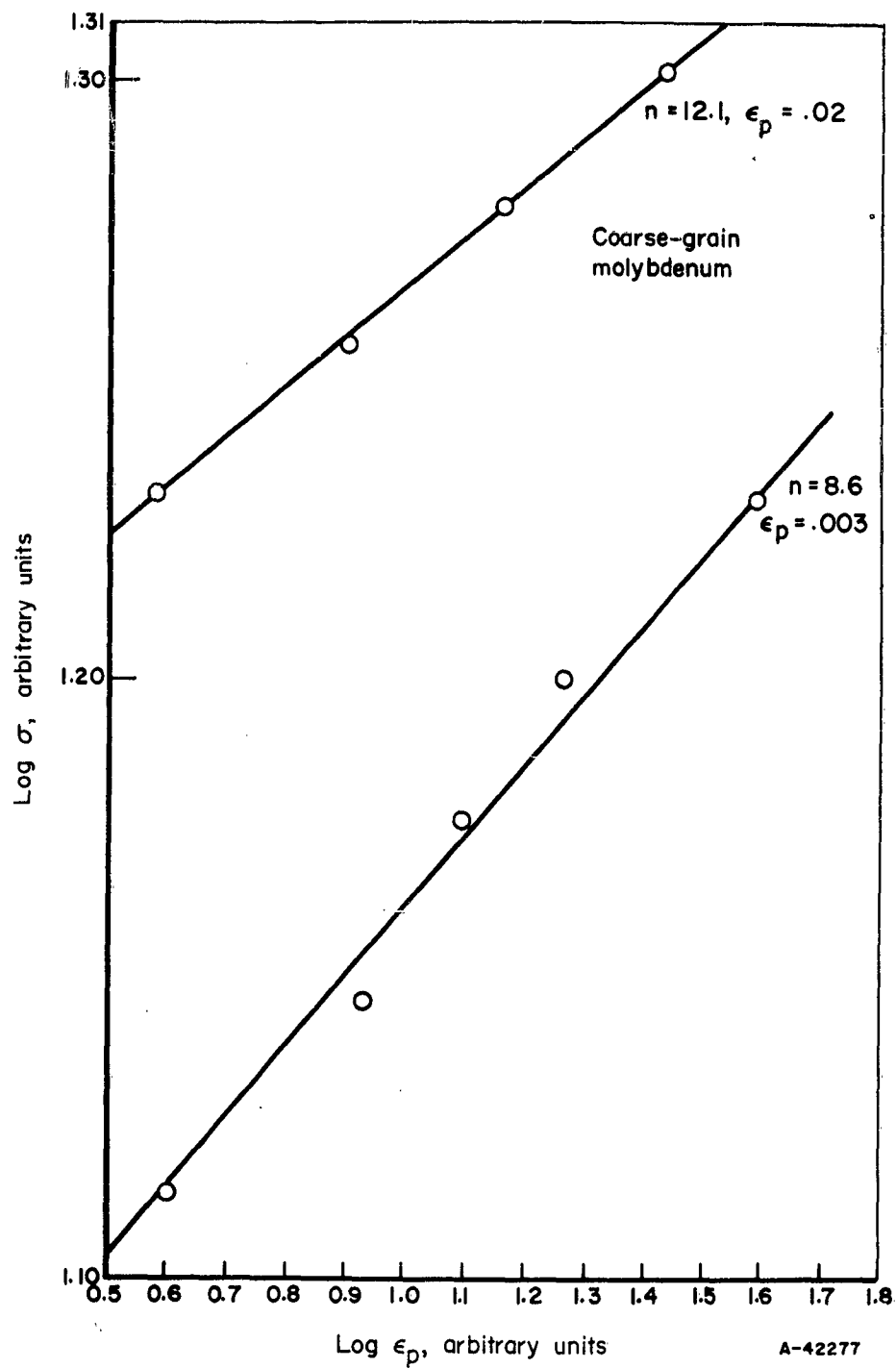


FIGURE 58. RELAXATION CURVES FOR COARSE-GRAINED MOLYBDENUM

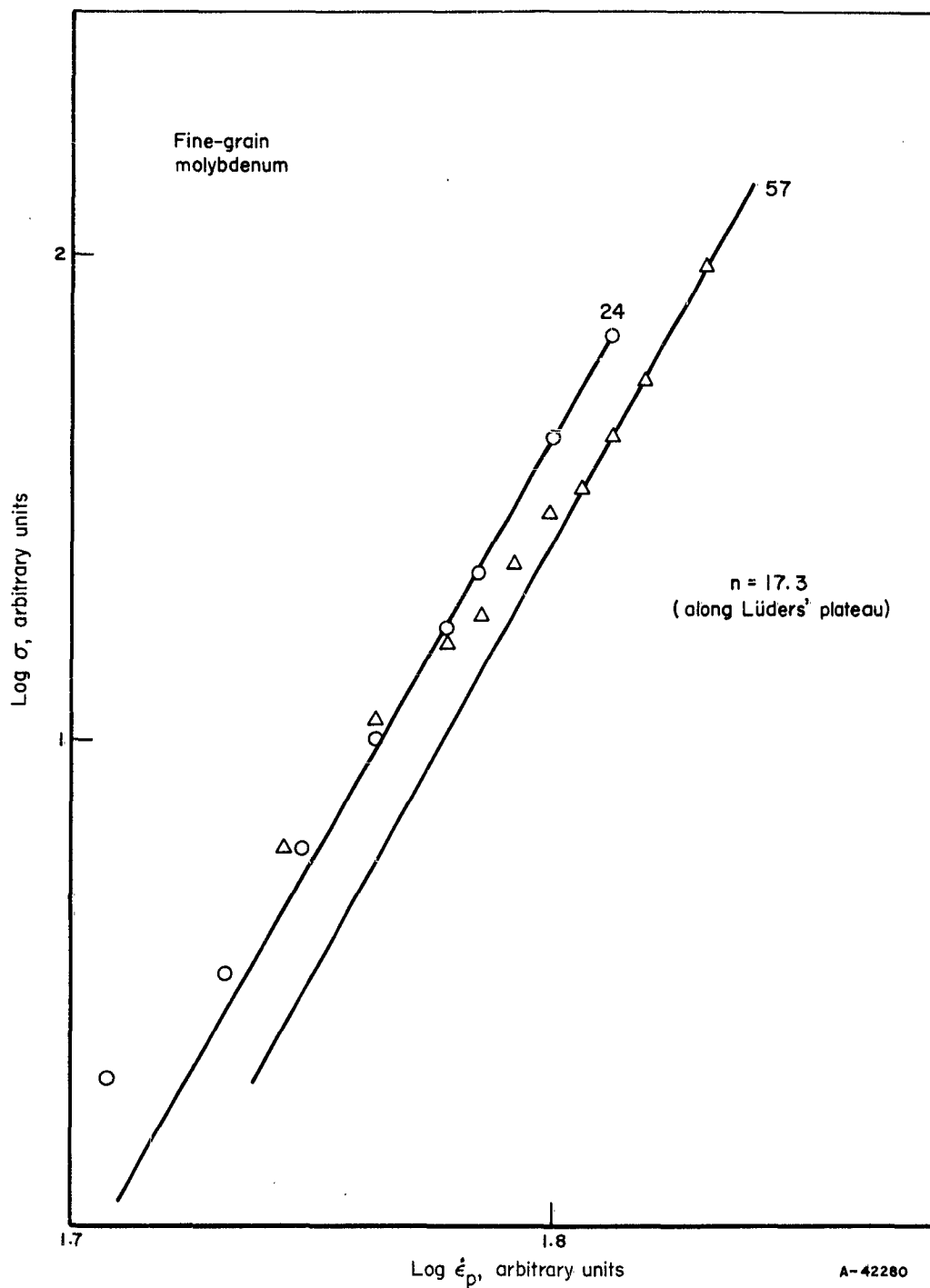


FIGURE 59. RELAXATION CURVES FOR FINE-GRAINED MOLYBDENUM

In the Lüders' band experiments, the dislocation velocity measured fell in the range 0.17 to 0.44 centimeters per second.

If then, by the preceding considerations, we accept a value of $n \approx 9$ for the coarse-grain material and $n = 14$ for the fine-grain material, we are left to explain the apparent grain-size dependence of this parameter, if the difference in yield strain does not account for all the discrepancy. This leads to the question of the nature of the forces governing n .

The only resistance to the movements of a dislocation through a perfect single crystal should be the Peierls Nabarro force. In a normal polycrystalline specimen however, there are, in addition to this force, forces due to interstitials, inclusions, other dislocations, and the complicating effect of grain boundaries. This variation in n may be due to the effect of the variation in grain size per se, or to the effect on impurity dispersion and initial dislocation structure of the different grain sizes. At this time, there is no evidence to differentiate between these alternatives.

GENERAL DISCUSSION

The research on notch sensitivity of refractory metals has been conducted from the viewpoints of theory, metallurgy, and design. This was done to provide information on notch sensitivity to three communities of interest: the materials scientist, the refractory metal producers, and the designers working with refractory metals. It should be recognized that the approach and evaluation from these three viewpoints necessarily is different, because the needs of the recipients differ.

In the study on mechanism of notch embrittlement, the theoretical treatment of notch initiation and fracture was applied to the specific case of refractory metals. However, the theory developed is general, and advances made in the theory will be available to other materials. The information on effects of metallurgical variables should be specifically useful to producers of refractory-metal products in their attempts to provide high-strength, high-performance materials with adequate notch toughness. The work on fracture toughness is intended to provide the designer of refractory-metal structures with information on the basis of which the strength of structures and the maximum flaws which can be tolerated in manufacture through quality control can be estimated. This design-based information is an outgrowth of extensive theoretical development of fracture toughness criteria in support of high-strength structures of other materials, and is a good example of the extension of theory developed in one class of materials to others.

How are the three viewpoints interrelated? In a broad sense, they are interrelated by having been conducted on common materials, refractory metals. However, the metallurgical phase of the study has been in progress for 3 years, whereas the theoretical and design-oriented studies were initiated within the last year. Thus, the theoretical work was done largely on unalloyed molybdenum, a subject covered from the metallurgical viewpoint during the first year of the investigation.

Correlation between the three viewpoints is another useful output of the three viewpoints. Necessarily, metallurgical variables are evaluated through arbitrary

criteria, hopefully of a discriminating nature, to reveal the notch sensitivity of materials under a wide variety of compositions and conditions. Such screening-type evaluations are of limited use in understanding the mechanism of fracture and in the design of structures. However, those common points where the three phases overlap provide the means for correlation between the viewpoints involved. Thus, the theoretical phase may have provided a basis for visualizing what is involved when the metallurgical variables are altered. Indeed, the mechanism studies provide a framework of thinking whereby the effects of metallurgical variables may be rationalized and future development work planned more effectively.

Beyond correlation between viewpoints, the ability to predict the results of one viewpoint from the starting point of the other is surely an outstanding achievement. This was done by the theoretical phase, when, from the properties of dislocations and the binding force between the atoms, the transition temperature for brittle fracture in molybdenum was predicted.

In the following sections, over-all conclusions from the individual viewpoints are presented.

Theoretical Aspects

Notch embrittlement arises from the modification brought about by the presence of a notch to the nominal stress and strain situation which a material would otherwise experience. In an effort to describe this modification, particularly with respect to a moving crack, an approach has been used which relies on the newly developed concepts of dislocation dynamics. Using these ideas, the stress-strain-time relationship experienced by material in front of an idealized moving elliptical crack has been calculated, using the stress-concentration factor appropriate to an instantaneously fixed crack, whose tip configuration is continuously modified by plastic flow. Using parameters specific to an individual material, the maximum stress concentration experienced by this material in the presence of a moving crack has been calculated as a function of crack velocity.

The results of these calculations show that the stress-concentration factor at the tip of a moving crack increases as the crack velocity increases, and is markedly dependent on the stress dependence of dislocation velocity in that material. The calculations further show that the introduction of free dislocations (for example by working or prestraining) should reduce the stress-concentration factor at the crack tip, effectively making the material more ductile.

As an indirect test of the usefulness of this type of approach, it is promising that the predicted transition temperatures, based on the results of such calculations, fall close to those actually determined in the Fracture Toughness Studies.

Experimentally, the aim was to determine for one material, molybdenum, the values of parameters necessary to the calculation. To this end, the variation of dislocation density with strain was determined by transmission electron microscopy, and several deductions from dislocation dynamics were in the main substantiated. More specifically, it was shown that, to a first approximation, indirect methods of determining

the stress dependence of dislocation velocity in molybdenum gave plausible and approximately similar values for n , the index in the relationship. Further, what difference existed in such determinations were rationalized on the basis of grain-size effects.

The success of the model, in respect to the semiquantitative prediction of transition temperature, and the substantiation of several predictions of dislocation dynamics give hope that in spite of the many simplifications implicit in such a derivation, the treatment will eventually lead to a fuller understanding of the effects of notches from a more fundamental standpoint than has been possible previously.

Metallurgical Aspects

The metallurgical phase has been the subject of research at Battelle since 1959, previous studies having been recorded in WADD TR 60-278 and ASD TR 61-474. These studies have treated various metallurgical and compositional variables relative to their effects on the mechanical behavior of refractory metals in the presence of mechanical notches.

The metallurgical phase included the following three types of variables, each of which will be discussed in following sections.

A. Metallurgical Structure Variables

(1) Grain Structure

- (a) Fibered (degree of fibering)
- (b) Recrystallized (grain size).

B. Compositional Variables

- (1) Group V versus Group VI base
- (2) Effects of interstitials
- (3) Effects of substitutional alloying

C. Mechanical Variables

- (1) Round versus sheet
- (2) Notch acuity.

Effects of Metallurgical Structure

Molybdenum and Mo-0.5Ti were produced in the recrystallized condition with three grain sizes. The transition temperature increased with increasing grain size, while strength decreased. Notch sensitivity increased with increased grain size, and the transition in reduction of area of notch specimens occurred at higher temperatures than in unnotched specimens.

Concerning grain shape, there was good documentation that lower transition temperatures combined with higher strength are found with a wrought condition compared with the recrystallized. Overall, as the structure progresses from wrought to fine-grained recrystallized to coarse-grained recrystallized, both the notch and unnotch strengths were decreased, transition temperatures increased, temperature dependence of strength and ductility decreased, and notch sensitivity increased. All the observations supported the conclusion that the wrought condition (both stress relieved and not stress relieved) was preferable to the recrystallized. Furthermore, fine grain size was preferable to coarse grain size.

The findings grouped tungsten generally similar to molybdenum and Mo-0.5Ti. Pure columbium and pure tantalum did not show appreciable dependence on structure, while tantalum showed considerably better behavior at low temperature than did columbium of comparable purity.

Effects of Composition

Concerning effects of interstitial impurities, there was no significant effect on the notch sensitivity of molybdenum when carbon varied from 20 to 300 ppm. On the other hand, oxygen greatly increased the transition temperature and structure dependence of the transition temperature for columbium and tantalum. Hydrogen increased the low-temperature notch sensitivity of columbium and tantalum when present in amounts greater than 100 ppm, without any appreciable effect on strength. Strain-aging embrittlement appeared at -75 F. In conclusion, interstitial contamination of any type is not beneficial, but there are significant interstitial levels below which the effects are tolerable.

Concerning substitutional alloying, the addition of 0.5Ti to molybdenum resulted in slightly lower tensile transition and lower notch sensitivity than for unalloyed molybdenum, combined with increased strengths. This result, which certainly could not be foreseen, indicates that Mo-0.5Ti is a better material than unalloyed molybdenum in all respects, including notch sensitivity.

The addition of 10 per cent tungsten to tantalum resulted in improved strength and loss of low-temperature ductility. Some structural sensitivity was introduced. However, at liquid-hydrogen temperatures, there was good ductility and no evidence of increased notch sensitivity.

F48 alloy, as an example of a solid-solution-strengthened and dispersion-strengthened Group V-A alloy, exhibited high strength and considerable structural sensitivity. The normal effects of structure on transition temperature and notch sensitivity were noted.

The over-all conclusion drawn concerning solid-solution strengthening was that strength is increased and there is a greater effect of structure on notch sensitivity and transition temperature. The effects of dispersions were not clear. In Mo-0.5Ti alloy, better notch properties were noted than for unalloyed molybdenum, but this may have been an effect of reduced soluble interstitial content. The dispersion of carbides in F48 certainly did not appear to benefit notch properties.

Effects of Mechanical Variables

For notched rounds compared to notched sheet specimens of the same K_T , there was increased notch sensitivity, higher transition temperature, and a greater degree of notch strengthening. All these are consistent with the greater constraint expected in a round specimen, because of a closer approach to plane-strain conditions (as opposed to plane stress).

Concerning notch acuity, recrystallized molybdenum and Mo-0.5Ti alloy exhibited little difference in going from $K_T = 3$ to $K_T = 6$. This might have been anticipated, since the recrystallized molybdenum-base materials were subject to brittle fracture in both cases, and the two notches were not sufficiently different to discriminate.

Fracture Toughness Aspects

The fracture toughness of unalloyed molybdenum, tungsten, tantalum, and columbium was investigated as a function of test temperature by testing sheet-tensile specimens containing sharp central notches. As discussed earlier, the fracture toughness, K_C , does not have a single value for a given material. In general, K_C will decrease as specimen thickness is increased, until it reaches a minimum value when it is independent of further thickness increase. This variation in K_C is associated with a change in fracture mode from full shear to transverse. When the fracture is entirely in the transverse mode, K_C has its minimum value and is referred to as K_{IC} , the plane-strain fracture toughness. According to Irwin, K_{IC} governs the propagation of small elliptical surface cracks through a sheet or plate, since such cracks extend in a transverse mode. Once the crack extends through the thickness, K_C governs further crack growth. If K_C for the thickness in question is not much greater than K_{IC} , fracture should proceed with little increase in load. If, however, it is considerably greater than K_{IC} , due to an appreciable percentage of shear-lip formation, much higher loads should be required to cause complete fracturing.

In this investigation, attention was centered on determination of K_{IC} and of the temperature above which K_C exceeds K_{IC} in 50-mil sheet. The variables studied were:

- (a) Metallurgical structure - fibered versus recrystallized
- (b) Orientation with respect to rolling direction (molybdenum only).

Conclusions

- (1) For molybdenum and tungsten, K_{IC} shows a transitional behavior as temperature is varied. The transition temperature is lower for molybdenum than for tungsten; for both materials, the recrystallized structure has a more gradual transition than the fibered structure.

- (2) The temperature above which K_{Ic} exceeds K_{Ic} in 50-mil sheet was found to be:

Molybdenum

Fibered (Longitudinal)	~90 C
Fibered (Transverse)	~90 C
Recrystallized (Longitudinal)	~150 C
Recrystallized (Transverse)	~150 C

Tungsten

Fibered	~260 C
Recrystallized	~400 C

Tantalum

Fibered	Below -196 C
Recrystallized	Below -196 C

Columbium

Fibered	Below -196 C
Recrystallized	Below -196 C

Above this temperature for each material, a crack extending under plane-strain conditions will presumably stop under plane-stress conditions if the stress remains constant.

- (3) In recrystallized molybdenum, the fracture toughness was found to be virtually independent of orientation; in fibered molybdenum, K_{Ic} was somewhat smaller in transverse specimens than in longitudinal specimens at test temperatures below about 50 C.
- (4) At room temperature, molybdenum exhibited a K_{Ic} (and K_{Ic}) value of approximately 30,000 psi $\sqrt{\text{in.}}$ and tungsten a value of 10,000 psi $\sqrt{\text{in.}}$ From fracture-mechanics theory, the critical through-crack length, $2a$ (where $2a \ll$ sheet width), at an imposed stress of 50,000 psi, would be approximately 1/4 inch and 1/40 inch for molybdenum and tungsten, respectively, at room temperature.
- (5) Tests at temperatures as low as -196 C on columbium and tantalum failed to provide fracture-toughness values for these materials, inasmuch as they remained completely ductile at these temperatures in the presence of the most severe stress concentrators.

REFERENCES

- (1) Imgram, A. G., Holden, F. C., Ogden, H. R., et al., "Notch Sensitivity of Refractory Metals", WADD TR 60-278, Battelle Memorial Institute, April, 1960.
- (2) Imgram, A. G., Mallett, M. W., Koehl, B. G., et al., "Notch Sensitivity of Refractory Metals", ASD TR 61-474, Battelle Memorial Institute, August, 1961.
- (3) Griffith, A. A., "The Phenomenon of Rupture and Flow in Solids", Philosophical Transactions, Royal Society of London, 221, 163 (1920).
- (4) Inglis, C. E., "Stresses in a Plate Due to the Presence of Cracks and Sharp Corners", Trans. Inst. Naval Arch., London, 55, 219 (1913).
- (5) Salzman, W. R., and Morrison, J. D., "An Investigation of the Crack Propagation Resistance of High-Strength Alloys and Heat Resistant Alloys", Southern Research Institute, Bimonthly Progress Report No. 7 for USN, NOW-61-0392-d, March 20, 1962.
- (6) Orowan, E., Report on Progress in Physics of the Physical Society, 12, 185 (1948-1949).
- (7) Irwin, G. R., Trans. Am. Soc. Met., 40A, 147 (1948).
- (8) Gilman, J. J., and Johnston, W. G., J. App. Phys., 30, 129 (1959).
- (9) Hahn, G. T., Gilbert, A., and Reid, C. N., (unpublished work).
- (10) Neuber, H., Theory of Notch Stresses, Springer Verlag, Berlin (1958) p 76, AEC-Tr-4547.
- (11) Hahn, G. T., Acta. Met., 10, 727 (1962).
- (12) Johnston, W. G., J. App. Phys. (to be published).
- (13) Keh, A. S., Trans. Am. Inst. Mining and Met. Engrs. (to be published).
- (14) Hull, D., and McIvor, I. (to be published).
- (15) Gregory, D. D., ASD-TDR-62-354, 1962.
- (16) Benson, R., Thomas, G., and Washburn, J. (to be published).
- (17) Schadler, H. W., and Low, J. R. Jr., Final Report on ONR Contract No. Nonr-2614(00), 1962.
- (18) Hahn, G. T., Reid, C. N., and Gilbert, A. (unpublished work).
- (19) Stein, D. I., and Low, J. R., Jr., J. Appl. Phys., 31, 362 (1960).

- (20) Hauser, F. E., Simmons, J. A., and Dorn, J. E., Response of Metals to High Velocity Deformation, Interscience Publishers, New York (1961), p 93.
- (21) Tankins, E. S., and Maddin, R., Columbium Metallurgy, Interscience Publishers, New York (1961), p 343.
- (22) Marcinkowski, M. J., WADC TR 59-294, 1959.
- (23) Reid, C. N., Gilbert, A., and Hahn, G. T. (unpublished work).
- (24) Bechtold, J. H., Trans. Amer. Inst. Mining and Met. Engrs., 197, 1469 (1953).
- (25) Carreker, R. P., Jr., and Guard, R. W., Trans. Amer. Inst. Mining and Met. Engrs., 206, 178 (1956).
- (26) Hendrickson, J. A., Wood, D. S., and Clark, D. S., Trans. Amer. Soc. Met., 48, 540 (1956).
- (27) Bechtold, J. H., Trans. Amer. Inst. Mining and Met. Engrs., 206, 142 (1956).
- (28) Wessel, E. T., France, L. L., and Begley, R. T., Columbium Metallurgy, Interscience Publishers, New York (1961), p 459.
- (29) Allen, G. A., Armstrong, R. W., and Bechtold, J. H., Trans. Amer. Inst. Mining and Met. Engrs., 212, 523 (1958).
- (30) Bechtold, J. H., and Shewmon, P. G., Trans. Amer. Soc. Met., 46, 397 (1954).
- (31) Ham, R. K., Phil Mag., 6, 1183 (1961).
- (32) Guard, R. W., Acta. Met., 9, 163 (1961).

APPENDIX I

METALLURGICAL-VARIABLE STUDIES

TABLE 11. TENSILE AND NOTCH TENSILE PROPERTIES OF AS-WROUGHT MOLYBDENUM WITH 25 PER CENT WORK

Test Temperature, C	Yield Strength (0.2 Per Cent Offset), psi	Ultimate Tensile Strength, psi	Elongation, per cent	Reduction in Area, per cent	Fracture at Maximum Load	Fracture Mechanism
<u>Unnotched Specimens</u>						
-196	--	85,000	0	(a)	Yes	C
-196	--	87,400	0	(a)	Yes	C
-75	136,100	136,700	2	0	Yes	C
-40	112,800	112,800	0	0.6	Yes	C
25	80,500	81,200	38	44.7	No	C
25	65,000	79,900	28	22.8	No	C
150	56,700	61,900	40	62.2	No	10% C
150	43,600	60,400	40	74.0	No	10% C
260	52,300	53,600	40	87.3	No	S
370	50,300	50,300	28	88.0	No	S
<u>Notched Specimens ($K_t = 3$)</u>						
-196		98,200		0	Yes	C
-196		43,900		0	Yes	C
-196		81,500		0	Yes	C
-75		66,300		0	Yes	C
-75		78,600		0	Yes	C
-40		42,100		0	Yes	C
-40		82,000		0	Yes	C
25		126,200		0	Yes	C
25		128,800		0	Yes	C
150		96,200		18.3	No	C
150		96,700		11.0	No	C
260		87,400		74.6	No	S
260		88,900		58.4	No	S
370		84,300		71.7	No	S
370		84,900		78.1	No	S

(a) Broke in threads.

TABLE 12. TENSILE AND NOTCH TENSILE PROPERTIES OF AS-WROUGHT MOLYBDENUM WITH 68 PER CENT WORK

Test Temperature, C	Yield Strength (0.2 Per Cent Offset), psi	Ultimate Tensile Strength, psi	Elongation, per cent	Reduction in Area, per cent	Fracture at Maximum Load	Fracture Mechanism
<u>Unnotched Specimens</u>						
-75	153,200	153,200	--	0	Yes	C
-75	153,100	153,100	2	0	Yes	C
-40	133,100	133,100	8	7.1	No	C
25	100,500	100,500	42	79.3	No	S
25	100,300	100,300	40	79.4	No	S
150	84,400	84,400	32	84.8	No	S
204	73,200	76,500	36	85.5	No	S
<u>Notched Specimens ($K_t = 3$)</u>						
-75		90,900		0	Yes	C
-75		58,800		0	Yes	C
-40		110,700		1.5	Yes	C
-40		92,700		0	Yes	C
25		159,900		4.8	?	C
25		148,800		0	Yes	C
150		132,300		31.0	No	S
150		133,900		25.6	No	S
204		125,300		54.1	No	S
204		126,300		64.4	No	S

TABLE 13. TENSILE AND NOTCH TENSILE PROPERTIES OF STRESS-RELIEVED MOLYBDENUM WITH 68 PER CENT WORK (1/2 HR AT 538 C)

Test Temperature, C	Yield Strength (0.2 Per Cent Offset), psi	Ultimate Tensile Strength, psi	Elongation, per cent	Reduction in Area, per cent	Fracture at Maximum Load	Fracture Mechanism
<u>Unnotched Specimens</u>						
-75	--	>90,000	0	$\alpha^{(b)}$	Yes	C
-75	155,100	155,600	--(a)	--(c)	Yes	C
-40	128,500	131,100	28	64.8	No	C
-40	129,100	129,100	16	28.5	No	C
25	102,500	102,500	40	74.8	No	S
150	83,900	84,000	28	78.8	No	S
204	79,000	79,000	26	84.8	No	S
<u>Notched Specimens ($K_t = 3$)</u>						
-75		140,200		0	Yes	C
-75		119,300		0	Yes	C
-40		187,100		0	Yes	C
-40		138,100		0	Yes	C
25		158,300		9.3	?	C
25		161,500		4.7	?	C
150		122,100		33.2	No	C
150		122,900		48.2	No	C
204		118,800		75.4	No	S
204		119,600		77.8	No	S

(a) Piece missing.

(b) Broke in threads.

(c) Double fracture - one in threads, one in reduced section.

TABLE 14. TENSILE AND NOTCH TENSILE PROPERTIES OF STRESS-RELIEVED MOLYBDENUM WITH 68 PER CENT WORK (1/2 HR AT 871 C).

Test Temperature, C	Yield Strength (0.2 Per Cent Offset), psi	Ultimate Tensile Strength, psi	Elongation, per cent	Reduction in Area, per cent	Fracture at Maximum Load	Fracture Mechanism
<u>Unnotched Specimens</u>						
-196	--	>81,000	--	--(a)	Yes	C
-196	--	>54,300	--	--(a)	Yes	C
+75	--	>53,100	--	--(a)	Yes	C
-75	160,500	160,500	2	3.4	Yes	C
-40	125,800	125,800	28	44.6	No	C
-40	134,600	134,600	30	57.2	No	C
25	106,400	106,400	40	75.5	No	S
25	102,200	102,200	44	78.7	No	S
150	78,700	78,700	40	81.6	No	S
204	80,200	80,200	26	83.3	No	S
<u>Notched Specimens ($K_t = 3$)</u>						
-75		97,800		0	Yes	C
-75		145,900		0	Yes	C
-75		133,800		0	Yes	C
-40		155,600		0	Yes	C
-40		133,500		0	Yes	C
25		149,100		0	Yes	C
25		155,500		0	No	C
150		125,300		49.7	No	90% C
150		122,600		48.2	No	90% C
204		120,300		67.7	No	10% C
204		122,400		49.7	No	10% C

(a) Broke in threads.

TABLE 15. TENSILE AND NOTCH TENSILE PROPERTIES OF RECRYSTALLIZED MOLYBDENUM WITH 68 PER CENT WORK (1/2 HR AT 1316 C)

Test Temperature, C	Yield Strength (0.2 Per Cent Offset), psi	Ultimate Tensile Strength, psi	Elongation, per cent	Reduction in Area, per cent	Fracture at Maximum Load	Fracture Mechanism
<u>Unnotched Specimens</u>						
-196	--	101,000	0	0	Yes	C
-75	--	87,500	--	--(a)	Yes	C
-75	--	80,100	--	--(a)	Yes	C
-75	83,700	83,700	0	0	Yes	C
25	75,400	75,400	52	47.4	No	C
25	65,800	72,500	52	46.9	No	C
150	46,200	56,200	46	46.8	No	C
150	35,500	54,500	58	73.7	No	C
260	27,000	48,300	58	88.5	No	10% C
370	25,400	43,500	60	92.0	No	S
<u>Notched Specimens ($K_t = 3$)</u>						
-196		35,600		0	Yes	C
-196		30,600		0	Yes	C
-75		72,000		0	Yes	C
-75		44,300		0	Yes	C
25		89,300		0	Yes	C
150		80,700		12.4	No	C
260		72,400		72.1	No	S
370		64,500		72.9	No	S
<u>Notched Specimens ($K_t = 6$)</u>						
-196		38,500		0	Yes	C
-196		58,200		0	Yes	C
-75		76,800		0	Yes	C
-75		24,000		0	Yes	C
25		96,300		0	Yes	C
25		98,100		0	Yes	C
150		61,000		4.7	?	C
150		71,400		9.4	?	C
260		71,400		57.0	No	50% C
260		71,100		45.8	No	C
370		64,400		75.4	No	S
370		65,500		79.2	No	S

(a) Broke in threads.

TABLE 16. TENSILE AND NOTCH TENSILE PROPERTIES OF RECRYSTALLIZED MOLYBDENUM WITH 68 PER CENT WORK
(1/2 HR AT 1928 C)

Test Temperature, C	Yield Strength (0.2 Per Cent Offset), psi	Ultimate Tensile Strength, psi	Elongation, per cent	Reduction in Area, per cent	Fracture at Maximum Load	Fracture Mechanism
<u>Unnotched Specimens</u>						
-196	--	>48,200	0	0 ^(a)	Yes	C
-196	--	>43,500	0	0 ^(a)	Yes	C
-75	--	>65,000	0	0 ^(a)	Yes	C
-75	--	>67,400	0	0 ^(a)	Yes	C
25	35,400	45,200	2	2.7	Yes	C
150	13,100	46,000	22	18.8	Yes	C
150	16,900	44,900	30	27.7	No	C
260	15,100	40,000	48	62.3	No	90% C
370	14,000	34,400	44	79.5	No	S
<u>Notched Specimens ($K_t = 3$)</u>						
-196		53,500		0 ^(a)	Yes	C
-196		52,800		0	Yes	C
-75		94,700		0	Yes	C
-75		45,200		0	Yes	C
25		64,700		1.5	Yes	C
25		58,100		0	Yes	C
25		57,000		0	Yes	C
150		40,600		1.7	Yes	C
150		52,500		3.2	?	C
150		53,600		7.9	?	C
260		57,100		11.0	?	C
260		59,200		6.3	?	C
370		51,700		50.4	No	C
370		55,900		43.4	No	C

(a) Broke in threads.

TABLE 17. TENSILE AND NOTCH TENSILE PROPERTIES OF RECRYSTALLIZED MOLYBDENUM WITH 68 PER CENT WORK
(1/2 HR AT 2096 C)

Test Temperature, C	Yield Strength (0.2 Per Cent Offset), psi	Ultimate Tensile Strength, psi	Elongation, per cent	Reduction in Area, per cent	Fracture at Maximum Load	Fracture Mechanism
<u>Unnotched Specimens</u>						
-196	--	59,000	0	0(a)	Yes	C
-75	--	53,800	0	0	Yes	C
25	33,400	38,700	2	1.3	Yes	C
150	10,400	36,700	8	6.6	Yes	C
260	14,400	38,200	40	57.4	No	C
370	13,000	33,600	46	83.1	No	S
<u>Notched Specimens ($K_t = 3$)</u>						
-196		>22,800		0(a)	Yes	C
-196		44,000		0	Yes	C
-75		71,200		0	Yes	C
-75		83,300		0	Yes	C
25		67,300		0	Yes	C
25		43,000		0	Yes	C
150		48,900		1.5	Yes	C
260		55,100		22.9	?	C
260		59,300		7.9	?	90% C
370		54,300		57.0	No	90% C
370		49,900		38.5	No	90% C

(a) Broke in threads.

TABLE 18. TENSILE AND NOTCH TENSILE PROPERTIES OF AS-WROUGHT MOLYBDENUM-0.5 PER CENT TITANIUM WITH 25 PER CENT WORK

Test Temperature, C	Yield Strength (0.2 Per Cent Offset), psi	Ultimate Tensile Strength, psi	Elongation, per cent	Reduction in Area, per cent	Fracture at Maximum Load	Fracture Mechanism
<u>Unnotched Specimens</u>						
-196	--	>150,100	0	0(a)	Yes	C
-75	--	>58,800	0	0(a)	Yes	C
-75	--	140,900	2	1.9	Yes	C
-40	--	82,100	0	0(a)	Yes	C
25	87,000	87,200	20	21.4	No	C
25	82,600	82,800	24	24.2	No	C
150	58,100	60,000	28	45.0	No	C
150	59,900	62,100	24	38.8	No	C
260	55,000	55,000	30	84.9	No	S
370	52,000	52,000	24	89.0	No	S
<u>Notched Specimens ($K_t = 3$)</u>						
-196		>85,600		0	Yes	C
-196		>56,700		0	Yes	C
-75		128,000		0	Yes	C
-75		80,500		0	Yes	C
-75		102,700		0	Yes	C
-40		99,400		0	Yes	C
-40		99,600		0	Yes	C
25		139,000		3.2	Yes	C
25		144,100		1.6	Yes	C
150		101,400		4.7	?	C
150		97,600		6.3	?	C
260		93,400		18.3	No	C
260		92,100		19.7	No	C
370		86,400		81.3	No	S
370		86,600		78.5	No	S

(a) Broke in threads.

TABLE 19. TENSILE AND NOTCH TENSILE PROPERTIES OF AS-WROUGHT MOLYBDENUM -0.5 PER CENT TITANIUM WITH 68 PER CENT WORK

Test Temperature, C	Yield Strength (0.2 Per Cent Offset), psi	Ultimate Tensile Strength, psi	Elongation, per cent	Reduction in Area, per cent	Fracture at Maximum Load	Fracture Mechanism
<u>Unnotched Specimens</u>						
-196	--	>175,300	0	0(b)	Yes	C
-196	--	>174,000	0	0(b)	Yes	C
-75	158,300	158,300	--(a)	3.2	?	C
-75	157,000	157,000	4	2.6	?	C
-40	132,900	132,900	38	49.5	No	C
-40	131,100	131,100	28	46.2	No	C
25	99,300	101,700	42	77.7	No	--
25	105,800	107,300	42	78.8	No	S
150	78,500	83,400	40	83.1	No	S
204	76,000	78,800	38	86.7	No	S
<u>Notched Specimens ($K_t = 3$)</u>						
-196		70,400		1.5	Yes	C
-196		126,500		0(b)	Yes	C
-40		143,800		0(b)	?	C
-40		140,500		0(b)	Yes	C
-40		115,400		0(b)	Yes	C
-75		>107,300		0(b)	?	C
-75		187,400		3.5	Yes	C
-75		136,600		1.7	Yes	C
25		172,800		1.5	Yes	C
25		177,300		3.2	Yes	C
150		135,300		7.9	No	C
150		135,000		4.8	No	C
204		126,600		76.9	No	S
204		127,800		64.4	No	S

(a) Piece missing.

(b) Broke in threads.

TABLE 20. TENSILE AND NOTCH TENSILE PROPERTIES OF STRESS RELIEVED MOLYBDENUM-0.5 PER CENT TITANIUM WITH 68 PER CENT WORK (1/2 HR AT 538 C)

Test Temperature, C	Yield Strength (0.2 Per Cent Offset), psi	Ultimate Tensile Strength, psi	Elongation, per cent	Reduction in Area, per cent	Fracture at Maximum Load	Fracture Mechanism
<u>Unnotched Specimens</u>						
-196	--	>165,600	0	0	Yes	C
-196	--	>104,400	0	0	Yes	C
-75	160,300	160,300	12	18.2	No	C
-75	162,400	162,400	2	0.3	Yes	C
-40	136,900	136,900	28	66.6	No	C
25	104,700	106,000	40	72.3	No	S
150	81,500	81,500	34	82.3	No	S
204	78,500	78,500	26	83.0	No	S
<u>Notched Specimens ($K_t = 3$)</u>						
-196		51,000		0	Yes	C
-196		79,900		0	Yes	C
-75		145,600		0	Yes	C
-75		159,700		0	Yes	C
-40		181,900		0	Yes	C
-40		182,100		0	Yes	C
25		168,900		21.1	No	C
25		168,400		23.8	No	C
25		172,100		3.2	Yes	C
150		126,100		74.2	No	S
150		127,300		71.7	No	S
150		128,800		24.0	No	S
204		122,100		76.9	No	S
204		123,900		77.8	No	S

TABLE 21. TENSILE AND NOTCH TENSILE PROPERTIES OF STRESS RELIEVED MOLYBDENUM-0.5 PER CENT TITANIUM WITH 68 PER CENT WORK (1/2 HR AT 1093 C)

Test Temperature, C	Yield Strength (0.2 Per Cent Offset), psi	Ultimate Tensile Strength, psi	Elongation, per cent	Reduction in Area, per cent	Fracture at Maximum Load	Fracture Mechanism
Unnotched Specimens						
-196	--	>164,900	0	0(a)	Yes	C
-196	--	>101,000	0	0(a)	Yes	C
-75	172,100	172,100	2	1.3	?	C
-75	--	>127,900	0	0(a)	Yes	C
-40	145,000	145,000	34	67.9	No	C
25	111,200	111,200	44	74.7	No	S
25	109,100	109,100	42	78.1	No	--
150	83,000	83,000	40	68.5	No	S
150	83,600	83,600	40	82.3	No	S
204	76,400	76,400	36	83.1	No	S
Notched Specimens ($K_t = 3$)						
-196		33,300		0	Yes	C
-196		64,200		0	Yes	C
-75		169,700		0	Yes	C
-75		165,600		0	Yes	C
-75		195,500		0	Yes	C
-40		169,200		0	Yes	C
-40		169,700		0	Yes	C
25		179,500		3.2	Yes	C
25		173,800		0	Yes	C
25		177,700		4.7	No	C
150		128,100		9.4	No	C
150		129,100		>7.9	No	C
150		124,500		26.7	No	C
204		122,600		62.0	No	S
204		123,800		80.3	No	S

(a) Broke in threads.

TABLE 22. TENSILE AND NOTCH TENSILE PROPERTIES OF RECRYSTALLIZED MOLYBDENUM-0.5 PER CENT TITANIUM WITH 68 PER CENT WORK (1/2 HR AT 1593 C)

Test Temperature, C	Yield Strength (0.2 Per Cent Offset), psi	Ultimate Tensile Strength, psi	Elongation, per cent	Reduction in Area, per cent	Fracture at Maximum Load	Fracture Mechanism
<u>Unnotched Specimens</u>						
-196	--	>98,300	0	0 ^(a)	Yes	C
-75	--	>88,100	0	0 ^(a)	Yes	C
-75	104,100	106,000	2	3.2	?	C
-40	82,900	103,200	12	11.3	Yes	C
25	57,600	78,600	30	29.7	No	C
25	56,000	75,600	22	19.9	No	C
150	19,700	55,200	50	29.0	No	50% C
150	19,200	56,400	46	44.4	No	C
260	16,000	48,300	58	89.6	No	S
370	16,200	42,600	62	94.2	No	S
<u>Notched Specimens ($K_t = 3$)</u>						
-196		73,300		0	Yes	C
-196		98,300		0	Yes	C
-196		61,400		0	Yes	C
-75		86,700		0	Yes	C
-75		121,600		0	Yes	C
-40		115,000		0	Yes	C
25		102,200		4.7	Yes	C
25		85,400		1.5	Yes	C
150		70,400		4.7	Yes	C
150		79,500		9.4	?	C
260		68,600		74.6	No	S
260		70,100		69.5	No	S
370		62,300		80.6	No	S
370		60,900		79.6	No	10% S
<u>Notched Specimens ($K_t = 6$)</u>						
-196		96,500		0	Yes	C
-196		41,200		0	Yes	C
-75		97,000		0	Yes	C
-75		90,100		0	Yes	C
25		88,300		0	Yes	C
25		90,300		0	Yes	C
150		74,000		10.8	?	C
150		75,800		10.8	?	C
260		71,200		29.4	No	C
260		73,300		22.6	?	C
370		63,400		79.2	No	S
370		62,900		82.7	No	S

(a) Broke in threads.

TABLE 23. TENSILE AND NOTCH TENSILE PROPERTIES OF RECRYSTALLIZED MOLYBDENUM-0.5 PER CENT TITANIUM WITH 68 PER CENT WORK (1/2 HR AT 1928 C)

Test Temperature, C	Yield Strength (0.2 Per Cent Offset), psi	Ultimate Tensile Strength, psi	Elongation, per cent	Reduction in Area, per cent	Fracture at Maximum Load	Fracture Mechanism
Unnotched Specimens						
-196	--	>55,100	0	0 ^(a)	Yes	C
-196	--	>52,800	0	0 ^(a)	Yes	C
-196	--	>34,100	0	0 ^(a)	Yes	C
-75	--	65,700	0	0	Yes	C
-40	63,300	73,600	0	1.4	Yes	C
25	42,900	57,600	4	45	No	C
150	19,700	44,400	20	22.8	?	C
260	13,600	37,100	42	80.3	No	S
370	13,400	32,600	58	81.1	No	S
Notched Specimens ($K_t = 3$)						
-196		58,700		0	Yes	C
-196		69,800		0	Yes	C
-196		32,300		0	Yes	C
-75		78,100		1.6	Yes	C
-75		61,100		0	Yes	C
-40		62,900		0	Yes	C
25		42,500		0 ^(a)	Yes	C
25		76,400		1.5	Yes	C
150		43,200		3.2	Yes	C
150		57,700		7.8	?	C
260		59,200		22.6	No	C
260		59,100		31.0	No	C
370		52,200		34.7	No	C
370		52,600		44.7	No	C
370		51,500		24.2	No	C

(a) Broke in threads.

TABLE 24. TENSILE AND NOTCH TENSILE PROPERTIES OF RECRYSTALLIZED MOLYBDENUM-0.5 PER CENT TITANIUM WITH 68 PER CENT WORK (1/2 HR AT 2096 C)

Test Temperature, C	Yield Strength (0.2 Per Cent Offset), psi	Ultimate Tensile Strength, psi	Elongation, per cent	Reduction in Area, per cent	Fracture at Maximum Load	Fracture Mechanism
<u>Unnotched Specimens</u>						
-196	--	>66,400	0	0 ^(a)	Yes	C
-75	--	74,200	0	0	Yes	C
-40	59,500	71,300	4	1.4	Yes	C
25	45,400	49,300	2	3.2	Yes	C
150	16,900	43,500	24	24.2	?	C
260	14,000	38,400	54	68.8	No	S
370	16,900	33,700	54	81.7	No	S
<u>Notched Specimens ($K_t = 3$)</u>						
-196		54,500		0	Yes	C
-196		36,900		0	Yes	C
-75		58,700		0	Yes	C
-75		62,600		0	Yes	C
-40		98,000		0	Yes	C
25		59,800		1.6	Yes	C
25		57,500		0	Yes	C
150		52,500		3.2	Yes	C
150		47,800		1.7	Yes	C
260		56,700		15.2	?	C
260		56,500		16.7	?	C
370		52,100		46.7	No	C
370		49,900		58.0	No	80% C
370		52,000		30.8	No	90% C

(a) Broke in threads.

APPENDIX II FRACTURE-TOUGHNESS STUDIES (TABULATED DATA)

TABLE 25. TENSILE STRENGTH AND FRACTURE-TOUGHNESS PROPERTIES OF WROUGHT, STRESS-RELIEVED MOLYBDENUM SHEET (LONGITUDINAL)

Specimen	Test Temp., C	Initial Slot Length, in.	Load at Pop-in, lb	Max Load, lb	Fracture Load, lb	Notch Tensile Strength, 1000 psi	Ultimate			Fracture Mode			
							Yield Strength, 1000 psi	K _{IC} , 1000 psi √in.	K _{IC} , 1000 psi √in.				
											Yield Strength, 1000 psi	K _{IC} , 1000 psi √in.	K _{IC} , 1000 psi √in.
Unnotched Specimens													
MS-5L	25					89.3		102.5					
MS-6L	93					80.0		90.1					
MS-7L	150					76.7		85.0					
Center-Notched Specimens													
MS-43L	-40	0.71	1650	1650	1650	26.6	~105	19.3	19.3				
MS-42L	-40	0.75	1540	1540	1540	25.7	~105	18.7	18.7				
MS-44L	25	0.75	2800	2800	2800	47.2	89.3	35.7	35.7				
MS-45L	25	0.74	2200	2200	2200	36.2	89.3	26.9	26.9				
MS-43L	93	0.78	>3900	5020	<5020	87.5	80.0	>55.7	>K _{IC}				
MS-35L	93	0.83	>3900	5090	<5090	89.5	80.0	>56.3	>K _{IC}				
MS-48L	150	0.76	>4500	5040	<5040	84.5	76.7	>65.6	>K _{IC}				
MS-49L	150	0.76	>3900	4840	<4840	82.5	76.7	>54.7	>K _{IC}				

TABLE 26. TENSILE STRENGTH AND FRACTURE-TOUGHNESS PROPERTIES OF WROUGHT, STRESS-RELIEVED MOLYBDENUM SHEET (TRANSVERSE)

Specimen	Test Temp., C	Initial Slot Length, in.	Load at Pop-in, lb	Max Load, lb	Fracture Load, lb	Notch Tensile Strength, 1000 psi	Yield Strength, 1000 psi	K _{IC} , 1000 psi √in.	K _C , 1000 psi √in.	Fracture Mode											
											Specimen	Test Temp., C	Initial Slot Length, in.	Load at Pop-in, lb	Max Load, lb	Fracture Load, lb	Notch Tensile Strength, 1000 psi	Yield Strength, 1000 psi	K _{IC} , 1000 psi √in.	K _C , 1000 psi √in.	Fracture Mode
Specimen	Test Temp., C	Initial Slot Length, in.	Load at Pop-in, lb	Max Load, lb	Fracture Load, lb	Notch Tensile Strength, 1000 psi	Yield Strength, 1000 psi	K _{IC} , 1000 psi √in.	K _C , 1000 psi √in.	Fracture Mode											
Unnotched Specimens																					
MS-5T	25					94.6		106.3													
MS-6T	93					84.7		90.3													
MS-7T	150					79.7		88.2													
Center-Notched Specimens																					
MS-49T	-70	0.80	320	320	320	5.6	~114	4.0	4.0	Transverse											
MS-43T	-40	0.80	280	280	280	5.0	~109	3.6	3.6	Transverse											
MS-48T	25	0.78	1970	1970	1970	34.3	94.6	25.4	25.4	Transverse											
MS-47T	25	0.77	2000	2000	2000	34.1	94.6	25.4	25.4	Transverse											
MS-44T	93	0.76	>4200	5180	<5180	89.0	84.7	>60.0	>K _{IC}	Shear											
MS-33T	93	0.75	>4200	5320	<5320	91.5	84.7	>59.1	>K _{IC}	Shear											
MS-35T	93	0.80	>3900	5290	<5290	92.8	84.7	>55.0	>K _{IC}	Shear											
MS-45T	150	0.79	>3900	4970	<4970	86.5	79.7	>55.1	>K _{IC}	Shear											
MS-46T	150	0.80	>4500	5160	<5160	89.7	79.7	>67.3	>K _{IC}	Shear											

TABLE 27. TENSILE STRENGTH AND FRACTURE-TOUGHNESS PROPERTIES OF RECRYSTALLIZED MOLYBDENUM SHEET (LONGITUDINAL)

Specimen	Test Temp., C	Initial Slot Length, in.	Load at Pop-in, lb	Max Load, lb	Fracture Load, lb	Notch		Yield Strength, 1000 psi	K _{Ic} , 1000 psi √in.	K _{Ic} , 1000 psi √in.	Fracture Mode
						Tensile Strength, 1000 psi	Yield Strength, 1000 psi				
Unnotched Specimens											
MR-8L	25				79.8		62.8		79.8		
MR-9L	93				56.2		41.3		56.2		
MR-10L	150				40.0		35.0		49.8		
Center-Notched Specimens											
MR-38L	-40	0.79	920	920	920	15.8		~105	11.5	11.5	Transverse
MR-39L	-40	0.80	890	890	890	15.5		~105	11.2	11.2	Transverse
MR-30L	25	0.75	1440	1440	1440	24.5		79.8	18.0	18.0	Transverse
MR-31L	25	0.67	2730	2730	2730	42.6		79.8	34.2	34.2	Transverse
MR-32L	93	0.77	2380	2380	2200	40.0		56.2	31.6	31.6	Transverse - dimple at notch tip
MR-33L	93	0.81	2070	2100	2070	37.5		56.2	28.6	28.6	Transverse - dimple at notch tip
MR-36L	150	0.76	1800	2680	<2680	28.1		40.0	24.1	>K _{Ic}	Shear
MR-37L	150	0.79	1980	2260	2260	23.3		40.0	27.4	>K _{Ic}	Transverse preceded by appreciable plastic flow

TABLE 28. TENSILE STRENGTH AND FRACTURE-TOUGHNESS PROPERTIES OF RECRYSTALLIZED MOLYBDENUM SHEET (TRANSVERSE)

Specimen	Test Temp., C	Upper Yield Stress, 1000 psi	Lower Yield Stress, 1000 psi	Ultimate Tensile Strength, 1000 psi	K _{IC} , 1000 psi √in.	K _C , 1000 psi √in.	Fracture Mode
Unnotched Specimens							
MR-8T	25	70.3	56.2	72.3			
MR-9T	93	57.0	42.3	57.0			
MR-10T	150	44.0	34.0	48.0			
Center-Notched Specimens							
		Initial Slot Length, in.	Load at Pop-in, lb	Max Load, lb	Fracture Load, lb	Notch Tensile Strength, 1000 psi	Yield Strength, 1000 psi
MR-42T	-40	0.80	1020	1020	1020	18.1	~90
MR-41T	-40	0.77	930	930	930	15.9	~90
MR-31T	25	0.66	2260	2260	2260	35.9	70.3
MR-32T	25	0.80	3070	3070	3070	54.6	70.3
MR-34T	93	0.78	2070	2080	2080	37.0	57.0
MR-36T	93	0.77	2410	2410	2270	41.6	57.0
MR-37T	150	0.74	1680	1840	1840	30.7	44.0
MR-38T	150	0.76	1920	2450	<2450	42.0	44.0
Fracture Toughness Data							
MR-42T	-40	0.80	1020	1020	1020	13.2	Transverse
MR-41T	-40	0.77	930	930	930	11.8	Transverse
MR-31T	25	0.66	2260	2260	2260	28.8	Transverse
MR-32T	25	0.80	3070	3070	3070	41.5	Transverse
MR-34T	93	0.78	2070	2080	2080	27.8	Transverse - dimple at notch tip
MR-36T	93	0.77	2410	2410	2270	33.1	Transverse - dimple at notch tip
MR-37T	150	0.74	1680	1840	1840	>K _{IC}	Transverse - dimple at notch tip
MR-38T	150	0.76	1920	2450	<2450	>K _{IC}	Transverse - dimple at notch tip
							Shear

TABLE 30. TENSILE STRENGTH AND FRACTURE-TOUGHNESS PROPERTIES OF RECRYSTALLIZED TUNGSTEN SHEET

Specimen	Test Temp., °C	Initial Slot Length, in.	Load at Pop-in, lb	Max Load, lb	Fracture Load, lb	Unnotched Specimens			K _{IC} , 1000 psi √in.	K _{IC} , 1000 psi √in.	Fracture Mode
						Upper Yield Stress, 1000 psi	Lower Yield Stress, 1000 psi	Ultimate Tensile Strength, 1000 psi			
Unnotched Specimens											
WR-9	121				(a)	(a)	(a)				
WR-10	399				18.5(b)	(b)	58.2				
WR-11	121				(a)	(a)	(a)				
Center-Notched Specimens											
WR-29	25	0.75	745	745	745	12.0	~100	8.6(c)	8.6	Transverse	Crack formed at notch tip prior to failure in grips
WR-30	25	0.75	790	790	790	12.4	~100	9.0(c)	9.0	Transverse	
WR-23	121	0.75	700	700	700	11.7	~65	8.5(c)	8.5	Transverse	
WR-24	121	0.75	1000	1000	1000	15.5	~65	11.4(c)	11.4	Transverse	
WR-25	260	0.75	670	670	670	10.6	~35	7.8(c)	7.8	Transverse	
WR-26	260	0.75	890	890	890	13.3	~35	9.8(c)	9.8	Transverse	Crack formed at notch tip prior to failure in grips
WR-27	399	0.75	~1320	1710(a)	1710(a)	>26.8	18.5	20.8(c)	1c	Crack formed at notch tip prior to failure in grips	
WR-28	399	0.75	~840	1150	1150	18.5	18.5	10.8(c)	10.8	Transverse	
WR-34	399	0.75	~990	1130	1130	19.1	18.5	14.0(c)	14.0	Transverse	Crack formed at notch tip prior to failure in grips
WR-33	538	0.75	>810	960(a)	960(a)	>15.5	~13	>10.7(c)	>K _{IC}	Crack formed at notch tip prior to failure in grips	
WR-32	538	0.75	>840	2220	<2220	35.8	~13	>12.6(c)	>K _{IC}	Shear	

(a) Failed in grips during loading.

(b) No yield point

(c) Notch radius varied from 0.001 to 0.003 inches; if sharper notch or crack had been used, values might have been lower.

TABLE 31. TENSILE STRENGTH AND FRACTURE-TOUGHNESS PROPERTIES OF WROUGHT, STRESS-RELIEVED TANTALUM SHEET

Specimen	Test Temp., C	Initial Crack Length, in	Load at Pop-in, lb	Max Load, lb	Fracture Load, lb	Notch Tensile Strength, 1000 psi	Yield Strength, 1000 psi	K _{Ic} , 1000 psi $\sqrt{\text{in.}}$	K _c , 1000 psi $\sqrt{\text{in.}}$	Fracture Mode
Unnotched Specimens										
TS-5	25					70.2			75.0	
TS-6	-196					143.0			151.0	
Center-Cracked Specimens										
TS-13	25	0.70	--	4220	1600	68.3	70.2	--	--	Shear
TS-12	-196	0.73	--	10,000	<10,000	164	143	--	--	Shear

TABLE 32. TENSILE STRENGTH AND FRACTURE-TOUGHNESS PROPERTIES OF RECRYSTALLIZED TANTALUM SHEET

Specimen	Test Temp., C	Initial Crack Length, in.	Load at Pop-in, lb	Max Load, lb	Fracture Load, lb	Yield Strength, 1000 psi		K _{IC} , 1000 psi $\sqrt{\text{in.}}$	K _C , 1000 psi $\sqrt{\text{in.}}$	Fracture Mode
						Upper Yield Stress, 1000 psi	Lower Yield Stress, 1000 psi			
Unnotched Specimens										
TR-8	25					41.4	33.6	47.5		
TR-9	-196					135.0	(a)	135.0		
Center-Notched Specimens										
TR-20	25	0.68	--	2520	~100	39.3	41.4	--	--	Shear
TR-19	-196	0.70	--	7800	6200	126	135	--	--	Shear

(a) Load dropped continuously after upper yield point.

(a) Load dropped continuously after upper yield point.

TABLE 33. TENSILE STRENGTH AND FRACTURE-TOUGHNESS PROPERTIES OF WROUGHT, STRESS-RELIEVED COLUMBIUM SHEET

Specimen	Test Temp., C	Initial Crack Length, in.	Load at Pop-in, lb	Max Load, lb	Fracture Load, lb	Notch Tensile Strength, 0 psi	Yield Strength, 1000 psi	K _{Ic} , 1000 psi √in.		Fracture Mode
								K _{Ic} , 1000 psi √in.	K _{IIc} , 1000 psi √in.	
Unnotched Specimens										
CS-5	25						52.0	46.0		
CS-6	-196						126.0	136.0		
Center-Cracked Specimens										
CS-11	25	0.70	--	3750	2000	60	52	--	--	Shear
CS-12	-196	0.70	--	8200	6250	131	126	--	--	Shear

TABLE 34. TENSILE STRENGTH AND FRACTURE-TOUGHNESS PROPERTIES OF RECRYSTALLIZED COLUMBIUM SHEET

Specimen	Test Temp., C	Initial Crack Length, in.	Load at Pop-in, lb	Max Load, lb	Fracture Load, lb	Upper Yield		Lower Yield		Ultimate Tensile		K _{Ic} , 1000 psi $\sqrt{\text{in.}}$	Fracture Mode
						Stress, 1000 psi	Yield Strength, 1000 psi	Stress, 1000 psi	Yield Strength, 1000 psi	Strength, 1000 psi	Tensile Strength, 1000 psi		
CR-8	25					37.7		34.9		45.6			
CR-9	-196					107.0(a)		(a)		114.0			
Notch													

(a) No yield point.

Aeronautical Systems Division, Dir./Materials and Processes, Metals and Ceramics Lab, Wright-Patterson AFB, Ohio.
Rpt No. ASD-TDR-62-1004. FURTHER INVESTIGATION OF NOTCH SENSITIVITY OF REFRACTORY METALS. Final report, Dec 62, 126p. incl illus., tables, 32 refs.

Unclassified Report

Molybdenum and Mo-0.5Ti alloy with various degrees of cold work and different recrystallized grain sizes were tested to determine their low-temperature properties. Sufficient cold work (> 25 per cent; about 68 per cent is sufficient) markedly reduced the ductile-to-brittle transition temperature of both materials, whereas increasing the recrystallized grain size increased this parameter. Mechanical notches resulted in pronounced degradation of properties in fibered structures, but were much less

(over)

detrimental to recrystallized structure. This behavior was attributed to the controlling (detrimental) effect of grain boundaries in the fracture of recrystallized molybdenum or Mo-0.5Ti, regardless of material geometry. The fracture toughness of unalloyed molybdenum, tungsten, tantalum, and columbium was studied over a range of temperatures chosen to include the ductile-brittle transition. Sheet specimens, 2 x 8 x 0.050 inc, containing sharp central notches were employed. Both wrought and recrystallized conditions were examined for each material. The effect of specimen orientation relative to the rolling direction was studied for molybdenum. Where possible, results were reported in terms of the fracture toughness parameters K_{IC} and K_{IS} . In an effort to provide some basic rationale^c for the behavior of a brittle material in the presence of notches, a model of an idealized partially relaxed crack was adopted. Using theoretical values of the stress at the tip of such a crack, the resultant macroscopic strain was calculated by means of parameters relating to dislocation density and velocity.

1. Refractory metals
2. Notch sensitivity
- I. AFSC Project 7351, Task 735101
- II. Contract AF 33 (616)-7604
- III. Battelle Memorial Institute, Columbus, Ohio

- IV. Aval fr OTS
- VI. In ASTIA collection

Aeronautical Systems Division, Dir./Materials and Processes, Metals and Ceramics Lab, Wright-Patterson AFB, Ohio.
Rpt No. ASD-TDR-62-1004. FURTHER INVESTIGATION OF NOTCH SENSITIVITY OF REFRACTORY METALS. Final report, Dec 62, 126p. incl illus., tables, 32 refs.

Unclassified Report

Molybdenum and Mo-0.5Ti alloy with various degrees of cold work and different recrystallized grain sizes were tested to determine their low-temperature properties. Sufficient cold work (> 25 per cent; about 68 per cent is sufficient) markedly reduced the ductile-to-brittle transition temperature of both materials, whereas increasing the recrystallized grain size increased this parameter. Mechanical notches resulted in pronounced degradation of properties in fibered structures, but were much less

(over)

detrimental to recrystallized structure. This behavior was attributed to the controlling (detrimental) effect of grain boundaries in the fracture of recrystallized molybdenum or Mo-0.5Ti, regardless of material geometry. The fracture toughness of unalloyed molybdenum, tungsten, tantalum, and columbium was studied over a range of temperatures chosen to include the ductile-brittle transition. Sheet specimens, 2 x 8 x 0.050 inc, containing sharp central notches were employed. Both wrought and recrystallized conditions were examined for each material. The effect of specimen orientation relative to the rolling direction was studied for molybdenum. Where possible, results were reported in terms of the fracture toughness parameters K_{IC} and K_{IS} . In an effort to provide some basic rationale^c for the behavior of a brittle material in the presence of notches, a model of an idealized partially relaxed crack was adopted. Using theoretical values of the stress at the tip of such a crack, the resultant macroscopic strain was calculated by means of parameters relating to dislocation density and velocity.